A review on the strain rate dependency of the dynamic viscoplastic response of FCC metals

Elsevier Editorial System(tm) for Progress in Materials Science

Manuscript Draft

Manuscript Number: PMS-D-15-00058

Title: A review on the strain rate dependency of the dynamic viscoplastic response of FCC metals

Article Type: Full Review Article

Keywords: Constitutive models
High strain rate
FCC metals
Modelling
Viscoplastic behaviour
Dynamic loading

Corresponding Author: Dr. Filipe Teixeira-Dias, BEng, MSc, PhD, Hab

Corresponding Author's Institution: University of Edinburgh

First Author: Francisco C Salvado

Order of Authors: Francisco C Salvado; Filipe Teixeira-Dias, BEng, MSc, PhD, Hab; Stephen M Walley; Lewis J Lea; João B Cardoso

Abstract: The response of structures and materials subject to impulsive loads remains a field of intense research. The dynamic loading and temperature increase affect the material's mechanical/failure response. For example, strains due to explosive blast will increase at rates from 102 to 104 s-1, leading to regimes of elastic/plastic wave propagation, plane stress and adiabatic deformations. Few constitutive models consider high strain rate effects, however some constitutive approaches that were developed and tested at low strain rate regimes will also be addressed here due to their relevance. Specific reference will be made to strain rate regimes close to 104 s-1, where shock waves may develop. The paper focuses on constitutive models for polycrystalline face-centred-cubic (FCC) metals since their behaviour under high strain rate regimes is not yet fully understood mostly due to path loading dependency. Reference is also made to aluminium alloys since they are widely used in virtually all fields of industry and in armour and protective structures and systems. A basic review of the main theoretical aspects that constitute the basis for most of the constitutive models described is also presented and the main features of each model are thoroughly discussed.

A review on the strain rate dependency of the dynamic viscoplastic response of FCC metals

Francisco C. Salvado , F. Teixeira-Dias , Stephen M. Walley, Lewis J. Lea , João B. Cardoso

Reply to reviewers

The authors thank the second set of comments received from the reviewers, which were considered and implemented to the maximum extent. The authors now hope that the resulting manuscript meets all the requirements of the reviewers.

Reviewer major changes:

1. The BP, SG, ZA, and MTS models are fine, but SL should be melded at the end of SG: Done.
2. The Kahn models are seldom used and should not be emphasized as much. There is hardly anything physical about them and they are clearly phenomenological. Thus, they belong in Section 5: They were moved to section 5.
3. The Chen Nemat Nasser model deals with dynamic strain aging, and this is another subject. There are dozens of DSA constitutive models. Hence it should be removed: It has been removed.
4. Section 2.2. Regarding dynamic recovery and recrystallization, Andrade et al. (Script Met, 1994, 30, 933-938) proposed an equation that incorporates the discontinuity due to the collapse of the strength. It might be worth mentioning it and showing its graphical expression. None of the other constitutive models treats the rapid strength decrease associated with such structural changes: Reference and comments to the work of Andrade et al. were added, and graphs from his paper were reproduced. Section 6 has been inserted to hold the comments on Andrade's equations instead of inserting them in Section 2, to avoid references to constitutive models before treating the subject.
5. Section 4.9 (Other Constitutive models) is far too long. It needs pruning. This is a painful process, but the authors will undoubtedly loose the reader. The authors have to decide on the relevance of the models and give proportionate importance: This section has been significantly shortened.
6. Section 5.1 Kocks-Mecking. This is not really a phenomenological model but is at the heart of the MTS model. Hence, this section should be moved to Section 4.4, with an explanatory transition. Kocks is the father of the MTS model and he used his earlier knowledge to develop it: Done.

Reviewer minor changes:

All minor changes suggested by the reviewers were implemented. Authors' replies in blue.

- Page 2: Period missing after [2]: Added.
- Page 3: BCC used before it is defined. In the first paragraph there are many repetitions of concepts such as Peierls stress and strain rate sensitivity: BCC defined. Paragraph was rephrased to avoid constant repetitions.
- Page 14: Do eqs 17-19 have specific citations? Citation [25], sentence rephrased.

- Page 15: What is the difference/advantage of eqs 23-26? These equations are similar in form but differ in how they account for the strain-rate dependency of the temperature. Sentence was rephrased to make this clearer.
- Page 19: Comma after "Due to their simplicity": Added.
- Page 20: Remove second period after "Zerilli and Armstrong [36] developed a constitutive relation based on dislocation mechanics and incorporating the effect of strain hardening, strain-rate hardening and grain size.": Removed.
- Fig 10 Caption: superscripts are missing: Corrected.
- All table titles should be above the table: All table captions are now above the table.
- The tables should also include the applicable references cited in the text: All applicable references added to tables.

A review on the strain rate dependency of the dynamic viscoplastic response of FCC metals

Francisco C. Salvado [a, c], *F. Teixeira-Dias* [b,*], *Stephen M. Walley* [d], *Lewis J. Lea* [d], *João B. Cardoso* [a]

[a] Department of Mechanical Engineering, Faculdade de Ciências e Tecnologia
Universidade Nova de Lisboa (FCT), 2829-516 Caparica, Portugal

[b] School of Engineering, The University of Edinburgh
Edinburgh EH9 3JL, UK

[c] Naval Research Centre (CINAV), Escola Naval
Alfeite, 2810-001 Almada, Portugal

[d] SMF Fracture and Shock Physics Group, Cavendish Laboratory
University of Cambridge, CB3 0HE, UK

Abstract

The response of structures and materials subject to impulsive loads remains a field of intense research. The dynamic loading and temperature increase affect the material's mechanical/failure response. For example, strains due to explosive blast will increase at rates from 10^2 to 10^4 s^{-1}, leading to regimes of elastic/plastic wave propagation, plane stress and adiabatic deformations. Few constitutive models consider high strain rate effects, however some constitutive approaches that were developed and tested at low strain rate regimes will also be addressed here due to their relevance. Specific reference will be made to strain rate regimes close to 10^4 s^{-1}, where shock waves may develop. The paper focuses on constitutive models for polycrystalline face-centred-cubic (FCC) metals since their behaviour under high strain rate regimes is not yet fully understood mostly due to path loading dependency. Reference is also made to aluminium alloys since they are widely used in virtually all fields of industry and in armour and protective structures and systems. A basic review of the main theoretical aspects that constitute the basis for most of the constitutive models described is also presented and the main features of each model are thoroughly discussed.

Keywords

Constitutive models, high strain rate, FCC metals, modelling, viscoplastic behaviour, dynamic loading

PACS codes

62.20.F-/fk/fq/Hg/M-, 62.50.Ef, 64.10.+h, 64.30.Ef, 81.05.Bx, 81.40.Lm, 81.70.Bt, 83.10.Ff/Gr, 83.60.Bc/Df/Fg/La/Uv, 83.80.Ab

[*] Corresponding author contacts: f.teixeira-dias@ed.ac.uk (F. Teixeira-Dias), Tel: +44 (0)131 50 6768.

A review on the strain rate dependency of the dynamic viscoplastic response of FCC metals

Francisco C. Salvado [a, c], *F. Teixeira-Dias* [b,*], *Stephen M. Walley* [d], *Lewis J. Lea* [d], *João B. Cardoso* [a]

[a] Department of Mechanical Engineering, Faculdade de Ciências e Tecnologia
Universidade Nova de Lisboa (FCT), 2829-516 Caparica, Portugal

[b] School of Engineering, The University of Edinburgh
Edinburgh EH9 3JL, UK

[c] Naval Research Centre (CINAV), Escola Naval
Alfeite, 2810-001 Almada, Portugal

[d] SMF Fracture and Shock Physics Group, Cavendish Laboratory
University of Cambridge, CB3 0HE, UK

Abstract

The response of structures and materials subject to impulsive loads remains a field of intense research. The dynamic loading and temperature increase affect the material's mechanical/failure response. For example, strains due to explosive blast will increase at rates from 10^2 to 10^4 s^{-1}, leading to regimes of elastic/plastic wave propagation, plane stress and adiabatic deformations. Few constitutive models consider high strain rate effects, however some constitutive approaches that were developed and tested at low strain rate regimes will also be addressed here due to their relevance. Specific reference will be made to strain rate regimes close to 10^4 s^{-1}, where shock waves may develop. The paper focuses on constitutive models for polycrystalline face-centred-cubic (FCC) metals since their behaviour under high strain rate regimes is not yet fully understood mostly due to path loading dependency. Reference is also made to aluminium alloys since they are widely used in virtually all fields of industry and in armour and protective structures and systems. A basic review of the main theoretical aspects that constitute the basis for most of the constitutive models described is also presented and the main features of each model are thoroughly discussed.

Keywords

Constitutive models, high strain rate, FCC metals, modelling, viscoplastic behaviour, dynamic loading

PACS codes

62.20.F-/fk/fq/Hg/M-, 62.50.Ef, 64.10.+h, 64.30.Ef, 81.05.Bx, 81.40.Lm, 81.70.Bt, 83.10.Ff/Gr, 83.60.Bc/Df/Fg/La/Uv, 83.80.Ab

[*] Corresponding author contacts: f.teixeira-dias@ed.ac.uk (F. Teixeira-Dias), Tel: +44 (0)131 50 6768.

1. Introduction

Considerable effort is being devoted to the investigation of the response of structures and materials subject to ballistic impacts or blast loads, due to public awareness about terrorist threats or the prevention of accidents such as in offshore oil and gas or chemical industries, where unwanted gas or fuel deflagrations can happen.

In general a blast or impact load will manifest itself by means of a sharp pressure wave travelling at ultrasonic speed impinging on the structure surface. The energy will be transmitted so quickly that deformation will develop at very high rates and stress waves may form and travel through the body. High temperature changes may also be present and both the dynamic loading and the temperature increase will affect the mechanical and failure response of the material. This rate dependent behaviour has been very intensely investigated for a number of materials, namely metals and composites. In broad terms, strains due to explosive blast will increase at rates from 10^2 to 10^4 s^{-1}, leading to a regime of elastic and plastic wave propagation, plane stress and deformation heating [1].

One important aspect in the research effort needed to understand the response of engineering materials to blast loads involves the definition of suitable constitutive models that can be used in numerical analysis. It is important to emphasize the relevance of numerical computations in these analyses since experiments may reveal themselves unpractical or expensive. Under blast loads, deformations will be quite large meaning that the elastic component of strain will be comparatively smaller than the plastic strain. This led many researchers to focus their attention on plastic constitutive expressions. However, many constitutive models for the response of metals in high speed and loading regimes exist and a compilation may be of some help for those involved in the field. Few models consider high strain rate effects but some others that were developed and tested at low strain rate regimes will also be addressed due to their relation with other models. Nonetheless, reference will be made to regimes around 10^4 s^{-1}, where shock waves may be present in the material. For the reader interested in extreme strain rate regimes, reviews are available [2].

The variety of engineering materials of interest (steel, non ferrous alloys, composites, foams, etc.) is too wide to be tractable and since studies on steel and ferrous alloys have been widely reviewed [3] the scope of this review will restrict itself to those constitutive models that can be used for the simulation of the dynamic behaviour of non-ferrous alloys (e.g. aluminium alloys) since the use of these materials spans for virtually all fields of industry (aeronautical, automotive, marine and civil), including in protective structures and armour. However, non-ferrous metals may exhibit different behaviour under dynamic loading and a preference will be made to those models that have been tested with aluminium. Aluminium is a widely used material in all sorts of civilian and military crafts, has a polycrystalline face centred cubic (FCC) structure, which is the main reason for its ductility. For plastic deformation at least five independent slip systems are needed, as pointed by von Mises by the first time [4], but although both FCC and BCC (body centred cubic) have those systems, FCC metals have a higher packing efficiency and the slip planes are more closely packed than BCC metals, which makes them more ductile as the energy required to move atoms along denser planes is smaller than for lesser packed planes. Emphasis will be put on those constitutive models that work better for FCC metals and, consequently, this review may ignore models and variants developed for other crystallographic structures such as BCC or hexagonal closed packed (HCP). The main difference is that in BCC metals the yield stress is determined by strain rate hardening and temperature softening and in FCC metals by strain rate hardening [5]. The plastic deformation of FCC metals is less sensitive to temperature than for BCC metals. Dislocation movement in BCC metals is more thermally activated than in FCC metals, meaning that the latter will maintain ductility at lower temperatures. In BCC metals dislocation motion is increasingly influenced by the periodic lattice potential such as the Peierls stresses while for the FCC there are the short range stresses induced by forest dislocations and solute atoms that mostly affect dislocation motion. BCC metals are also more strain-rate sensitive than FCC metals.

The problem of the simulation of explosively driven deformation of metals and alloys is a complex one, that requires suitable and realistic models of plastic constitutive behaviour [6]. The range of variation of mechanical and thermodynamic state variables can be extremely wide (plastic strain of several hundreds per cent, pressures exceeding 10 GPa and plastic strain rates of millions per second, and temperatures up to melting point). Many models are available, each one emphasizing a few aspects of material response but none being completely satisfactory. For instance, those constitutive equations that

were derived from thermally activated dislocation glide theory are known not to work properly for strain rates above 10^5 s^{-1} where a sharp increase in the flow stress is observed. It will be discussed that this increase is due to phonon drag and most constitutive methods do not consider this effect in the equations.

One of the most interesting aspects related to high strain rate loading regimes is the increase of flow stress with strain rate and the strain rate sensitivity. Both phenomena can be observed in Fig. 1, which shows how the stress-strain curves move upwards with strain rate but also how a structure alteration due to the change in strain ratio will affect the stress-strain curve. A strain rate insensitive material strained at a certain rate (lower curve of Fig. 1a) will start following the upper curve if there occurs an increase in strain rate. However if a structure alteration occurs due to the change in strain rate (if the material is sensitive to strain rate) the stress-strain curve may follow a different path as shown in Fig. 1b [7]. This aspect will be a main issue in most constitutive model discussions. A basic review of the main theoretical aspects that constitute the basis for most of the constitutive models described is presented below. To help to understand the formulations proposed below the reader is referred to the sources for a more detailed and complete treatment of these matters.

2. Constitutive behaviour theory

At the micro-scale level, polycrystalline metals show crystal defects termed dislocations. Under load, dislocations will move along various glide planes resulting in plastic flow. Mobile dislocations will move rapidly until they are arrested by energy barriers lying in their paths. The rate of deformation is controlled by the interaction of dislocations with defects such as grain boundaries, forest dislocations, second phase particles, etc. For FCC metals the dominant short-range obstacles are expected to be other dislocations (forest dislocations). However, for solid solution or dispersion strengthened alloys other effects will come into play. When encountering barriers, dislocations will need to overcome them in order that deformation can proceed and that requires energy. For low strain rates, where dislocation drag is not significant, thermal activation will be the main mechanism for deformation rate control. Thermal activation will be expressed in terms of large and random vibrations that allow the overcoming of the obstacles by the dislocations, which will then accelerate until they are stopped by another obstacle and the same process has to be repeated.

Obstacles vary with temperature. For low temperatures (below 25% of melting temperature) the main rate-controlling mechanism in FCC metals it is the intersection of forest dislocations which controls the thermally activated process (Conrad, H., "The cryogenic properties of metals, in High Strength Materials", John Wiley, New York, 1964, cited by Read et al. [8]).

The plastic deformation behaviour of metals and alloys depends not only on the instantaneous value of strain rate but also on the strain history [9]. This is true for FCC and HCP metals while BCC metals are considered as not path dependent and makes it difficult to establish reliable constitutive relations that account for strain history. Walley [10] investigated a Taylor impact experiment in copper and found a good agreement between measured data and numerical data obtained with the path-dependent constitutive method from Goldthorpe [11]. We will observe different dislocation structures for the same level of plastic strain, depending on the rate of deformation imposed on the material. The same happens for plastic deformation at different temperatures. Therefore, flow stress is not a unique function of strain, strain rate and temperature but it is accepted that plastic deformation is the result of displacement of many dislocations and plastic deformation rates can be described in terms of thermally activated processes.

A few theoretical notes that are presented below following the work of Meyers et al. [7, 12] present a more detailed introduction to the mechanism of thermally activated dislocation motion.

It is normally stated in most papers on the subject of plasticity that dislocations or strain rate follow an Arrhenius law. This comes from an observation made by Arrhenius that there are "activation states" in chemical reactions between reactants and products. He suggested that the reaction rate could be expressed by a constant *K* given by

$$K = A \exp\left(\frac{-\Delta E_a}{KT}\right) \tag{1}$$

where *A* is a frequency factor, ΔE_a is the activation energy for the process and *KT* are the Boltzmann constant and temperature, respectively. Proof for this equation or a theoretical treatment of these matters are beyond the scope of this work. For the moment it is assumed that dislocations will pass through an activated state. If we consider *N* dislocations that are arrested at obstacles then, considering the dislocations as oscillators, each one will have its own energy level. These energy levels, e_i are quantised

(i.e. they are discrete) and for each energy level we will have a number of dislocations n_i which distribution can be mathematically represented by an exponential function

$$n_i = Ae^{-\beta e_i} \tag{2}$$

This is the Boltzmann distribution, where A and β are the distribution parameters. The probability that a dislocation has an energy equal or greater than E is given by

$$P_E = \frac{A\int_E^\infty e^{-\beta e_i}\mathrm{d}e_i}{A\int_0^\infty e^{-\beta e_i}\mathrm{d}e_i} = e^{-\beta E} \tag{3}$$

From thermodynamics it can be shown that $\beta = 1/(KT)$, and that the probability of a dislocation having an energy greater than E is

$$P_E = e^{-E/(KT)} \tag{4}$$

It is assumed that dislocations will overcome an obstacle when their energy exceeds the height of the obstacle. Also, from basic thermodynamic relations, we can conclude that the internal energy is approximately equal to enthalpy, since the PV term is negligible in condensed solids. Thus,

$$p = \exp\left(-\frac{\Delta H}{KT}\right) = \exp\left(-\frac{\Delta G - T\Delta S}{KT}\right) = \exp\left(-\frac{\Delta G}{KT}\right)\exp\left(-\frac{\Delta S}{K}\right) = A\exp\left(-\frac{\Delta G}{KT}\right) \tag{5}$$

The term $\exp(\Delta S/K)$ becomes the coefficient A. Most constitutive models are based on this expression, meaning that given a barrier of height ΔG, the probability that a dislocation will jump over it is p. When temperature rises, this probability increases because the energy of the dislocation will increase due to the thermal contribution. The frequency of successful jumps, v_1, is related to this probability p, by $p = v_1/v_0$, where v_0 is the frequency of vibration of the dislocations. Thus,

$$v_1 = v_0 A\exp(-\Delta G/KT) \tag{6}$$

The Orowan equation applied to Eq. (6) relates the strain to the movement of dislocations:

$$\dot{\gamma} = \frac{1}{M}\rho b\frac{\Delta l}{\Delta t} \tag{7}$$

where M is an orientation factor, ρ is the dislocation density, b is the Burgers vector and Δl is the distance between dislocation barriers. The total transit time of a dislocation is the sum of the waiting time to jump

over the obstacle and the travel time between obstacles. The travel time may be assumed to be negligible and Δt, the waiting time, is the inverse of the successful jump frequency, v_1. Substituting Eq. (6) in Eq. (7) yields

$$\dot{\gamma} = \frac{v_0 \rho b \Delta l}{M} A \exp\left(-\frac{\Delta G}{KT}\right) = \dot{\gamma}_0 \exp\left(-\frac{\Delta G}{KT}\right) \tag{8}$$

where all the terms outside the exponential were grouped together and named $\dot{\gamma}_0$. Other authors use similar constitutive relations for thermally activated dislocation mechanism, such as [9]

$$\dot{\gamma} = v(\tau, s_\alpha, T) \exp\left[-\frac{\Delta G(\tau^*, s_\alpha, T)}{KT}\right] \tag{9}$$

where v is a reference value, ΔG is the activation free energy, K is the Boltzmann constant, τ and γ are shear stress and shear strain, respectively, and τ^* is the effective shear stress. The s_α family of parameters is intended to account for the history of metal structure change. Eq. (8) can be solved for, ΔG, leading to

$$\Delta G = KT \ln \frac{\dot{\gamma}_0}{\dot{\gamma}} \tag{10}$$

The barriers can have different shapes and may lead to different constitutive equations. Several authors attempted to find suitable barrier shapes and a generalised form has been proposed by Kocks et al. (1975, Kocks UF, Argon AS, Ashby MF, *Thermodynamics and kinetics of slip*, Prog. Mater. Sci. vol. 19, Pergamon Press, Oxford, cited by [12]) using two parameters to define the shapes, p and q. These authors proposed an equation of the form

$$\Delta G = \Delta G_0 \left[1 - \left(\frac{\tau}{\tau_0}\right)^p\right]^q \tag{11}$$

Combining Eqs. (10) and (11) a general constitutive equation is obtained relating stress, strain rate and temperature.

It is usual to decompose stress into two components, one dependent on temperature and another independent of thermal effects. Some authors define an effective stress, τ^*, associated to successful thermal activation that is related to the applied stress by means of a term independent of temperature, called athermal stress τ_a:

$$\tau^* = \tau - \tau_a \quad (12)$$

The athermal stress is the stress necessary to overcome long-range obstacles. The other term, called the effective stress, is temperature dependent and is related to the force necessary to overcome short-range obstacles [13]. At very high strain rates the applied stresses are sufficient to overcome the obstacles without any aid from thermal activation. At these strain rates dislocation drag will be the main damping mechanism for dislocation movement. The thermal stress component decreases with temperature and increases with strain rate. The athermal component increases with the accumulation of dislocations as the elastic field will hinder the motion of mobile dislocations [14]. This elastic field will not depend directly on temperature but will be affected by it in two ways: (i) by means of temperature dependence of elastic moduli and (ii) through the effect of temperature on the density of far-field dislocation forests. At certain temperature levels metals will anneal, which will reduce dislocation density and this may have to be taken into account when high temperature regimes are present. Temperature history is also dependent of strain rate, which will affect the current density of dislocations. A schematic explanation of how thermal energy can help the dislocation to overcome obstacles is shown in Fig. 2.

The figure shows the energies necessary to overcome a barrier (the areas under the force-distance curve) and as temperatures increases the respective thermal energies will also increase (represented by the hatched areas) decreasing the effective height of the barrier to be overcome. So the stress necessary to move the dislocation past the barrier decreases as temperature increases.

2.1. Twinning

There are two basic modes of plastic deformation in polycrystalline metals, slip and twinning [8]. Twinning can be dominant at high strain rates under shock loading and constitutive models for high strain rate loading should consider both twinning and slip. Twinning at low temperatures and high strain rates is responsible for higher predicted yield stress values than experimental results. This has been reported from the findings of Zerilli and Armstrong for instance [12] and was attributed to the change of the major deformation mechanism from dislocation slip to twinning at high strain rates and low temperature. Other occurrences of twinning are reported for shock-induced deformation [15]. However, twinning is seldom addressed in most widely used constitutive models.

2.2. Dynamic recovery and recrystallization (DRV and DRX)

When a metal deforms plastically at high temperatures two softening mechanisms such as dynamic recovery (DRV) and dynamic recrystallisation (DRX) may take place which have a strong effect on the microstructure and mechanical properties of the material. At the microstructure level DRX will begin when strain hardening and recovery can no longer store more immobile dislocations. Strain-hardening plus recovery and DRX are important mechanisms responsible by the stress-strain response of FCC metals although not restricted to these.

Dynamic recovery consists of a re-arrangement, at high temperatures, of crystal defects of a plastically deformed metal. Some restoration of the original structure and properties may occur through annihilation of point defects and dislocations and a spatial re-distribution of dislocations that will soften the metal. As deformation progresses the flow stress increase as dislocations interact and multiply but as the dislocation density increases the rate of recovery also increases and at a certain strain a dynamic equilibrium will be found between the rates of work hardening and recovery. Work hardening rates are therefore counterbalanced by DRV or DRX.

DRX can be characterised by a nucleation rate of low dislocation density grains and a posterior growth rate that can produce a homogeneous grain size at a reached equilibrium status.

Recovery and recrystallisation are competing processes and the temperature regimes where they operate may overlap. Recrystallisation will usually be the first phenomena to occur and once it has occurred no further recovery will take place since the driving force for both mechanisms is the reduction in the stored energy of the deformed material. Conversely recovery will retard recrystallisation. DRX occurs during straining of metals at high temperature and will affect crystallographic texture and thus material anisotropy. As dislocation are eliminated by DRX the hot plasticity of materials is improved. DRV is typical of high stacking-fault energy (SFE) such as Al, where the flow stress saturates after an initial period of work hardening. DRX

Shear stresses and strain rates will determine which dislocation mechanism controls the mechanical response. For shear stresses smaller then the quasi-static yield stress the response will remain elastic and below the level of τ (see Eq. 10) the plastic flow will be in the thermally activated regime [8].

For stresses above τ the strain rate regimes will influence the mechanism that controls dislocation motion. At very small strain rates rate effects are negligible and the strain hardening characteristics of the material will determine the stress strain response. For small strain rates thermal activation will be the rate-controlling mechanism. At higher strain rates viscous drag will control the plastic flow. When increasing the shear stress even further it is observed that for very high rates relativistic effects will influence the process, setting a limit for dislocation velocity. The transitions between these dislocation motion regimes are not precise and vary with the material and the temperature. Meyers [7] points that, as a rule, relativistic effects start becoming important for mean dislocation velocities above 0.8 of shear-wave velocity. For titanium the drag-controlled plasticity regime starts at above a strain rate of 10^4 s^{-1}.

It is important to note that the flow stress at a given temperature T is typically proportional to the shear modulus μ, [16] at this temperature. This allows the activation work done by the applied forces to be independent of material properties and so ΔG is proportional to $\mu(T)$. This allows the definition of a normalised activation energy,

$$g \equiv \frac{\Delta G}{\mu b^3} = g\left(\frac{\tau \mu_0}{\hat{\tau}\mu}\right)$$

where μ_o is the shear modulus at 0 K [16]. Inverting the equation and combining with Eq. (10) gives

$$g = \frac{KT}{\mu b^3} \ln\left(\frac{\dot{\varepsilon}_0}{\dot{\varepsilon}}\right) \tag{13}$$

As deformation progresses the material structure changes as the result of a balance between dislocation accumulation and dynamic recovery. The strain hardening θ can be decomposed into components due to dislocation accumulation and dynamic recovery respectively, which can be written as $\theta = \theta_a - \theta_r(T, \dot{\varepsilon}, \hat{\sigma})$ [17], where $\hat{\sigma}$ is the mechanical threshold stress. The dynamic recovery term depends strongly on strain rate and temperature. If the strain-hardening rate $(\mathrm{d}\hat{\sigma}/\mathrm{d}\varepsilon)$ is plotted against $\hat{\sigma}$ as a function of strain rate and temperature, a Voce (linear) behaviour is observed for a limited range of strain, as can be seen in Fig. 3. A closed-form description for dynamic recovery has been proposed [16] in the form

$$g = g_0 \left[1 - \left(\frac{\tau \mu_0}{\hat{\tau}\mu}\right)^p\right]^q \tag{14}$$

This equation has been used for dynamic recovery with the exponent $q = 2$. It may be concluded [16] that an expression of the form

$$\Delta G = KT \ln\left(\frac{\dot{\varepsilon}_0}{\dot{\varepsilon}}\right) = \mu b^3 g_0 \left[1 - \left(\frac{\tau \mu_0}{\hat{\tau} \mu}\right)^p\right]^q \quad (15)$$

can describe the mechanism of dislocation and obstacle interaction.

The strain hardening representations for a given strain rate and temperature can be grouped into two categories: (i) the Voce type group where a saturation stress is approached at large strain and (ii) the Hollomon or power-law group [18] that are unbounded at large strains. Due to dynamic recovery most metals do not show Voce behaviour, that is strain hardening rate decreasing to zero with increasing stress or strain.

For strain rates up to 10^4 s^{-1} the dominant mechanism of viscoplastic flow is glide kinetics of dislocations overcoming obstacles with the assistance of thermal fluctuations. Above the mechanical threshold this thermally activated dislocation glide is no longer the dominant mechanism that controls viscoplastic flow but, instead, the continuous glide of mobile dislocations that are subject to damping and relativistic effects.

Thermally activated stored deformation energy will control the softening mechanisms. The DRX activation energy will be an important parameter determining the critical conditions for DRX initiation.

The increase in strain rate or the decrease in deformation temperature prevents the occurrence of softening due to DRX and DRX and the material will exhibit a work hardening behaviour. For a given strain rate the work hardening effect will predominate in the first stages of deformation and the flow stress rapidly increases to a critical value. Then DRV and DRX become predominate and the true stress-strain curves of most materials will tend to adopt a shape of a plateau after the flow stress curve may show an inflexion after its peak value. DRX thus occurs after a critical amount of strain, which is dependent on the temperature and strain rate and also on initial grain size. It will become the dominant stress-strain response mechanism in FCC metals after the critical strain is attained. However, normally the effect of DRX has not been included in the constitutive equations although DRX causes significant changes in the thermomechanical response of the material, particularly in the high-strain rate regimes. A

procedure exists that incorporates the contribution of DRX into the constitutive equations. Such contribution will be shown in Section 6, after a review of relevant constitutive models since its discussion is more appropriate after the relevant constitutive model and their underlying assumptions have been presented.

3. Constitutive equations

The mechanisms of plastic deformation and their relation with applied loads can be mathematically described by constitutive laws which are basically sets of relations between stresses, stress derivatives, strains, strain derivatives, temperature, microstructure and damage. The deformation and failure responses of engineering materials require the knowledge of suitable constitutive equations if accurate predictions are to be numerically obtained. A constitutive model is a combination of independent functions of strain, strain rate and temperature which are generally represented as $f(\varepsilon), g(\dot{\varepsilon})$ and $h(T)$. A constitutive model is therefore a relation of the type:

$$\sigma = F(\varepsilon, \dot{\varepsilon}, T, \text{deformation history}) \tag{16}$$

where $\varepsilon, \dot{\varepsilon}, T$ are the strain, strain rate and temperature, respectively. Some constitutive models also consider internal variables that characterize the metal structure. The deformation history is required due to the irreversible nature and path dependence of the plastic deformation, particularly for FCC metals. The effects of each of the above three variables can be combined with the other in a multiplicative or additive way [18] allowing many possible different constitutive equations. Many will be modifications of existing ones. The strain rate will have, for instance, hardening or softening effects on certain aluminium alloys, depending on the strain rate range and temperature. That is the main difficulty in identifying a suitable constitutive law, as often they are normally limited to certain classes of materials and limited ranges of strain rates. The many researchers that have addressed this problem have in many cases tried to circumvent this difficulty by introducing modifications to existing models when calibration from experimental data failed to produce good agreement between model and experiments. These efforts result in dozens of constitutive models, for as many materials and loading regimes.

From the many possible regimes of loading we can identify our range of interest of strain rate, from 10^2 s^{-1} upwards. For strain rates higher that 10^3 s^{-1} thermal and wave propagation effects become

noticeable and at 10^5 s^{-1} or higher, shock waves will propagate through the material making thermodynamic behaviour important as transition from isothermal to adiabatic behaviour is observed. The thermal behaviour of yield and flow stress of FCC metals is more complex to describe than strain rate. The yield stress follows a curve like the one depicted in Fig. 4.

Four regions can be noticed in the curve [19]: (i) a low temperature region in which the pattern of the flow stress depends on the material, (ii) a region where the material is subjected to higher temperatures and the flow stress decreases with increasing temperature, (iii) a region where the temperature has no effect on flow stress and, finally, (iv) a very high temperature region, where the flow stress decreases again with increasing temperatures. Not all materials exhibit the four regions and some metals can behave in accordance with only one or two parts of the curve. It will be seen that most constitutive models combine strain rate and temperature effects.

Constitutive equations can be broadly classified in two major categories: physically based or phenomenologically based, depending on the assumptions adopted for each of them. The recent trend has increased the focus on physically based models, which extends their application to a wider range of strains [20]. However, the empirical approach is often preferred as it produces simpler equations and, although they are not derived from first principles, they are consistent with the laws of physics. Dimensional analysis is one way to obtain phenomenological equations. Physically based models can also be addressed in different ways [21]:

- A microscopic approach describing the mechanics of deformation at the molecular or crystalline level, in which macroscopic behaviour results from integrating or averaging microscopic variables over a volume element;
- A thermodynamic approach that assumes a homogeneous continuum equivalent to the real material and represents the microscopic physical phenomena by means of macroscopic internal variables [22].

A considerable number of constitutive models are available, many of them having been implemented in computer codes. It is important to remember that the material dynamic behaviour at high strain rates is affected by the microstructural evolution during deformation, which is not considered in

phenomenological models. This is one reason why physically based models are preferred in some situations.

Another way of categorising constitutive equations [23] considers the main loading mechanism: high-pressure loading, where the dominant effect is the shock wave high pressure such as is observed in pressure-shear plate impact tests; or the regular-pressure type which does not include the pressure as a state variable and is observed in one-dimensional-stress experiments like Split Hopkinson Pressure Bar (SHPB) tests. In the second case deviatoric stresses will induce different microstructural responses than those induced by pressure [7]. The available constitutive models for these high-pressure regimes will be referred to in what follows, as reviewed by Remington [2]. The regular-pressure models can be reviewed in the works of Chaboche [3] and Lin and Chen [24].

Before addressing strain rate dependent models, it is relevant to cite classic constitutive models that describe flow stress changes depending on the deformation conditions, such as temperature and strain rate. These models do not usually consider deformation history but are accurate for cases where strain hardening is the dominant factor. The following well-known equations are part of this group [25]:

The Hollomon equation: $\sigma_p = C\varepsilon^n$ (17)

The Ludwick equation: $\sigma_p = \sigma_{po} + C\varepsilon^n$ (18)

The Voce equations: $\sigma_p = \sigma_{ps} - \left(\sigma_{ps} - \sigma_{po}\right)^{-n\varepsilon}$ (19)

There are many other equations but none has proven to be satisfactory for all materials and deformation conditions [25]. For higher strain rates the exponential forms such as Voce equation, are more suitable. Other models have been developed such as:

Fields and Backofen equation: $\sigma_p = C\varepsilon^n\dot{\varepsilon}^m$ (20)

The Hart equation: $\sigma_p = \sigma_p^* \exp\left[\left(-\frac{\dot{\varepsilon}^*}{\dot{\varepsilon}}\right)^{\lambda}\right] + \sigma_0(\dot{\varepsilon})^{\frac{1}{M}}$ (21)

where the first term describes thermally activated plastic flow and the second describes dislocation slip.

The Wagoner equation: $\sigma_p = C(\varepsilon + \varepsilon_0)^n \left(\frac{\dot{\varepsilon}}{\dot{\varepsilon}_0}\right)^m$ (22)

Another group of equations that include the effect of temperature may assume the following forms, where the most significant difference is the way temperature depends on strain and strain rate [25]:

$\sigma_p = C\varepsilon^n \exp(n_1\varepsilon)\, \dot{\varepsilon}^m \exp(a_1 T)$ (23)

$\sigma_p = C\varepsilon^n \exp(n_1\varepsilon)\, \dot{\varepsilon}^{(m+bT)} \exp(a_1 T)$ (24)

$\sigma_p = C\varepsilon^{(n+b_2 T)} \exp(n_1\varepsilon)\, \dot{\varepsilon}^{(m+bT)} \exp(a_1 T)$ (25)

$\sigma_p = C\varepsilon^n \exp\left(\frac{n_1\varepsilon}{\varepsilon_m}\right) \dot{\varepsilon}^{(m+b/T)} \exp(a_1 T)$ (26)

A few variations on the equations above can also be used, where the forms of the exponents have been slightly modified. In the above equations the indices for the stress symbol σ, are: p for flow stress, p_0 for yield point, p_m for the flow stress at the ultimate tensile strength and p_s for saturation stress. σ_p^* and $\dot{\varepsilon}^*$ are the current states of stress and strain rate, respectively. The indices n and n_1 are the strain hardening coefficients, m is the strain rate sensitivity, ε_o is the pre-strain, ε_m is the critical strain and C, M, λ, a, a_1, b and b_1 are experimentally determined material parameters.

Zener and Hollomon considered a modification for the effect of temperature on the strain rate, proposing the following term:

$\sigma_p = f\left[\dot{\varepsilon} \exp\left(\frac{Q}{RT}\right)\right] = f(Z)$ (27)

where Q is the activation energy and Z is the Zener-Hollomon parameter [25]. A number of variations have been developed by several authors, which include Z type parameters, as will be shown below. Classical approaches are good starting points for more recent constitutive models but will not be covered.

They normally follow Duvaut, Lion and Perzyna formulations [13, 26]. As an example [27] used the Fields – Backhofen equation to investigate the mechanical behaviour of AZ31 magnesium alloy sheets but considered low strain rates, which excludes their work from this review.

4. Physically based constitutive equations

Early work is well described in a review from Armstrong and Walley [5] presenting some pioneering results on attempts to relate strain rate and viscoplastic behaviour. The introduction of the dislocation concept is very well documented. This idea was developed by Taylor [28, 29] and other authors in the 1930s. More recent work, particularly from the last three or four decades, has benefited from the rapid increase in the processing capacity of computers that has been translated into more sophistication of the numerical models available.

From this group of more recent work one interesting attempt to obtain a physically based model was published by Read and co-workers [8] who developed a rate-dependent physically based constitutive model for polycrystalline metals. They assumed that most of the plastic flow at a point was due to slip along planes on which the resolved shear stress has its maximum value. Plastic strain was assumed to depend on the density of mobile dislocations, N_m, by the following expression:

$$\dot{\varepsilon}_p = \frac{4}{3} b N_m v \tag{28}$$

where b is the Burgers vector and v is the mean velocity of the mobile dislocations. Expressions were developed for each of the terms of the equations above to construct the constitutive equation [8]. considered that the applied stress could be decomposed into a thermally activated component τ^*, a viscous drag component τ_D, and an athermal component τ_μ. Combining the expressions for Eq. (1) and those for the stresses, the constitutive equation they obtained becomes

$$\dot{\varepsilon}_p = \frac{4}{3} \frac{b u_g [N_{m\infty} + (N_{m0} - N_{m\infty} + M_1 \varepsilon_p^2) \exp(-A_1 \varepsilon_p)]}{1 + \beta |u_g| \exp\left(-\frac{v^* \tau^*}{kT}\right)} \tag{29}$$

where u_g is the glide velocity (function of the viscous drag stress), N_m is the mobile dislocation density in which subscript "0" refers to its initial value and subscript "∞" refers to the saturation value of the mobile dislocation density. M_1 and A are a coefficient and an annihilation factor, respectively, and k is the

Boltzman constant. v^* is an activation volume, T is assumed to be a fixed temperature and β is a function of temperature, activation energy and vibration frequency. It is possible to simplify the equation neglecting the thermally activation stress, which may be adopted for metals in which thermal activation is not a major player at a given temperature. In that case:

$$\dot{\varepsilon}_p = \frac{4}{3}\frac{bu_g[N_{m\infty}+(N_{m0}-N_{m\infty}+M_1\varepsilon_p^2)\exp(-A_1\varepsilon_p)]}{\sqrt{1+\frac{\phi^2}{C_s^2}}} \quad (30)$$

where ϕ is a function of the viscous drag stress and C_s is a coefficient to be determined. Read and co-workers [8] tested the model for 6061-T6 aluminium alloy to assess the effectiveness of the model in considering hardening, thermal activation, Bauschinger effect, viscous drag, dislocation multiplication and annihilation and the limiting dislocation velocity (relativistic effect). Their model is limited to isotropic behaviour and considerable simplifications were introduced due to the lack of knowledge at the time.

Evidence of the importance of the strain rate effect has been studied by many researchers together with the combined effect with temperature history effects [9]. The first relationship found was described by a thermally activation process and the second resulted from an evolutionary process, in which the structure changes during plastic deformation.

4.1. Bodner and Partom (BP)

Bodner and Partom [30] developed an elastic-viscoplastic equation for large deformation analysis considering the effects of strain hardening and viscosity and has been used with success in many applications. Results published in the original work were obtained for very small strain rates of the order 10^{-3} to 10^{-5} s^{-1} but in a more recent application much higher strain rates were investigated. The model is based on the separation of the total deformation rate into an elastic and a plastic component during the deformation process, that is,

$$d_{ij} = d_{ij}^e + d_{ij}^p \quad (31)$$

where d_{ij} is the symmetric part of the velocity gradient and the elastic component of the deformation rate is related to Cauchy stress rate tensor by Hooke's generalised law [31]

$$d_{ij}^{e} = \frac{\dot{t}_{ij}}{G} - \frac{\lambda \dot{t}_{kk}\delta_{ij}}{2G(3\lambda+2G)} \tag{32}$$

in which G is the elastic shear modulus and λ is a Lamé constant. The plastic deformation rate d_{ij}^{p} can be related to the deviatoric part of the Cauchy stress tensor s_{ij}

$$d_{ij}^{p} = \gamma s_{ij} \tag{33}$$

where γ is a material parameter. When this equation is squared we obtain $\gamma^2 = D_2^p/J_2$ or $D_2^p = f(J_2)$, where D_2^p is the second invariant of the plastic deformation rate, J_2 is the second invariant of the Cauchy deviatoric tensor and f is a function of J_2. Bodner and Partom [30] deemed appropriate to consider the particular form of that function

$$D_2^p = D_0^2 \exp\left[-\left(\frac{n+1}{n}\right)\left(\frac{Z^2}{3J_2}\right)^n\right] \tag{34}$$

where D_o is the maximum strain rate and Z is an internal variable. The strain rate sensitivity is governed by the parameter n. Z is assumed to be a function of the plastic work

$$Z = Z_1 + (Z_0 - Z_1)\exp\left(-m\frac{W_p}{Z_0}\right) \tag{35}$$

The original Bodner and Partom (BP) model for uniaxial stress is

$$\dot{\varepsilon}_x^p = \frac{2D_0}{\sqrt{3}}\frac{\sigma}{|\sigma|}\exp\left[-\frac{1}{2}\left(\frac{3A^2}{\sigma^2}\right)^n\right] \tag{36}$$

$$A^2 = \frac{1}{3}(Z^2)\sqrt{\frac{n+1}{n}} \tag{37}$$

where $\dot{\varepsilon}_x^p$ and W_p are the plastic strain rate and plastic work, respectively, and D_0, n, m, Z_0 (initial value) and Z_1 (saturation value) are material constants.

The interest of the BP model rests on its solid physical foundation [32] and has been widely used although it is not very sensitive to the strain rate and it does not consider temperature effects. An example of its application to high-speed impact of a projectile was proposed by Song [33]. Results obtained with this constitutive model are shown in Fig. 5 for aluminium deformed at two values of strain rate of the order of 10^3 s^{-1}.

A modification to the BP model was later introduced, consisting of an explicit introduction of thermal softening effect [32] to study the behaviour of 30CrMnSiA steel after a high rate heating. The thermal softening effect introduced by Chen consisted in a modification of Eq. (37):

$$A^2 = \frac{1}{3}\left[Z\exp\left(C_1 T'^{n1}\right)\right]^n \sqrt{\frac{n+1}{n}} \tag{39}$$

where C_1 and n_1 are more material constants and the non-dimensional temperature

$$T' = \frac{T - T_0}{T_{\text{melt}} - T_0}$$

with T_0 referring to room temperature and T_{melt} being the melting temperature. Z depends on the deformation history of the material and relates to the dislocation density while n relates to dislocation velocity. Results for 30CrMnSiA showing the softening effect of increasing the temperature above 200 K obtained with the BP and other constitutive equations are presented in Fig. 6.

4.2. Steinberg-Guinan (SG)

Due to their simplicity, elastic-perfectly plastic constitutive models were implemented early on in most hydrocodes but the need to account for work hardening was soon recognised [34] and some modifications that took account of this phenomenon were developed and implemented. Shear modulus G and yield stress Y also increase with increasing pressure and decrease with increasing temperature and a constitutive model has been developed to take account of this [35]. The authors admitted that an unbounded growth of the flow stress with increasing strain rate was unreasonable and a limit was found for strain rates close to 10^5 s^{-1}. They stated that this was due to the increase in temperature with increasing stress. The temperature effect together with the strain rate effect were combined into the Steinberg-Guinan (SG) constitutive model, relating these state variables to the shear modulus G and yield strength Y. In this equation the yield strength is expressed as a first-order Taylor expansion in pressure and temperature about the ambient state, that is,

$$G = G_0\left[1 + \left(\frac{G'_p}{G_0}\right)\frac{P}{\eta^{\frac{1}{3}}} + \left(\frac{G'_T}{G_0}\right)(T - 300)\right] \tag{40}$$

$$Y = Y_0[1 + \beta(\varepsilon + \varepsilon_1)]^n \left[1 + \left(\frac{Y_P'}{Y_0}\right)\frac{P}{\eta^{\frac{1}{3}}} + \left(\frac{G_T'}{G_0}\right)(T - 300)\right] \quad (41)$$

subject to the constraint that $Y_0[1 + \beta(\varepsilon + \varepsilon_1)]^n \leq Y_{\max}$. β and n are work-hardening parameters, ε_i is the initial plastic strain (usually zero), the subscript $_0$ refers to the reference state ($T = 300$ K, $P = 0,\ \varepsilon = 0$), primed parameters mean their derivatives at the reference state, with respect to either P or T, shown using appropriate subscripts. Note that the model includes semi-terms such as the work hardening term, $[1 + \beta(\varepsilon + \varepsilon_1)]^n$ which fits data for a wide number of metals at high strain-rates, namely the results of Wilkins and Guinan [34], who determined the yield strength of a number of materials through computer simulation of cylinder deceleration experiments at high strain rate regimes (10^5 s^{-1} on average). The effects of the state variables P, T and ε (pressure, temperature and strain) on Y and G has been checked for impact experiments with 6061-T6 Al alloy (results shown in Fig. 7), along with the data that resulted from adding, step-by-step, the effects of those parameters on the constitutive equations. The results for the induced wave profiles show the differences in the arrival times of both the calculated and the measured waves from which the pressure and temperature dependencies of the shear modulus can be examined. The effects of these parameters on yield stress were also shown to be much stronger than work-hardening.

However, the saturation of microstructural processes above a critical strain rate (10^5 s^{-1}) and the rate-independent plastic deformation above this critical strain rate gives a good description of metal plastic response behind the shock front but not at the shock front. The SG model remains one of the few constitutive equations used for strain rates around 10^5 s^{-1}.

4.3. Steinberg and Lund (SL)

This is an extension of the Steinberg-Guinan [35] constitutive model to extend its regime of validity to strain rates as low as 10^{-4} s^{-1}. The form used is based on the work of Hoge and Mukherjee [36]. This modified model is simpler, has fewer coefficients and is more stable when running in hydrocodes. The increase in the range of applicability was achieved by splitting the yield strength into its thermal and athermal components where the former is a function of strain rate and temperature. The equation of Hoge and Mukherjee (1977) [36] was used for the thermal part of the constitutive model but any other

expression for plastic strain rate as a function of yield stress and temperature could have been used [37]. The equation is as follows:

$$\dot{\varepsilon}_p = \frac{1}{C_1} \exp\left[\frac{2U_k}{KT}\left(1 - \frac{\sigma_t}{\sigma_p}\right)^2\right] + \frac{C_2}{\sigma_t} \tag{42}$$

where σ_p is the Peierls stress, $2U_k$ is the energy necessary to form a pair of kinks in a dislocation segment of length L and K is the Boltzmann constant. $C_2 = D/\rho b^2$ where D is the drag coefficient, ρ is the dislocation density and b is the Burgers vector. Additionally,

$$C_1 = \frac{\rho L a b^2 v}{2} w^2 \tag{43}$$

where a is the distance between Peierls valleys, w is the width of a kink loop and v is the Debye frequency. σ_t is the thermally activated component of the yield stress. The method is applied to a wide range of strain rates, from 10^{-4} to 10^6 s^{-1}, which makes it suitable for shock-induced phenomena representation. Results for a shocked tantalum target are shown in Fig. 8, where excellent agreement between experimental and calculated data is evident although at such a high stress level the model loses sensitivity. The method seems to be applicable to crystalline structures other than BCC, although the only published data corresponds to tantalum, a BCC material

4.4. Zerilli and Armstrong (ZA)

Zerilli and Armstrong [38] developed a constitutive relation based on dislocation mechanics and incorporating the effect of strain hardening, strain-rate hardening and grain size. They also wanted to include in constitutive models the different behaviour of materials due to their crystalline structures as they observed different dislocation interactions for FCC and BCC metals. The dislocations must overcome barriers of forest dislocations. To overcome those barriers, a certain thermal activation energy is necessary which decreases with plastic strain due to the increase in dislocation density. Therefore, the flow stress is divided into a thermal and an athermal component, $\sigma = \sigma_a + \sigma_{th}$. The thermal flow stress is given as

$$\sigma_{th} = \frac{M \Delta G_0}{Ab} e^{-\beta T} \tag{44}$$

$$\beta = -C_3 + C_4 \ln \dot{\varepsilon} \tag{45}$$

where M is a direction factor, ΔG_o is the free energy of thermal activation at 0 K, A is the activation area, b is the Burgers vector and β is a parameter associated with strain and strain rate [24].

For BCC metals dislocations must overcome Peierls-Nabarro barriers, thermal activation does not depend on strain and *A* is constant. As mentioned above, yield stress in FCC metals is determined by strain hardening and that of BCC metals is determined by strain rate hardening and thermal softening. Therefore *A* is not constant but instead proportional to $\varepsilon^{-1/2}$. Based on such considerations, the Zerilli-Armstrong (ZA) model has been developed with two formulations, one for FCC and another for BCC metals. The expression for FCC is within the scope of this review and is

$$\sigma = \sigma_a + C_2 \varepsilon^{\frac{1}{2}} \exp(-C_3 T + C_4 T \ln \dot{\varepsilon}) + k l^{-\frac{1}{2}} \tag{46}$$

where σ is the von Mises equivalent stress, σ_a is an athermal component of stress that considers the contribution of the initial dislocation density for the yield stress. C_i are parameters to be determined experimentally. The last term brings in the effect of grain diameter l and of a micro-structural stress intensity factor k.

The model assumes independency between work-hardening rate, temperature and strain rate increase which is true for most metals but will not accurately model materials that exhibit that type of dependency. It is also observed that the parameters of the model should not be used as constants as this will reduce the accuracy of predictions. Zhang et al. (2009) [39] proposed a modification to the ZA method by considering the integrated effects of the temperature, strain-rate and deformation history on the flow behaviour of alloy IC10. For FCC materials the modified expression is [39]

$$\sigma = C_0 + C_2 \varepsilon^{\frac{1}{2}} \exp\left[\left(-C_3'' T + C_4' T \ln\left(\frac{\dot{\varepsilon}}{r(\varepsilon) r(\dot{\varepsilon})}\right)\right) f(T)\right] \tag{47}$$

where the dislocation density $r(\varepsilon) = \rho_o + M\varepsilon$ increases linearly with the plastic strain. In this expression M is a material constant relative to the increasing rate of dislocation density and ρ_o is the initial dislocation density. Parameters C_i, C_3' and C_4'' of the modified ZA equation are material constants. Expressions for $f(T)$ and $r(\dot{\varepsilon})$ are given by Zhang et al. (2009) [39]. The results from the modified ZA

model fit better than those from the original model. However, the use of these modifications is limited as they are particular to certain materials. Other modified versions of the ZA model were derived to improve the fitting of predictions with data from experiments with materials such as alloy D9 [40], a titanium-modified austenitic stainless steel or S15C, S50C and SKS93 carbon steels [41]. More general modifications have been derived [42, 43, 44] to correct some inaccuracies found in results obtained with the method. Reference will be made below to the method of Gao and Zhang (2010) [44] that may be generalized to FCC metals and show good results for strain rates up to 10^4 s^{-1}. The modified expression is

$$\sigma = \hat{\sigma}_a + \hat{Y}\varepsilon^n \exp\left[C_3 T \ln\left(\frac{\dot{\varepsilon}}{\dot{\varepsilon}_{so}}\right)\right]\left\{1 - \left[-C_4 T \ln\left(\frac{\dot{\varepsilon}}{\dot{\varepsilon}_o}\right)\right]^{\frac{1}{q}}\right\}^{\frac{1}{p}} \tag{48}$$

where $\hat{Y} = \lambda\hat{\sigma}_{so}$ is the actual reference thermal stress, $\hat{\sigma}_{so}$ is the reference saturated threshold stress, $\hat{\sigma}_a$ is the athermal stress, λ and n are material constants and p and q are parameters representing the shape of potential barriers. $C_3 = k/g_{so}\mu b^3$ and $C_4 = k/g_o\mu b^3$ are also material constants. Fig. 9 shows results predicted with the modified equation for OFHC copper.

4.4. Mecking and Kocks (MK)

This is a single internal variable model suitable for high strain rate viscoplastic response of metals (in the range 10^2-10^4 s^{-1}) based on total dislocation density. Mechanical properties (i.e. the flow stress) depend on current metallurgical structure and this structure evolves with strain. Dislocation density is generally used as the parameter that relates the metallurgical structure with strain. The model considers that the flow stress is related to the dislocation density by means of a multiplicative combination of two terms, one being a rate sensitive term dependent on thermal activation and the other a structure sensitive term [43] representing the flow stress at zero temperature $\hat{\sigma}$:

$$\sigma = s(\dot{\varepsilon}, T)\hat{\alpha}\mu b\sqrt{\rho} \tag{49}$$

This relation was shown to be valid for small strains at all temperatures or to apply to a finite range of strain at low temperatures. This behaviour breaks down as strain hardening becomes rate sensitive as dynamic recovery increases. To relate the described relation with dynamic recovery the s function has been redefined as

$$s = \left(\frac{\dot{\varepsilon}}{\dot{\varepsilon_0}}\right)^{1/m} \exp\left(-F\frac{\theta_r}{\theta_h}\right) \quad (50)$$

and

$$s = \left(\frac{\dot{\varepsilon}}{\dot{\varepsilon_0}}\right)^{\frac{1}{m}} \left(1 - F\frac{\theta_r}{\theta_h}\right) \quad (51)$$

where F is an adjustable parameter that decreases from 1 as dynamic recovery increases, θ_r is an athermal hardening rate and θ_h is a normalization factor. Flow stress is then given as the product of a strain only dependent stress $\hat{\sigma}$ and which depends on strain rate and temperature, with the given s function. Above the mentioned strain rate range the dislocation evolution and stress-strain behavior will follow different patterns. In FCC metals it has been observed that flow stress increases disproportionally when strain rate exceeds the 10^3-10^4 s^{-1} range [45].

4.5. Mechanical Threshold Stress (MTS)

The work of Kocks [45] is very important as it was the precursor of the MTS method.Experimental results have shown that strain rate sensitivity change at constant strain must be due to a change in the structure evolution of the metal [17]. It was observed that a representative state variable for such an internal microstructure state could be the mechanical threshold stress, i.e. the flow stress measured at 0 K. Follansbee et al. found that this stress is a function of the strain rate at constant strain, meaning that structural evolution is rate dependent. This led to the formulation of a constitutive model based on state variables that describe the current state of the material. This model, the Mechanical Threshold Stress (MTS) model, uses strain, strain rate and temperature to define the yield stress of a material at a specific internal state. The model evolved from previous work [45], extending their range of application to the high strain rate regime. The equations that describe the model are

$$\sigma = \hat{\sigma}_a + (\hat{\sigma} - \hat{\sigma}_a)\left\{1 - \left[\frac{KT\ln\left(\dot{\varepsilon}_0/\dot{\varepsilon}\right)}{g_0\mu b^3}\right]^{\frac{1}{q}}\right\}^{\frac{1}{p}} \quad (52)$$

where σ is the flow stress, which is a function of the mechanical threshold stress $\hat{\sigma}$, the athermal stress $\hat{\sigma}_a$ (a parameter to be found). K is the Boltzmann constant, μ is the shear modulus (temperature dependent), b is the Burgers vector, g_0 is the total activation energy, p and q are constants, as well as $\dot{\varepsilon}_o$ which is a reference strain rate. Voce behaviour has been considered and then the state variable $\hat{\sigma}$ can be determined through a strain-hardening rate

$$\theta = \frac{\mathrm{d}\hat{\sigma}}{\mathrm{d}\varepsilon} = \theta_0 \left[1 - \left(\frac{\hat{\sigma}-\hat{\sigma}_a}{\hat{\sigma}_s-\hat{\sigma}_a}\right)\right] \tag{53}$$

where $\hat{\sigma}_s$ is the saturation stress or the stress at zero strain hardening rate (temperature and strain rate dependent) and θ_0 is the hardening due to dislocation accumulation. Together with the equation

$$\ln\left(\frac{\dot{\varepsilon}}{\dot{\varepsilon}_{so}}\right) = \frac{\mu b^3 A}{KT} \ln\left(\frac{\hat{\sigma}_s}{\hat{\sigma}_{so}}\right) \tag{54}$$

where $\dot{\varepsilon}_{so}$, A and $\dot{\sigma}_{so}$ are constants. $\dot{\sigma}_{so}$ is the saturation threshold stress for deformation at 0 K, these two expressions allow the evolution of the state variable mechanical threshold stress to be determined. The MTS model accounts for the influence on flow stress of the strain, strain rate and temperature histories, but requires a large number of experiments to determine the material parameters necessary to calibrate the equation, rendering it difficult to use. The method attempts to correctly predict the flow stress behaviour in the high strain rate regime (above 10^3-10^4 s^{-1}).

Other authors have attempted to describe strain and strain rate history effects in FCC metals at high strain rates. Klepaczko proposed a model based on dislocation density and considered a strain rate dependence on dislocation accumulation. The model was revised later by Klepaczko and Chiem based on dislocation accumulation and recovery effects (Klepaczko JR, 1975. Mat Science Engng, 18: 121 and Klepaczko JR and Chiem CY, 1986, J. Mech. Phys. Solids, 34: 29 both cited by Follansbee and Kocks [17]). The citation adds that the Klepaczko-Chiem model has never been used for rates above 10^3 s^{-1}, which makes it less interesting for this review.

Dorward and Hasse reported that flow stresses of aluminium alloys are independent of strain rates below 10^3 s^{-1}. These authors used the following constitutive equation [46]

$$\sigma = \sigma_0 \varepsilon^n \dot{\varepsilon}^m (1 - \beta \Delta T) \tag{55}$$

to perform a number of analysis. However, the range of strain rates was, in general, below 10^3 s^{-1}. Their conclusions are in line with other authors as they report an increase in the flow stress above that value of strain rate.

Zhao and Gary (1995) [47] derived a constitutive model suitable for car crash test simulation. Based on dynamic and quasi-static experiments a phenomenological model has been derived [47] for strain rates from 10^{-4} to 10^4 s^{-1}. The authors examined Johnson and Cook (JC) (which will be discussed under section 5), ZA and SG empirical equations but adopted a Ludwig-type expression in which the coefficients depend on strain rate:

$$\sigma = \left[A(\dot{\varepsilon}) + B(\dot{\varepsilon})\varepsilon_p^{n(\dot{\varepsilon})}\right](1 - \mu\Delta T) \tag{56}$$

with

$$A = a_1 + a_2 \log\left(\frac{\dot{\varepsilon}}{\dot{\varepsilon}_o}\right) + a_3 \left[\log\left(\frac{\dot{\varepsilon}}{\dot{\varepsilon}_o}\right)\right]^3; \quad B = b_1 - b_2 \log\left(\frac{\dot{\varepsilon}}{\dot{\varepsilon}_o}\right) + b_3 \left[\log\left(\frac{\dot{\varepsilon}}{\dot{\varepsilon}_o}\right)\right]^{0.5} \tag{57}$$

and

$$n = n_1 + n_2 \log\left(\frac{\dot{\varepsilon}}{\dot{\varepsilon}_o}\right) + n_3 \left[\log\left(\frac{\dot{\varepsilon}}{\dot{\varepsilon}_o}\right)\right]^3 \tag{58}$$

where σ, ε_p and $\dot{\varepsilon}$ are stress, plastic strain and strain rate, respectively, ΔT is the temperature increment in respect to room temperature (23℃) and a_i, b_i, n_i, μ, $\dot{\varepsilon}_o$ are constants to be determined. μ is a thermal softening coefficient to be determined assuming adiabatic conditions during deformation. Good agreement with experimental data was achieved with this model within the range 10^{-4} to 10^4 s^{-1} for steel sheets.

Banerjee [48] compared results from the MTS and JC models for the response of AISI 4340 steel under blast loading. This author concluded that both models give similar results but the JC model is numerically more efficient and is better suited for large numerical simulations. Results for the deformation of copper obtained with the MTS model, Eq. (4), are presented in Fig. 10.

4.6. Nemat-Nasser and Li (NNL)

A dislocation physically based constitutive model has been proposed by Nemat-Nasser [14] to calculate finite deformations of FCC polycrystals. These authors had previously derived a phenomenological model [49] for single FCC crystals considering the history of the deformation divided into three regimes depending on the number of active slip systems. The authors followed previous work for BCC and FCC metals [49, 50, 51].

A computer implementation using a plastic-predictor and an elastic-corrector was used in that formulation. The underlying physical model of inelastic response of metals based on dislocation motion and accumulation considers thermal activation and dislocation drag has a significant degree of complexity and is not easily mathematically modelled for implementation in computer codes. In many cases simplifying assumptions have to be adopted to make models more tractable. Nemat-Nasser and Li [14] expressed plastic strain rate $\dot{\gamma}$ in the classic way, as a function of the dislocation density, velocity and Burgers vector b, then using a power law to derive the final form of the constitutive equation. An empirical relation was used for the average dislocation spacing and the resulting equation is

$$\tau(\dot{\gamma},\gamma,T)=\tau^{o}\left\{1-\left[-\frac{KT}{G_0}\left(\ln\frac{\dot{\gamma}}{\dot{\gamma}_0}+\ln\left(1+a(T)\gamma^{\frac{1}{2}}\right)\right)\right]^{\frac{1}{2}}\right\}^{\frac{3}{2}}\left[1+a(T)\gamma^{\frac{1}{2}}\right]+\tau_a^{o}\gamma^{n_1} \tag{59}$$

$$\tau^{o}=\frac{G_0}{b\lambda l_0},\quad \dot{\gamma}_0=b\rho_m\omega_0 l_0,\quad a(T)=a_0\left[1-\left({}^{T}/_{T_m}\right)^{2}\right] \tag{60a, b, c}$$

where the variables have their usual meaning. $a(T)$ and n_1 are experimentally derived parameters. K is obtained empirically and $G_o=\hat{\tau}b\lambda l$, where $\hat{\tau}$ is the thermal stress for zero absolute temperature and λ, l_o are the average barrier width and the initial dislocation spacing associated with an initial temperature, respectively. The superscripts "o" in the above equations indicate initial values. For instance τ_a^o is the initial value for the athermal part of the resistance to the motion of dislocations. This method differs from others because it is iterative rather than a closed form solution. In Fig. 11 material responses (stress-strain) are shown for a number of strain rates and temperatures.

Another physical constitutive model was developed under the same framework suggested by Nemat-Nasser and Li (1998) for 3003 Al-Mn alloy [52]. The equation is not of general use as it is calibrated for that particular alloy. It will not be mentioned further because of its very particular application.

Fig. 11 shows results obtained with the NNL constitutive model. Fig. 12 shows an application of the method to FCC metals comparing results with experimental data gathered in the work of Nemat-Nasser and Li [14]. Fig. 12 shows calculated and measured material responses for polycrystalline annealed OFHC copper at strain rates of 8000, 0.1 and 0.001 s^{-1} A remarkably good correlation with the experimental results has been obtained [53]. The modified model has been successfully used to model the dynamic response of molybdenum [54] and titanium [55]. The modified expression is given by

$$\tau = \tau^o \left\{1 - \left[-\frac{KT}{G_0}\left(\ln\frac{\dot{\gamma}}{\dot{\gamma}_0} + \ln\left(1+\alpha(T)\gamma^{\frac{1}{2}}\right)\right)\right]^{\frac{1}{2}}\right\}\left[1+\alpha(T)\gamma^{\frac{1}{2}}\right] + \tau_a^o \gamma^{n_1} \tag{61}$$

$$\tau_0 = \frac{G_0}{b\lambda l_0} \tag{62}$$

where the parameters have the usual meanings.

4.7. Other constitutive models

As we have seen above several approaches have been followed for the prediction of flow stress in the high strain regime. such approaches has been the consideration of phonon drag effects [56]. Based on experimental uniaxial compression test results on AL-6XN austenitic stainless steel Nemat-Nasser, Guo and Kihil developed a physically based model that considers also the viscous-drag effect. The tests were performed between 10^{-3} and 8000 s^{-1} and at temperatures ranging from 77 to 1000 K. Plastic flow stress of this alloy was shown to depend on the temperature, the strain-rate and their histories. At low strain rates dynamic strain-aging occurs at the range of temperatures 500 to 1000 K peaking at 800 K. Dislocation motion faced viscous-drag resistance at a range of strain-rates and the microstructure of this material evolved mainly with the temperature history. Thus the constitutive equations were developed to include all these effects following previous work [14, 50, 54, 55] on several polycrystalline metals. The model assumes a thermal and an athermal part of the resistance to dislocation motion, the main deformation mechanism considered. The flow stress, τ, is considered to be divided into three components: one due to short-range thermally activated effect which may include the Peierls stress and point defects, designated as τ^*; the second part is the athermal component τ_a, due to long-range effects such as the stress field of dislocation forests and grain boundaries; and the third part is the viscous-drag

component, τ_d. The flow stress will be a function of strain rate $\dot{\gamma}$, temperature, T, and some microstructural parameters such as the distribution of the density of dislocations, ρ. Then,

$$\tau = \tau_a + \tau_d + \tau^* \tag{63}$$

The viscous-drag stress depends on the dislocation motion which average velocity, v is related with the strain rate $\dot{\gamma}$ by $\dot{\gamma} = \rho_m b v / M$, where ρ_m is the mobile dislocation density, and b and M are the magnitude of Burgers vector and the Taylor factor respectively. Using these relations

$$\tau_d = m_0[1 - \exp(-\alpha\dot{\gamma})] \tag{64}$$

$$\alpha = \frac{M^2 B}{\rho_m b^2 \tau_y} \tag{65}$$

where m_0 is a material constant measured directly measured at a very high-strain rate and α represents an effective damping of the dislocation motion.

The thermally activated component of the flow stress depends on temperature, T, strain rate, $\dot{\gamma}$, and an internal variable characterising the microstructure of the material. The average dislocation density ρ has been considered the dominant microstructural parameter. A relation between τ^*, T and $\dot{\gamma}$ can be obtained using the concept of activation free energy ΔG, Eq. (11), and a final expression for τ^* has been defined as,

$$\tau^* = \tau^0 \left\{1 - \left[-\frac{KT}{G_0}\ln\left(\frac{\dot{\gamma} f(\gamma,T)}{\dot{\gamma}}\right)\right]^{\frac{1}{q}}\right\}^{\frac{1}{p}} f(\gamma,T) \quad \text{for } T \le T_c \tag{66}$$

$$\tau^0 = \frac{G_0}{b\lambda l_0} \tag{67}$$

$$\dot{\gamma_0} = b\rho_m \omega_0 l_0 \tag{68}$$

$$f(\gamma,T) = 1 + a\left[1 - \left(\frac{T}{T_m}\right)^2\right]\gamma^m \tag{69}$$

where

$$T_c = -\frac{G_0}{K}\left[\ln\left(\frac{\dot{\gamma} F(\gamma,T_c)}{\dot{\gamma}_0}\right)\right]^{-1} \tag{70}$$

In these equations the parameters p and q define the profile of the short-range energy barrier, T_m is the melting temperature, the index m is a free parameter to be obtained from experimental data, l_0 is an initial average dislocation spacing, K is the Boltzmann constant, λ is the average effective barrier width, a is a free parameter and $\omega_0$is the attempt frequency of barrier overcoming. Results from the use of this constitutive model for the AL-6XN stainless steel are shown below in Fig. 13.

Preston et al. [6] also developed a physically based model suitable for explosive loading and high-speed impacts. It has been applied to strain rates from 10^{-3} to 10^{12} s^{-1} which makes it one of the few that can cope with hypervelocity phenomena. It is known that for high stresses the Arrhenius form for the strain rate, which is the basis of many constitutive equations, becomes less accurate as thermal activation mechanisms cease to be dominant and dislocation drag predominates. Their model is based on the same mechanisms as for the hybrid SL models, such as thermal activation for shear stresses lower than the dominant dislocation barriers and a viscous drag mechanism for shear stresses greater than the barriers [2]. At strain rates of up to 10^4 s^{-1} the model is calibrated using conventional data obtained from Hopkinson bar experiments. For higher strain rates the model includes formulations that reproduce overdriven shock[†] waves with strain assumed to have a power law dependence on strain rates, represented by an Arrhenius form. Alternatively, data can be extrapolated from strength curves between the two limiting regimes (the low end thermal activation and the high end nonlinear viscous drag). The equations that describe the model are as shown below in their simpler form for the lower strain rate regimes:

$$\hat{\tau} = \hat{\tau}_s + \frac{1}{p}\left(s_0 - \hat{\tau}_y\right)\ln\left\{1 - \left[1 - \exp\left(-p\frac{\hat{\tau}_s - \hat{\tau}_y}{s_0 - \hat{\tau}_y}\right)\right]\exp\left[-p\theta\psi\left[\left(s_0 - \hat{\tau}_y\right)\left[\exp\left(p\frac{\hat{\tau}_s - \hat{\tau}_y}{s_0 - \hat{\tau}_y}\right) - 1\right]\right]^{-1}\right]\right\} \quad (71)$$

For shock regimes a function of the type $\hat{\tau} = \hat{\tau}_s G(p,T)$ has to be used, where $\hat{\tau}_s$ is a normalised work-hardening saturation stress. The flow stress normalisation has been performed assuming a proportionality with shear modulus G: $\hat{\tau} = \tau/G(\rho,T)$ where ρ is the mass density and T is the temperature. Temperature was also scaled on the basis of melting temperature T_m, such that $\hat{T} = T/T_m(\rho)$. The work hardening saturation stress and the yield stress in the thermal activation regime are given by

[†] An overdriven shock wave is one in which the plastic wave has overrun the elastic precursor producing a shock wave front steeper than that, which would result from adiabatic elastic compression

$$\hat{\tau}_s = s_0 - (s_0 - s_\infty)\,\mathrm{erf}\left[K\hat{T}\ln\left(\gamma\dot{\xi}/\dot{\psi}\right)\right] \tag{72}$$

$$\hat{\tau}_y = y_0 - (y_0 - y_\infty)\,\mathrm{erf}\left[K\hat{T}\ln\left(\gamma\dot{\xi}/\dot{\psi}\right)\right] \tag{73}$$

that take the following form of a power law in the overdriven shock regime:

$$\hat{\tau}_s = \hat{\tau}_y = s_0\left(\frac{\dot{\psi}}{\gamma\dot{\xi}}\right)^{\beta} \tag{74}$$

It is worth noting that at these high strain rate regimes work hardening may be neglected as it is probably saturated. In the transition gap between the thermally activated regime and the overdriven shock regime the saturation stress is taken as the greater of the two values given by Eqs. (72) and (73). A similar expression is obtained for the yield stress, to allow for a maximum in the strain-rate sensitivity. It has been shown [57] that a jump in the strain rate sensitivity occurs at about 10^3 s^{-1} exceeding that calculated at strain rates above 10^9 s^{-1}. To allow for such a maximum in the small strain rate sensitivity, Preston and co-workers introduced two additional parameters: y_0 and y_1. The final expression for the yield stress in the transition gap from thermally activated to overdriven shock regimes is then

$$\hat{\tau}_y = \max\left\{y_0 - (y_0 - y_\infty)\,\mathrm{erf}\left[K\hat{T}\ln\left(\frac{\gamma\dot{\xi}}{\dot{\psi}}\right)\right]\min\left[y_1\left(\frac{\dot{\psi}}{\gamma\dot{\xi}}\right)^{y_2}, s_0\left(\frac{\dot{\psi}}{\gamma\dot{\xi}}\right)^{\beta}\right]\right\} \tag{75}$$

where s_o is the value of $\hat{\tau}_s$ at 0 K, s_∞ is the value of $\hat{\tau}_s$ close to the melting temperature, y_o, y_∞ are the values of $\hat{\tau}_y$ at 0 K and close to the melting temperature, respectively. K and γ are material constants. $\dot{\psi} = \dot{\psi}_0\exp[-\Delta\phi(\tau)/K_BT]$ is the plastic strain rate in an Arrhenius form, where the activation energy $\Delta\phi(\tau)$ is a decreasing function of the applied stress and K_BT is the thermal energy. $\dot{\xi}$ is a scaling factor (the time required for a transverse wave to cross an atom) and is used to obtain a normalised strain rate variable, $\dot{\psi}/\dot{\xi}$, where

$$\dot{\xi} = \frac{1}{2}\left(\frac{4\pi\rho}{3M}\right)^{\frac{1}{3}}\sqrt{\frac{G}{\rho}} \tag{76}$$

where M is the atomic mass.. The model has been employed for wider ranges of strain rates and temperatures and obtained good correlation between predictions and experimental data for wide ranges of strain rates and temperatures by modifying the strain-hardening term in the original PTW model using the Voce equation [58].

A new constitutive equation has evolved from the work of Klepaczko JR, [9] that reported the response of polycrystalline FCC metals within the range of strain rates from 10^{-4} to 10^{3} s^{-1} obtained through experiments. This work was the basis for a further development [59] of the model to describe the viscoplastic behaviour of the metal sheet under test. The method considers the addition of an internal stress and an effective stress corresponding to a strain hardening and a thermal activation process, respectively. The thermal stress is given by an Arrhenius relation coupling strain rate and temperature. The corresponding constitutive relation is

$$\sigma = \frac{E(T)}{E_0}\left[B_0\theta_m^{-v}(\varepsilon_0 + \varepsilon^p)^{n_0(1-D_2\theta_n)} + \sigma_0^*(1 - D_1\theta_m)^m\right] \tag{77}$$

In the above equations σ is the shear stress,

$$\theta_m = \frac{T}{T_m}\log\left(\frac{\dot{\varepsilon}_{\max}}{\dot{\varepsilon}^p}\right) \quad \text{and} \quad \theta_n = \frac{T}{T_m}\log\left(\frac{\dot{\varepsilon}^p}{\dot{\varepsilon}_{\min}}\right) \tag{78}$$

are two homologous temperatures modified by the strain rate. The other parameters are the plasticity modulus B_o, the temperature sensitivity v and the hardening coefficient n_o. The effective stress σ_o^* at T = 0 K and D_1 and D_2 are experimentally derived material constants, ε and $\dot{\varepsilon}$ are strain and strain rate and E and E_o are the Young moduli at current and 0 K temperatures, respectively. An upper bound was set for the strain rate $\dot{\varepsilon}_{\max}$ and the minimum strain rate $\dot{\varepsilon}_{\min}$ is reached at a critical temperature. T_m is the melting temperature. The Young modulus also evolves with temperature in accordance with the following expression

$$E(T) = E_0\left\{1 - \frac{T}{T_m}\exp\left[\theta^*\left(1 - \frac{T_m}{T}\right)\right]\right\} \tag{79}$$

where θ^* is the characteristic homologous temperature.

The method was later modified when it was verified that the RK model could not accurately describe certain aspects relating the thermo-viscoplastic behaviour. To improve the method extensions were produced later [60] by adding a third term to the stress σ. The new term, σ_{ns}, is the stress component that accounts for the negative strain rate sensitivity observed in aluminium alloys as the method was improved to study applications of these alloys. A new extension to the RK method has been

presented by Rusinek and co-workers [61], the modified RK model (MRK) where the von Mises stress is decomposed in the following way

$$\bar{\sigma} = \frac{E(T)}{E_0}\left[\bar{\sigma}_{\mu} + \bar{\sigma}^{*}\right] + \bar{\sigma}_{vs} \tag{80}$$

The temperature dependent Young modulus ratio $E(T)/E_o$ defines its evolution with temperature. The internal stress component σ_{μ} is equal to Y, the flow stress of the undeformed material. The effective stress component $\bar{\sigma}^{*}$ is given as

$$\sigma^{*} = \sigma_0^{*}\left[1 - \xi_1\left(\frac{T}{T_m}\right)\log\left(\frac{\dot{\varepsilon}_{\max}}{\dot{\varepsilon}^{p}}\right)\right]^{1/\xi_2} \tag{81}$$

where ξ_1 and ξ_2 are material constants that describe temperature and rate sensitivity of the material and $\dot{\varepsilon}_{max}$ is the maximum strain-rate for a particular material. The viscous-drag component $\bar{\sigma}_{vs}$ is given as a function of the Taylor factor M, the drag coefficient B and the mobile dislocation density ρ_m, b is the Burgers vector and an expression based on experimental data has been proposed [62]

$$\bar{\sigma}_{vs} = \chi[1 - \exp(-\alpha)\,\dot{\bar{\varepsilon}}^{p}] \tag{82}$$

$$\alpha = \left(\frac{M^2 B}{\rho_m b^2 \tau_y}\right) \tag{83}$$

where χ is a material constant, α is an effective damping coefficient affecting the dislocation motion and τ_y is the athermal yield stress. Figs. 14a and 14b show how this model fits experimental results. The MRK model was also used to obtain the temperature sensitivity description of 2024-T3 aluminium alloy [63] in low velocity perforation tests, with good results.

A reference is due to more classical works such as the Hollomon and Voce constitutive models [18] which introduced a multiplicative type phenomenological equation containing three functions

$$\sigma = \sigma(\varepsilon, \dot{\varepsilon}, T) = f(\varepsilon, T)g(\dot{\varepsilon})h(T) \tag{84}$$

Function *f* accounts for the temperature sensitivity of the strain-hardening rate by means of a linear combination of Hollomon and Voce strain hardening equations. This combination showed how the

strain-hardening rate varies with temperature, being lower at higher temperatures. This is a behaviour that is not captured by most existing constitutive models. The proposed function was

$$f(\varepsilon, T) = \alpha(T) f_h + [1 - \alpha(T) f_v] \tag{85a}$$

$$\alpha(T) = \alpha_1 - \alpha_2 (T - T_0) \tag{86b}$$

$$f_h = H\varepsilon^n \tag{87c}$$

$$f_v = V(1 - Ae^{B\varepsilon}) \tag{88d}$$

where T_o is a reference temperature and $\alpha_1, \alpha_2, H, n, B$ are material constants. Function $\alpha(T)$ can reproduce a Voce type curve at high temperatures and a Hollomon type behaviour at lower temperatures or vice-versa, depending on the sign of α_1.

Austin and McDowell a have also developed a physically based model to include slip in FCC polycrystalline metals subjected to very high strain rates (10^4 to 10^8 s^{-1}) corresponding to loadings in the weak shock loading regime were deviatoric stresses are significant and the shock waves display distinct elastic and plastic wave fronts. For strain rates higher than 10^8 s^{-1}, i.e. strong shock waves (longitudinal stress amplitudes of the order of 50 to 100 GPa) the deviatoric stresses can be neglected due to the high pressures present [64]. Other models for shock-induced plasticity considering that the kinetics of viscoplastic deformation are based on thermally-activated dislocations at the shock front [65, 66] have been considered by Austin and McDowell to model the metal response at higher shock stress amplitudes. However, the model also considers the weak shock loading regime, were slip is the ruling mechanism for plastic deformation and deviatoric stresses and strains have important effects. Volumetric responses using various equations of state are well studied and deviatoric stress-strain models are difficult to tackle. This is mostly due to the complexity of the deformation mechanisms, the microstructure evolution and the related dependencies on pressure, temperature and rate of deformation [67]. This is why most constitutive models for dynamic strength of metals are underdeveloped. The work of Austin and McDowell (2011) [64] addresses this and consists of the following set of differential equations:

$$\frac{d\lambda_1^p}{d\zeta} = \frac{2}{3}\frac{\lambda_1^p}{D}\Phi \tag{89}$$

$$\frac{d}{dx}(\Delta\theta^p) = \frac{4}{3}\frac{\beta\lambda_1\tau}{\rho_0 C_\eta D}\Phi \tag{90}$$

$$\frac{dN_m}{d\zeta} = -\frac{\dot{N}_m}{D} \tag{91}$$

$$\frac{dN_{im}}{d\zeta} = -\frac{\dot{N}_m}{D} \tag{92}$$

In the above equations C_η is the specific heat (per unit mass) at constant elastic configuration, β is the fraction of plastic work that is converted to heat, D is the shock wave velocity defined by an empirical equation of state, ρ_0 is the initial mass density, $\Delta\theta^p$ is the temperature change produced by plastic work, λ_1^p and λ_1 are the plastic and elastic stretch ratios components in the longitudinal direction, N_m and N_{im} are the mobile and immobile dislocation densities, respectively, and τ is the shear stress. The dots represent rates of change of these quantities. An expression for Φ is provided by the Orowan equation,

$$\Phi = bN_m\bar{v} \tag{93}$$

where b is as usual the Burgers vector and $\bar{v}$ is the mean dislocation velocity. The independent variable in the differential equations is

$$\zeta = \frac{B_0 c_s}{2\tau_{eff} b} \tag{94}$$

where B_0 is the nominal value of the damping coefficient, c_s is the shear wave speed and τ_{eff} is the effective stress. Fig. 15 shows comparative results for 6061-T6 AA.

The same authors refined their own model based on previous works [67, 68] for higher shock stresses by considering homogeneous dislocation nucleation. As in their previous work, this model is unique in the sense that it separates the mobile and immobile dislocation populations, making it possible to distinguish the dislocation segments that cause plastic deformation from those which contribute only to material strength. The model also considers homogeneous and heterogeneous dislocation nucleation. These will be considered in accordance with a microstructure-sensitive criterion depending on the stress wave amplitude ranges in which heterogeneous or homogeneous dislocation nucleation are expected to dominate. The later model extended the range of validity to higher shock stresses by developing a treatment of homogeneous dislocation nucleation. The model has a significant number of parameters to

be determined from experiments and proved to be difficult to calibrate. However, it was the first approach that resolved the structure of the shock front. Results were considered to be reasonable for shock-wave induced viscoplastic deformation in polycrystalline Cu, Ni and Al. The constitutive model is also suitable for shockless high-strain-rate loading, e.g. quasi-isentropic compression waves. In these regimes the high strength of the loaded materials observed have been attributed to dislocation drag [5] and this feature is already incorporated in the model.

Zhang, McCormick and Estrin (2001) have developed a constitutive model that although not being referenced very often has been considered to be promising [69]. Since aluminium alloys containing magnesium show a discontinuous yielding behaviour known as the Portevin Le Chatelier (PLC) effect, it is relevant as it is one of the few constitutive models that take account of this behaviour. PLC effects are believed to be a consequence of dynamic strain ageing (DSA). An increase in strain rate within certain ranges of temperature and strain rate will change the local time dependent concentration of solute atoms at temporarily arrested dislocations [70]. The resulting reduction of the solute concentration will justify negative strain sensitivity of the flow stress in the DSA regime. The resulting instability of the plastic flow will give rise to strain localisation and a repeating phenomenon of initiation and propagation of deformation bands will manifest by means of a serrated yielding. The associated equivalent plastic strain $\dot{\varepsilon}^p$ is given by

$$\dot{\varepsilon}^p = \dot{\varepsilon}_0 \exp\left(\frac{\sigma_v - \sigma_d}{S} - P_1 C_s'\right) \tag{95}$$

The stress σ_d introduces the strain hardening effect associated with the dislocation density

$$\sigma_d = d_1 + d_2\left[1 - \exp\left(-\frac{\varepsilon^p}{d_3}\right)\right] \tag{96}$$

S is the strain rate sensitivity and is given by $S = s_1 + s_2\sqrt{\varepsilon^p}$ Coefficients $\dot{\varepsilon}_o, P_1, d_1, d_2, d_3, s_1, s_2$ are experimentally derived constants. The non-dimensional solute concentration is

$$C_s = \{1 - \exp[-P_2(\varepsilon^p)^\alpha (t_a^n)]\} C_m \tag{97}$$

where C_m is a saturation value to which the solute concentration will tend as the effective ageing time t_a approaches infinity. P_2, α and n are constants. The method has been used to simulate the deformation

behaviour of an Al-Mg-Si alloy and it reproduced the conic morphology of the deformation band associated with the PLC effect as shown in Fig. 16. The arrows point the direction of propagation of a localized deformation zone. However results are only available for low strain rate regimes.

Voyadjis and Abed [71] investigated the Zerilli and Armstrong (1987) [38] model proposing some modifications such as the evolution of mobile dislocation density. In FCC metals the long-range dislocations intersection controls the mechanism of thermal activation and thermal activation is strongly dependent on the plastic strain. This implies that the distance d, between dislocations and consequently the activation volume is determinant for a formulation that introduces the effect of plastic strain on the thermal component of the material flow stress. Their work presents two models for each type of crystalline structure (BCC or FCC). The following constitutive equation for FCC metals has been proposed for the first model:

$$\sigma = B\varepsilon_p^n \left[1 - \left(\beta_1 T - \beta_2 T \ln \dot{\varepsilon}_p\right)^{1/q}\right]^{1/p} + Y_a \tag{98}$$

where Y_a is the initial temperature independent yield stress, p and q are constants and B and n are plastic hardening constants. At the onset of plastic deformation $\sigma = Y_a$ which is not in total agreement with FCC metal behaviour and led to the introduction of a slight strain and temperature dependence of the initial yield stress. The parameters β_1 and β_2 are related to the material behaviour in accordance with the respective expressions:

$$\beta_2 = \frac{K}{G_0} \tag{99}$$

$$\beta_1 = \frac{K}{G_0}\left(\frac{\tilde{m}b\rho_m v_0}{1-\frac{\tilde{m}l\lambda_1}{b}+\tilde{m}bl\lambda_2\rho_m+\tilde{m}l\lambda_3\sqrt{\rho_f}}\right) \tag{100}$$

where v_0 is the reference dislocation velocity, G is the shear stress-dependent free energy of activation, K is the Boltzmann's constant , b is the Burgers vector, λ_i are constants related, respectively, to the multiplication of mobile dislocations λ_1, their mutual annihilation λ_2 , and their immobilization through intersection with forest dislocations λ_3 , and the remaining variables were previously defined before.

The second model, was based on a different formulation for the activation volume, based on experimental results from Hoge and Mukherjee [36] , and yielded the following equation:

$$\sigma = \left(Y_0 + B\varepsilon_p^n\right)\left(1 + \beta_0 T^m - \beta_1 T + \beta_2 T \ln \dot{\varepsilon}_p\right) + Y_a \tag{101}$$

where β_0 is a function of strain rate. Another form of the above constitutive Eq. (102) was developed later [19] considering a power variation for the temperature dependence

$$\sigma = B\varepsilon_p^n \left[1 + B_1 T\left(\dot{\varepsilon}_p\right)^{1/m} - B_2 T \exp\left[A\left(1 - \frac{\tau}{\tau_1}\right)\right]\right] + Y_a \tag{102}$$

The temperature independent stress Y_a is independent of the plastic strain or strain rate and A, B, B_1, B_2, m and n are determined from experimental data. This constitutive model relates stress with strain rate by means of a power term. The power law appears to be more suitable to describe the strain rate dependence for a wider range of rates. The model has been compared with experimental results from other sources for OFHC copper. In Fig. 17 results have been compared with experimental data from Nemat-Nassser and Li [14]. The constitutive models Eq. (102) is similar to the Zerilli-Armstrong (1977) [38]. for the stress-strain behavior of a carbon-steel under different strain rate loading.

Holmedal based his model on the well-known MTS constitutive equation [17] whose applicability is limited due to predictions of negative stresses outside of a limited range of strain rates. Consequently, Holmedal considered the use of an algebraic expression for the activation energy term [72], which made the formulation more general with the equations

$$\dot{\gamma} = \dot{\gamma}_0 \exp\left(-\frac{\Delta G}{KT}\right) - \dot{\gamma}_{\min} \tag{103}$$

$$\tau_t = \frac{\mu}{\mu_0}\left\{1 - \left(\frac{KT}{\frac{g_0}{p\mu b^3}}\right)^{\frac{1}{q}} \ln\left(\frac{\dot{\gamma}_0}{\dot{\gamma}+\dot{\gamma}_{\min}}\right)\left|\ln\left(\frac{\dot{\gamma}_0}{\dot{\gamma}+\dot{\gamma}_{\min}}\right)\right|^{\frac{1-q}{q}}\right\}^{1/p} \hat{\tau}_t \tag{104}$$

where g is a function of the ratio of the stress and the threshold stress, the meaning of the remaining coefficients was described earlier. Eq. (104) provides a value for the thermal stress component of the flow stress [73]. The new mathematically derived elastoplastic formulation has been applied to OFE copper and compared with the original MTS model.

Another physically based constitutive model for FCC metals that considers temperature and strain-rate effects on the material response has been proposed by Voyadjis and Almasri [19]. It considers the dependence of activation energy on temperature, strain-rate and stress. This is an approach similar to the

one of Voyiadjis and Abed (2005) [71] but now a power term relates stress and strain rate while Voyiadjis and Abed (2005) used the logarithm of the strain rate for the stress dependence.

Comparisons were presented for OFHC copper between NNL and the presented method (VA). The VA method gave better predictions at low strains than at higher strains although the NNL model gives a slightly better approximation (see Fig. 18).

The Gao and Zhang constitutive model describes the dynamic plasticity of FCC metals using the thermal activation mechanism of dislocation motion under the coupled effect of high strain rate (within the range 10^{-3} to 10^{4} s^{-1}). The equations were successfully applied to the plasticity response of OFHC [46]. This is a physical one-dimensional model based on the idea of thermally activated dislocation motion for moderate strain rates (10^{4} s^{-1}) and dislocation drag deformation mechanism for higher strain rates. The model showed better results than either the JC or the ZA models when applied to OFHC copper over a broad range of temperatures (from 77 to 1096 K) and strain rates (from 10^{-3} to 10^{4} s^{-1}). The limit of validity for the strain rate in the GZ model was found to be 10^{4} s^{-1}. A new constitutive model was established by the authors to extend that limit to higher strain rates [23]. It is generally not possible to develop a single equation applicable to both the conventional strain rate (10^{-4} to 10^{4} s^{-1}) and the high strain rate ranges (10^{4} to 10^{6} s^{-1}). Most models do not cope with both regimes of strain rate and even the PTW model has a piecewise constitutive form to patch together the low-rate and the extremely high-rate regimes. Therefore, a new unified model was developed considering the athermal and thermal stresses:

$$\sigma_f = \sigma_{ath} + \sigma_{th} =$$

$$\sigma_G + B[1-\exp(-k_{a0}\varepsilon)]^{1/2} + \hat{C}\sqrt{1-\exp\left[-k_0\left(\frac{\dot{\varepsilon}}{\dot{\varepsilon}_{s0}}\right)^{-C_1T}\varepsilon\right]}\sqrt{\left\{1+\tanh\left[C_0\log\left(\frac{\dot{\varepsilon}}{\dot{\varepsilon}_{s0}}\right)\right]\right\}\left(\frac{\dot{\varepsilon}}{\dot{\varepsilon}_{s0}}\right)^{C_1T}}\left\{1-\right.$$

$$\left.-C2T\ln\varepsilon\varepsilon s01/q1/p\right. \qquad (105)$$

where σ_G is the stress due to initial defects, $\hat{C}$ is the reference thermal stress, C_1 is the absolute rate sensitivity due to defect annihilation, $C_2 = K/(g_o\mu b^3)$ and $B, k_{a0}, \dot{\varepsilon}_{s0}, p, q, n$ are constants to be determined. The above equation is applicable to very high strain rates.

Results from this model for OFHC copper for a high strain rate can be seen in Figs. 19 and 20 where a comparison with other constitutive models is also presented.

Goldthorpe has developed a path-dependent constitutive method [11] for gilding copper. The method is said to work well with FCC metals, which depend upon their prior deformation history through the evolution of the structure of dislocations at different strain rates and temperatures. These two variables will influence dislocation generation and annihilation. The resulting effects of these changing deformation conditions can only be reproduced if the load-path history is considered. The method is a modification of the work of Follansbee and Kock [17] and makes comparisons with results obtained with the Zerilli-Armstrong method [74,75].

4.8. Critical analysis of the selected physically based models

Though far from complete the extents of the list of cited models makes an overall understanding of their differences rather difficult, Some may have result from small changes to other existing models but others resulted from novel approaches and different assumptions. Such understanding requires a systematization of the described models in a way that permits their main features to be pointed. In Table 1 such a comparison has been presented and a compilation of the respective proposed constitutive equations is given in Table 2.

In the preceding sections some comments on the limitations and capacities of each of the considered models were presented. Most of the methods presented were able to consider strain rates in the high velocity regime ($>10^3$). A few could be used for the specific treatment of materials under shock (such as the Steinberg–Guinan [35], Steinberg-Lund [37], Preston-Tonks-Wallace [6] and Austin & McDowell [64]). Theoretical treatment of shock response has normally been addressed by considering the spherical components of stress. The consideration of deviatoric stress-strain models has been much more complex as it involves micro-structure evolution, deformation mechanism and the described dependencies on temperature and rate of deformation. Most authors based their work on dislocation mechanics as shown above and in Table 1, below and although the equations obtained are not the same their physical foundations have a lot in common. Zerilli-Armstrong [38] proposed the thermal activation analysis of dislocation motion in which they had many followers. An exception is the MTS [17] method in which structural evolution has been based on the flow stress value at 0 K. However, this method has many

parameters that are hard to obtain and therefore its calibration is difficult and makes the method far from tractable. Voyadjis-Abed [71] method came to correct a limitation of the Zerilli-Armstrong model where it was not capable of handling the deformation of metals under high temperature. The Nemat-Nasser-Li method used a varying reference strain rate [44]. The Khan–Huang–Liang [76] and Holomon-Voce [18] cannot properly describe the dynamic behaviour of a metal at high strain rates [44].

In general, the more recent work follows previous principles (dislocation mechanics, decomposition of stress in thermal and athermal components, thermal activation, etc..) using other models as starting points. In many cases modification are introduced to obtain better agreement with results of a particular material under test [11].

Table 1 – Comparison of the major characteristics of physically based constitutive models.

Year	**Model**	**Strain rate**	**Main features**
1975	Bodner and Parton [30]	10^{-3} to 10^{0} s^{-1}	• Based upon separation of the total deformation rate into elastic and plastic components • Incorporates strain hardening effects through a plastic work term • Assumes a dependency on J2 invariant • No temperature effects;
1980	Steinberg and Guinan [35]	10^{5} s^{-1}	• Incorporates temperature effects, • Considers the effect of shock pressure • Based on equivalent plastic strain
1987	Zerilli-Armstrong [38]	$4x10^{3}$ s^{-1}	• Considers temperature effects • Considers grain size. • Based on dislocation mechanics • Considers thermal activation
1988	Mechanical threshold stress [17]	10^{-4} to 10^{4} s^{-1}	• Incorporates temperature effects • Based on thermal activation • Uses the flow stress at 0 K (MTS) • Based on dislocation density as state variable
1989	Steinberg and Lund [48]	10^{-4} to 10^{6} s^{-1}	• Considers thermal activation • Includes the effect of temperature • Extends the Steinberg and Guinan model • Based on equivalent plastic strain • Considers the pressure
1998	Nemat-Nasser and Li [14]	10^{-3} to 10^{4} s^{-1}	• Considers dislocation mechanics • Considers thermal activation • Considers temperature
2001	Nemat-Nasser, Guo and Kihl [66]	10^{-2} to $\approx 10^{4}$ s^{-1}	• Based on dislocation motion mechanics • Includes viscous drag effects on dislocation motion
2003	Preston, Tonks and Wallace [6]	10^{-3} to 10^{9} s^{-1}	• Uses an Arrhenius form for plastic strain rate but with an activation energy • Suitable for explosive loading
2001	Rusinek and Klepaczko [69]	10^{-4} to 10^{3} s^{-1}	• Includes temperature effects • Based on two components of stress: effective and internal • Uses an Arrehnius type eq. for the effective component of stress
2011	Austin and McDowell [74]	10^{4} to 10^{8} s^{-1}	• Based on dislocation densities as state variables • Uses J2 flow theory

			• First plastic-wave analysis using dislocation mechanics in the weak shock regime
2001	Zhang, McCormick and Estrin [80]	10^{-3}	• Models the Portevin-Le Chatelier effect • Based upon separation of the total deformation rate into elastic and plastic components
1982	Anand [81]	10^{-2}	• Considers temperature • Activation energy • Considers dynamic recovery
2005	Voyadjis and Abed [82]	10^{-3} to 10^{4} s^{-1}	• Modified ZA model • Based on dislocation mechanics • Considers thermal activation
2007	Holmedal [84]	10^{-4} to 10^{9}	• Modification of MTS method
2008	Voyadjis and Almasri [19]	10^{-4} to 10^{4}	• Based on VA model • Based on dislocation density • Considers temperature effects • Considers activation energy
2012	Gao and Zhang [23]	10^{-3} to 10^{4}	• Based on dislocation motion • Considers thermal activation • Considers dislocation drag for high strain rates
2009	Huang et al. [85]	10^{-5} to 10^{6} s^{-1}	• Dislocation mechanics • Thermal activation • Temperature
2000	Gould and Goldthorpe [11]	Not indicated	• Based on Follansbee and Kocks [17] model • Temperature effect • Dislocation motion • Thermal activation

Table 2 – Constitutive equations of the indicated models.

Bodner and Partom [30]	$\dot{\varepsilon}_x^p = \frac{2D_0}{\sqrt{3}}\frac{\sigma}{\lvert\sigma\rvert}\exp\left[-\frac{1}{2}\left(\frac{3A^2}{\sigma^2}\right)^n\right]$
Steinberg and Guinan [35]	$Y = Y_0[1+\beta(\varepsilon+\varepsilon_1)]^n\left[1+\left(\frac{Y_p'}{Y_0}\right)\frac{P}{\eta^{\frac{1}{3}}}+\left(\frac{G_T'}{G_0}\right)(T-300)\right]$
Zerilli and Armstrong [36]	$\sigma = \sigma_a + C_2\varepsilon^{\frac{1}{2}}\exp(-C_3T + C_4T\ln\dot{\varepsilon}) + kl^{-\frac{1}{2}}$
MTS [17]	$\sigma = \hat{\sigma}_a + (\hat{\sigma}-\hat{\sigma}_a)\left\{1-\left[\frac{KT\ln\left({\dot{\varepsilon}_0}/{\dot{\varepsilon}}\right)}{g_0\mu b^3}\right]^{\frac{1}{q}}\right\}^{\frac{1}{p}}$
Steinberg and Lund [48]	$\dot{\varepsilon}_p = \frac{1}{C_1}\exp\left[\frac{2U_k}{KT}\left(1-\frac{\sigma_t}{\sigma_p}\right)^2\right]+\frac{C_2}{\sigma_t}$
Nemat-Nasser and Li [14]	$\tau(\dot{\gamma},\gamma,T) = \tau^o\left\{1-\left[-\frac{KT}{G_0}\left(\ln\frac{\dot{\gamma}}{\dot{\gamma}_0}+\ln\left(1+a(T)\gamma^{\frac{1}{2}}\right)\right)\right]^{\frac{1}{2}}\right\}^{\frac{3}{2}}\left[1+a(T)\gamma^{\frac{1}{2}}\right]+\tau_a^o\gamma^{n_1}$
Nemat-Nasser, Guo and Kihil [66]	$\tau^* = \tau^0\left\{1-\left[-\frac{KT}{G_0}\ln\left(\frac{\dot{\gamma}f(\gamma,T)}{\dot{\gamma}}\right)\right]^{\frac{1}{q}}\right\}^{\frac{1}{p}} f(\gamma,T) \quad \text{for } T \le T_c$
Preston-Tonks-Wallace [6]	

$$\hat{\tau} = \hat{\tau}_s + \frac{1}{p}(s_0 - \hat{\tau}_y)\ln\left\{1 - \left[1 - \exp\left(-p\frac{\hat{\tau}_s - \hat{\tau}_y}{s_0 - \hat{\tau}_y}\right)\right]\exp\left[-p\theta\psi\left[(s_0 - \hat{\tau}_y)\left[\exp\left(p\frac{\hat{\tau}_s - \hat{\tau}_y}{s_0 - \hat{\tau}_y}\right) - 1\right]\right]^{-1}\right]\right\}$$

Rusineck-Klepcazko [69] $\sigma = \frac{E(T)}{E_0}\left[B_0\theta_m^{-v}(\varepsilon_0 + \varepsilon^p)^{n_0(1-D_2\theta_n)} + \sigma_0^*(1 - D_1\theta_m)^m + \sigma_{ns}\right]$

Voyadjis-Abed [82] $\sigma = B\varepsilon_p^n\left[1 - \left(\beta_1 T - \beta_2 T\ln\dot{\varepsilon}_p\right)^{1/q}\right]^{1/p} + Y_a$

Voyadjid-Almasri [19] $\sigma = B\varepsilon_p^n\left[1 + B_1 T\left(\dot{\varepsilon}_p\right)^{1/m} - B_2 T\exp\left[A\left(1 - \frac{T}{T_t}\right)\right]\right] + Y_a$

Gao-Zhang [23] $\sigma = \hat{\sigma}_a + \hat{Y}\varepsilon^n\exp\left[C_3 T\ln\left(\frac{\dot{\varepsilon}}{\dot{\varepsilon}_{s0}}\right)\right]\left\{1 - \left[-C_4 T\ln\left(\frac{\dot{\varepsilon}}{\dot{\varepsilon}_0}\right)\right]^{1/q}\right\}^{1/p}$

Huang [85] $\tau = \alpha\mu b\sqrt{\rho} + \left[B_{wind}^0 + \frac{B_{flutter}^0}{1 - \left(\frac{\dot{\gamma}}{b\rho_m C_t}\right)^2}\right]\frac{T}{\theta_D}\frac{\dot{\gamma}}{b^2\rho_m}$

Gould and Goldthorpe [11] $\bar{\sigma} = \sigma_a + \phi\eta\left\{1 - \left[\alpha - \theta\frac{\varepsilon}{\eta} + 1\right]^{\frac{1}{1-\alpha}}\right\}$

5. Phenomenological constitutive equations

Phenomenological constitutive relations are equations normally derived from experimental data rather than from physical principles. However, they are widely used because they are simple to implement and the parameters are often easier to obtain. Although they are not derived from first principles they have physical meaning and can provide accurate results. The main phenomenological constitutive relations will be presented in the next sections.

5.1. Molinari-Ravichandran (MR)

This is a single internal variable phenomenological model based on a characteristic length scale of the microstructure that develops in the metal during deformation. A scaling law was considered for the evolution of this characteristic or effective length δ during experimental observations as this variable mimics the cell size δ_c, which is an important structure parameter. The evolution of δ can be described by

$$\frac{d\delta}{d\varepsilon} = -\frac{\delta_r}{\delta_s}[\delta^2 - \delta_s\delta] \tag{106}$$

where the expressions for the microstructure refinement rate δ_r, and the saturation value of the microstructure length δ_s at large strains, are empirical or may be derived from the theory of thermally activated processes, and are functions of temperature and strain rate. Using the second approach, the following expressions were derived:

$$\frac{\delta_r}{\delta_{r0}} = \left\{1 - \left[k_r\left(\frac{T}{T_{r0}}\right)\log\left(\frac{\dot{\varepsilon}_{r0}}{\dot{\varepsilon}}\right)\right]^{p_r}\right\}^{q_r} \tag{107}$$

$$\frac{\delta_s}{\delta_{s0}} = \frac{1}{\left\{1-\left[k_r\left(\frac{T}{T_{r0}}\right)\log\left(\frac{\dot{\varepsilon}_{r0}}{\dot{\varepsilon}}\right)\right]^{p_s}\right\}^{q_s}} \tag{108}$$

where δ_{ro} and δ_{so} are the reference values of δ_r and δ_s, respectively, and $k_r, p_r, q_r, k_s, p_s,$ and q_s are constants that describe the dependence of micro-structural refinement and steady state characteristic length on strain rate and temperature. $T_{ro}, T_{so}, \dot{\varepsilon}_{ro}$ and $\dot{\varepsilon}_{so}$ are reference temperatures and strain rates for modelling the observed behaviours in micro-structure refinement and steady state characteristic length. The flow stress is a function of the intrinsic resistance of the material and the strain-rate and it is expressed as [68]:

$$\sigma = \sigma_0\left(\frac{\dot{\varepsilon}}{\dot{\varepsilon}_0}\right)^{1/m} \tag{109a}$$

$$\sigma_0 = \hat{\sigma}(d)\left(\frac{\delta}{\delta_0}\right) \tag{109b}$$

where $\dot{\varepsilon}_o$ is the reference strain-rate and m is the instantaneous material strain rate sensitivity which is a function of the temperature. It accounts for part of the thermal softening of the material due to the change in ambient temperature and the rise of temperature during adiabatic deformation. The other part of the thermal softening is controlled by the temperature dependence of δ_{ro} and δ_{so}. d is the grain size and is the internal characteristic length which reduces when the plastic strain ε increases in accordance with a phenomenological evolution equation. This internal variable, governed by an evolution law with temperature and rate-dependent coefficients, expresses the response of the material in a simple way, adequate for engineering applications. Other authors used the same approach based on a single internal parameter as micro-scale models demand too much computational time for applications to high-speed

dynamics [77]. Their work used part of the MR model [68]. It reproduced strain-rate history effects for various materials at a range of strain rates from $8x10^{-3}$ to 10^3 s^{-1}. Fig. 21 shows results for copper at a strain rate of 5000 s^{-1}.

5.2. Johnson and Cook (JC)

Perhaps the most widely used constitutive model for high strain rate applications is the Johnson-Cook (JC) [78] empirical equation. One of the reasons for this preference resides in its simplicity as it only requires calibration of five parameters and has been successfully used for a wide range of materials at different temperatures and strain-rates. It has also been the object of many modifications, which demonstrates the generalised interest that it raises throughout the scientific and engineering community. This model assumes that the material is isotropic and its constitutive relation is

$$\sigma_{eq} = (A + B\varepsilon^n)(1 + C \ln \dot{\varepsilon}^*)(1 - T^{*m}) \tag{110}$$

where σ_{eq} is the von Mises equivalent flow stress, ε is the equivalent plastic strain, $\dot{\varepsilon}^* = \dot{\varepsilon}/\dot{\varepsilon}_o$ is a dimensionless plastic strain rate ($\dot{\varepsilon}_o$ is a reference strain-rate, set to 1 s^{-1}) and $T^* = (T - T_o)/(T_m - T_o)$ is a dimensionless temperature where T_m is the melting temperature and T_o is room temperature. A is the yield stress at a reference temperature and a reference strain-rate, B is a strain-hardening coefficient and n is the strain-hardening exponent. C and m are material constants that represent the coefficient of strain-rate hardening and a thermal softening coefficient, respectively.

The equivalent flow stress is then the product of three factors taken independently without concern about strain-rate or temperature history effects, strain hardening, strain rate and the softening effect temperature. The constants are parameters to be obtained from experiments (e.g. Split Hopkinson Tension Bar) although originally they were obtained from Taylor impact. When the loading approaches static conditions (low plastic strain rate, $\dot{\varepsilon}^*$) the $\ln \dot{\varepsilon}^*$ term tends to infinity and so a modification to the JC equation has been suggested by Borvik [79]. The modified equation is:

$$\sigma_{eq} = \left(a + B\varepsilon_{eq}^n\right)\left(1 + \dot{\varepsilon}_{eq}^*\right)^C (1 - T^{*m}) \tag{111}$$

Another modification to the J-C model was proposed to account for the strengthening exhibited by many ductile metals at strain rates above 10^4 s^{-1} [80]. To better reproduce that high strain rate sensitivity, Rule and Jones proposed the following revised Johnson-Cook equation (RJC):

$$\sigma = (C_1 + C_2\varepsilon^n)\left[1 + C_3 \ln \dot{\varepsilon}^* + C_4\left(\frac{\dot{1}}{C_5 - \ln \dot{\varepsilon}^*} - \frac{1}{C_5}\right)\right](1 - T^{*m}) \tag{112}$$

where C_1 to C_5 are material constants. The term $1/(C_5 - \ln \dot{\varepsilon}^*)$ increases the strain rate sensitivity at higher rates and parameter C_4 controls how much the RJC model deviates from the original. To solve the problem of the yield stress being unbounded and tending to infinity as $(C_5 - \ln \dot{\varepsilon}^*)$ approaches zero these authors defined an extra non-dimensional parameter, C_6, defined as

$$\left[1 + C_3 \ln \dot{\varepsilon}^* + C_4\left(\frac{\dot{1}}{C_5 - \ln \dot{\varepsilon}^*} - \frac{1}{C_5}\right)\right] \leq C_6 \tag{113}$$

This way the strain rate sensitivity term will be limited to a maximum value. A number of other authors have been experimenting with other modifications to the JC model. Rule and Jones (1998) [80] cite two modifications (Holmquist TJ, Johnson GR, *J. Phys. France*, 1, C3-853, 1991 and Kang WJ, Cho SS, Huh H and Chung DT, *Int. J. Vehicle Design*, Vol 21, Nos. 4/5, 1999, pp.424-435). The first has not been widely used due to the fact that the modified version did not produce a significant enhancement over that provided by the original formulation. The second modification introduced a quadratic form for the strain rate sensitivity such that

$$\sigma_{eq} = (A + B\varepsilon^n)(1 + C_1 \ln \dot{\varepsilon}^* + C_2(\ln \dot{\varepsilon}^*)^2)(1 - T^{*m}) \tag{114}$$

Another modification [81] considered the effect of temperature on the strain rate-hardening behaviour of IC10, and can be expressed as:

$$\sigma = [A(1 - T^m) + BT^*\varepsilon^n](1 + C \ln \dot{\varepsilon}^*) \tag{115}$$

where the coefficients maintain their original meanings and the following additional function $B(T^*)$ is introduced:

$$B(T^*) = \frac{\sigma_{br}(1 - T^{m_1}) - \sigma_{0.2r}(1 - T^{*m})}{\left[\varepsilon_{br}(1 - P_1T^* - P_2T^{*P_3})\right]^n} \tag{116}$$

where m_1, P_1, P_2 and P_3 are material constants, σ_{br} is designated by the author as *broken stress* at room temperature and reference strain rate and ε_{br} is the corresponding strain at room temperature and reference strain-rate. Finally $\sigma_{0.2r}$ is the yield stress at $\varepsilon = 0$.

Vural and Cairo (2009) [82] derived another modified version of the JC equation noting that experiments show that strain-hardening decreases faster than predicted by the thermal softening rate term in the original JC model. To provide a direct coupling between temperature and strain-hardening they introduced the modification $B = B_o(1 - T^{*P})$ [93] where P is a material constant. They also noted that the original JC model does not provide an enhanced strain rate effect at high rates and gives a too small and unrealistic strain rate dependence at high temperatures, and introduced a temperature dependence in the strain-rate sensitivity parameter C. The MJC equation has the following final form:

$$\sigma = \left\{\sigma_0 + B_0\left[1 - \left(\frac{T-T_0}{T_m - rmT_0}\right)^P\right]\varepsilon_p^n\right\}\left[1 + (C_1 T_r^{*P} + C_2 H)\ln\left(\frac{\dot{\varepsilon}}{\dot{\varepsilon_0}}\right)\right]\left[1 - \left(\frac{T-T_0}{T_r - T_0}\right)^P\right] \quad (117)$$

where

$$H(\dot{\varepsilon}, \dot{\varepsilon}_t, k) = \frac{1}{2} + \frac{1}{2}\tanh\left[k\ln\left(\frac{\dot{\varepsilon}}{\dot{\varepsilon}_r}\right)\right]$$

C_1 and C_2 are the rate sensitivity in the quasi-static strain rate regime ($\dot{\varepsilon} < \dot{\varepsilon}_t$) and the enhancement in rate sensitivity in the dynamic strain-rate regime ($\dot{\varepsilon} > \dot{\varepsilon}_t$), respectively. H is a smooth approximation of the Heaviside step function. The transition interval between quasi-static and dynamic regimes can be made to vary thanks to the scaling factor k. Examples of results obtained with the MJC are shown in Fig. 22 where comparison is made with experimental data for a 2139-T8 aluminium alloy subject to uniaxial compression and tension experiments over a range of strain rates up to 10^4 s^{-1}.

Lin and co-workers (2010) [83] proposed another modified JC equation considering the coupled effects of temperature and strain rate, giving the following expression [84]:

$$\sigma = (A_1 + B_1\varepsilon + B_2\varepsilon^2)(1 + C_1\ln\dot{\varepsilon}^*)\exp[(\lambda_1 + \lambda_2\ln\dot{\varepsilon}^*)(T - T_r)] \quad (118)$$

where $A_1, B_1, B_2, C_1, \lambda_1, \lambda_2$ are material constants and all the other parameters keep their original meanings.

Other modifications of the JC model are available in the literature but most of them were developed for specific materials [85, 86, 87]. However, it is important to refer to a hybrid model resulting from the Johnson-Cook and Zerilli-Armstrong constitutive models, namely a physically based model developed to describe the response of 42CrMo alloy steel to hot compression [88]. Another JC equation for use with aluminium alloys, in particular an Al-Cu-Mg alloy under hot forming loads has been published-[89]. The authors tried to use the JC model but it failed to provide accurate results for the high temperature flow stress of the alloy studied. Modifications were introduced based on the Zener-Hollomon parameter but as only low strain rates were considered, the model will not be described here. The method is an extension of the JC constitutive model. This method has been widely used by the research and engineering community and a large amount of data has been and still continuous to be published based on its use.

5.3. Khan-Huang (KH) and Khan-Huang-Liang (KHL)

Khan and Huang (1992) introduced a viscoplastic constitutive model (KH model) to simulate the response of alloy AA 1100 to a wide range of strain rates. They proposed a relation between the second invariant of the deviatoric stress J_2, and functions of the equivalent strain and the second invariants of the plastic deformation rate [76]:

$$J_2 = f_1(\varepsilon) f_2\left(D_2^p\right) \tag{119}$$

This expression can be simplified for a one-dimensional case giving $\sigma = g_1(\varepsilon) g_2(\dot{\varepsilon})$ where g_1 describes the correlation of the stress with the plastic strain at the reference strain-rate and g_2 represents the dependence on the strain-rate, that is,

$$g_1(\varepsilon) = \left[3 f_1\left(\frac{3}{4}\varepsilon^2\right)\right]^{\frac{1}{2}} \tag{120}$$

$$g_2(\dot{\varepsilon}) = \left[f_2\left(\frac{3}{4}\dot{\varepsilon}^2\right)\right]^{\frac{1}{2}} \tag{121}$$

Particular forms for the above functions were presented as

$$g_1(\varepsilon^p) = \sigma_0 + E_\infty \varepsilon^p - a e^{-\alpha \varepsilon^p} \tag{122}$$

$$g_2(\dot{\varepsilon}^p) = 1 \Big/ \left[1 - \frac{\ln(\dot{\varepsilon}^p)}{\ln(D_0^p)}\right] \tag{123}$$

where the five constants necessary to calibrate the model are n, E_∞, σ_o, a and α. D_2^p has been chosen to be 10^6 s^{-1} by Khan and co-workers. The model is capable of predicting the strong work-hardening behaviour at larger strain rate regimes than those of the BP model. However, it is worth noticing that no temperature effects have been included in these constitutive equations. The lack of temperature effects led to further modifications. Meanwhile, a constitutive model has been proposed based on BP model assumptions [31]. A modification to that model was proposed by Khan and Liang (1999) [90] to introduce the coupled work hardening dependence of flow stress on strain, strain rate and the temperature dependency that was lacking in the previous model. Basically, a temperature multiplicative factor similar to that of JC equation was introduced to improve correlation with experiments. Khan and Liang (1999) [90] started with a new relation between D_2^p and J_2,

$$J_2 = f_1\left(\varepsilon_2, D_2^p\right) f_2(T) \tag{124}$$

where ε_2 is the equivalent strain, f_1 describes the coupled strain and strain rate effects on the work-hardening behaviour. The resulting constitutive equation is known as the KHL model,

$$\sigma = \left[A + B\left(1 - \frac{\ln(\dot{\varepsilon}^p)}{\ln(D_0^p)}\right)^{n_1} \varepsilon^{n_0}\right](1 - T^{*m}) e^{C \ln(\dot{\varepsilon})} \tag{125a}$$

$$T^* = \frac{T - T_r}{T_m - T_r} \tag{125b}$$

where σ, ε, $\dot{\varepsilon}$ are the von Mises equivalent stress, strain and strain-hardening, respectively, and T, T_m and T_r are absolute temperature, melting temperature and reference temperature, respectively. The other parameters A, B, n_o, n_1, C and m are empirical constants. As in other constitutive models the number of parameters to be determined is within tractable limits. Better agreement with experimental data has been obtained but only BCC metals were tested. Later work on tantalum alloy and AerMet 100 steel tested the suitability of the new model to predict complex loading paths of current experimental results [91]. The model successfully predicted non-proportional experimental results.

In a later study Khan and co-workers adopted the Hall-Petch relation $\sigma_y = a + k/\sqrt{d}$ in the KHL equation, where σ_y is the yield stress, d is the polycrystal average grain size and a and k are material constants) obtaining a model for coarse-grained polycrystalline materials [92]. The KHL model was further modified to account for grain size dependence, work hardening, rate sensitivity and temperature effect, as deemed necessary to reproduce the behaviour of fully compacted nanocrystalline iron. Results have shown that the modified KHL model correlates reasonably with both isothermal and adiabatic experimental results. The modified equation is

$$\sigma = \left[\left(a + \frac{k}{\sqrt{d}}\right) + B\left(1 - \frac{\ln(\dot{\varepsilon}^p)}{\ln(D_0^p)}\right)^{n_1} \varepsilon^{n_0}\right](1 - T^m)\dot{\varepsilon}^C \tag{126}$$

A modified version of the KHL model [93] was used for the Ti-6Al-4V alloy to compare with the JC model and experimental results. The KHL model, as given by the following equation, led to much better predictions than the JC model,

$$\sigma = \left[A + B\left(1 - \frac{\ln(\dot{\varepsilon}^p)}{\ln(D_0^p)}\right)^{n_1} \varepsilon^{n_0}\right]\left(\frac{T_m - T}{T_m - T_r}\right)^m \left(\frac{\dot{\varepsilon}^p}{\dot{\varepsilon}^{p*}}\right)^C \tag{127}$$

where σ is the stress and ε^p is the plastic strain, T_m, T and T_r are melting, current and reference temperatures, respectively, $D_o^p = 10^6$ s^{-1}, which is an arbitrary value chosen as an upper bound strain rate, $\dot{\varepsilon}^* = 1$ s^{-1} is a reference strain rate at which some material constants are determined, $\dot{\varepsilon}$ is the current strain rate and A, B, n_1, n_0, C and m are material constants. This model can reproduce the decreasing work-hardening behaviour observed with increasing strain rate through the material constant n_1. The KHL model has a simple temperature dependent term in a multiplicative form. Because of this, the temperature dependence of different metals may not be easy to describe and many attempts led to modified versions of the model, with more constants to be determined.

In 2006, the analysis of the mechanical properties of nanocrystalline aluminium and iron led to another modification to the method [94], including the following bilinear Hall-Petch type relation:

$$\sigma = \left(a + \frac{k}{\sqrt{d}}\right)\left[1 + \frac{B}{a}\left(1 - \frac{\ln(\dot{\varepsilon}^p)}{\ln(D_0^p)}\right)^{n_1} \varepsilon^{n_0}\right]\left(\frac{T_m - T}{T_m - T_r}\right)^m \left(\frac{\dot{\varepsilon}^p}{\dot{\varepsilon}^{p*}}\right)^C \tag{128}$$

The KHL model was also applied to the microscopic stress and strain rate of a nanocrystalline iron and copper mixture (80% Fe and 20% Cu) [95] assuming the equivalence between macroscopic and microscopic properties:

$$\sigma_M = \left[\sigma_0 + B\left(1 - \frac{\ln(\dot{\varepsilon}_M)}{\ln(D_0^p)}\right)^{n_1} \varepsilon_M^{n_0}\right](1 - T^{*m})\dot{\varepsilon}_M^C \tag{129a}$$

$$T^* = \frac{T - T_r}{T_m - T_r} \tag{129b}$$

where σ_M, ε_M and $\dot{\varepsilon}_M$ are microscopic von Mises equivalent stress, strain and strain rate, respectively, in the matrix material. T is the absolute temperature, T_m is the melting temperature of the material and T_r is a reference temperature. The remaining parameters are material constants as described before.

Yu and co-workers also used the KH model to analyse data from impact experiments in a dual phase 600 steel (DP600) at strain rates ranging from 10^{-4} to 1.6 x 10^3 s^{-1}. However, the results show a gap between experimental and model predictions at higher strains. This led the authors to propose a new modified KH plastic constitutive model [96] expressed as follows:

$$\sigma = f(\varepsilon^p, \dot{\varepsilon}^p) = \sigma_0 \hat{f}_2(\dot{\varepsilon}^p) + E_\infty \varepsilon^p - ae^{-\alpha\varepsilon^p} \tag{130a}$$

with

$$f_2(\dot{\varepsilon}^p) = 1 + D\left(\ln\frac{\dot{\varepsilon}^p}{\dot{\varepsilon}_0^p}\right)^m \tag{130b}$$

where D and m are material constants. As in the former constitutive model KH, temperature effects were ignored in this new model. In Fig. 23 results for the modified KHL model are presented for the stress strain curves at various strain rates, together with measured results. A new grain size and temperature dependent viscoplastic model [97] was derived from the KHL (Khan – Huang – Liang) constitutive equation [92, 93, 94] to account for different polycrystalline plastic behaviour as a result of grain refinement. This new constitutive model (see Fig. 24), can be described by the following relation:

$$\sigma = \left[\left(a + \frac{k}{d^{n^*}}\right) + B\left(\frac{d}{d_0}\right)^{n_2}\left[\left(1 - \frac{\ln(\dot{\varepsilon}^p)}{\ln(D_0^p)}\right)\left(\frac{T_m}{T}\right)\right]^{n_1}(\varepsilon^p)^{n_0}\right]\left(\frac{T_m - T}{T_m - T_{ref}}\right)^m\left(\frac{\dot{\varepsilon}^p}{\dot{\varepsilon}^{p^*}}\right)^C \tag{131}$$

where $\dot{\varepsilon}^p, \varepsilon^p$ are plastic strain and current strain rate, σ is the flow stress, T_m, T and T_{ref} are melting, current and reference temperatures, respectively. D_o^p is an arbitrarily chosen upper bound strain rate, $\dot{\varepsilon}^{p*} = 1$ is a reference strain rate at which certain material constants are obtained and $n^* = 0.5$ (while material follows the Hall-Petch relationship). Coefficients d and d_0 are the average grain size of the material under test and its corresponding coarse-grained counterpart respectively ($d_0 \approx 50\ \mu m$). $a, k, n1$, n_2, c, m and B are material constants.

The proposed model adds a few extra terms to simulate the change in work hardening behaviour as the result of grain refinement and different temperatures. Good correlations were obtained for mechanically milled Cu and Al and it can capture the change in yield stress and work-hardening behaviour with variation in the grain size. The model also captures well the strain-rate sensitivity of nanocrystalline Cu and Al at wide ranges of strain rate

5.3. Other phenomenological models

Voce and Kocks based a model on the fact that true stress-strain curves of FCC metals are adequately represented by an exponential law to a saturation stress. The exponential law was first proposed by Voce [98] and later expanded by a number of authors. One of these developments [68] expanded Voce's work to describe the temperature and strain-rate dependence and to give it a physical foundation. Voce's equation, presented in 1948 as cited by Lin [24] was

$$\sigma = \sigma_s + \left[(\sigma_0 - \sigma_s) \exp\left(-\frac{\varepsilon}{\varepsilon_r}\right)\right] \tag{132}$$

where σ_s is the saturation stress and σ_o is the initial yield stress and ε_r is the relaxation strain. Kocks (1976) [99] developed a description of the saturation stress σ_s as a function of temperature and stain-rate:

$$\sigma_s = \sigma_{s0} \left(\frac{\dot{\varepsilon}}{\dot{\varepsilon_0}}\right)^{KT/A} \tag{133}$$

where K is the Boltzmann constant, b is the Burgers vector, σ_{so} is the saturation threshold stress at zero Kelvin and A and $\dot{\varepsilon}_o$ are material parameters. The initial yield stress is can be obtained as [100]

$$\sigma_0 = \sigma_{k0}\left(\frac{\dot{\varepsilon}}{\dot{\varepsilon_{k0}}}\right)^{KT/A_0} \tag{134}$$

where $A_o = A\mu(T)b^3$ and μ is the elastic modulus and A , $\dot{\varepsilon}_{ko}$ are material parameters. An expression for the relaxation strain ε_r is also given as

$$\varepsilon_r(\dot{\varepsilon}, T) = \frac{\sigma_s(\dot{\varepsilon},T) - \sigma_0(\dot{\varepsilon},T)}{\theta_0} \tag{135}$$

where θ_o is the initial work-hardening rate. Naderi (2008) [100] combined MR and VK models to obtain results for 22MnB5 boron steel. However, only fairly low strain-rates were considered (up to 10 s^{-1}). The results, shown in Fig. 25, although slightly better than the MR model showed that in spite of this, the constitutive model has more flexibility since history effects (e.g. rapid changes in strain rate or temperature history) can be taken into account via the evolution law of the internal parameter. Lin et al. developed equations to obtain the flow stress of metals and alloys under hot deformation from the Arrhenius equation, using a Zener-Hollomon parameter to describe the stress-strain curve [101]. These authors investigated very high temperature deformation of 42CrMo steel at strain rates up to 50 s^{-1}. The modifications introduced were applied to a 2124-T851 aluminium alloy [83]. The effect of temperature and strain rate behaviour can be represented by a Zener-Hollomon parameter in an exponent-type equation. The Arrhenius type equation is chosen as it provides a better approximation between the Zener-Hollomon parameter and the flow stress:

$$\dot{\varepsilon} = AF(\sigma)\exp\left(-\frac{Q}{RT}\right) \tag{136}$$

$$Z = \dot{\varepsilon}\exp\left(\frac{QR}{T}\right) \tag{137}$$

$$F(\sigma) = \begin{cases} \sigma_n \Leftarrow \alpha\sigma < 0.8 \\ \exp(\beta\sigma) \Leftarrow \alpha\sigma > 1.2 \\ [\sinh(\alpha\sigma)]^n \Leftarrow \text{all } \sigma \end{cases} \tag{138}$$

in which σ is the flow stress, R is the universal gas constant, T is the absolute temperature, $\dot{\varepsilon}$ is the strain-rate, Q is the hot deformation activation energy, and A, α and n are material constants ($\alpha = \beta/n$). The method has been used to predict the flow stress of a 42CrMo steel at strain rates up to 50 s^{-1}.

A more recent and comprehensive constitutive model has been developed from the previous approach to predict the stress-strain curve of 42 CrMo steel (see Fig. 26). Again the authors had in mind hot forming processes at relatively low strain rates (up to 10 s^{-1}) which makes this method depart from the object of this review. Further details on this model are available in the literature [102].

5.4. Comparison between the presented phenomenological models

Tables 3 and 4 compare those constitutive models described in section 5 and compares the main parameters selected by the authors to base the development of their equations. Mecking –Kocks [45], Molinari-Ravichandran [68] and Johnson-Cook [78] are the most cited and from these the Johnson-Cook is by far the most popular due to the simplicity of implementation in hydrocodes.

Table 3 - Comparison of the major characteristics of some empirical constitutive models.

Year	Model	Strain rate	Main features
2003	Kocks and Mecking [72]	10^{2} to 10^{4} s^{-1}	• Based on dislocation density • Considers thermal activation • Considers flow stress at 0 K
2005	Molinari & Ravichandran [68]	10^{-3} to $8.5x10^{4}$ s^{-1}	• Based on a characteristic length scale of the microstructure • Considers temperature effects • Considers grain size
1983	Johnson and Cook [78]	Up to 10^{4} s^{-1}	• Purely empirical model • Considers the effect of temperature • Considers strain rate effects
1976	Voce and Kocks [98]	10 s^{-1}	• Uses the concept of saturation stress as a function of temperature and strain rate
2008	Lin, Chen and Zhong [101]	5x10 s^{-1}	• Defines flow stress in terms of the Zener-Hollomon parameter
1992	Khan and Huang [76]	10^{-5} to 10^{4} s^{-1}	• Does not includes temperature effects • Based upon separation of the total deformation rate into elastic and plastic components • Assumes a dependency on J2 invariant
1992	Khan, Huang and Liang [90]	10^{-6} to 10^{4} s^{-1}	• Adds temperature effects to the KH model
2009	Khan, Liang and Farrokh [97]	10^{-4} to 10^{3} s^{-1}	• Derived from KHL method • Includes temperature effects • Considers grain size
			•
			•

Table 4 - Constitutive equations of the indicated phenomenological models.

Kocks and Mecking [72]	$s = \left(\frac{\dot{\varepsilon}}{\dot{\varepsilon_0}}\right)^{1/m} \exp\left(-F\frac{\theta_r}{\theta_h}\right)$ and $s = \left(\frac{\dot{\varepsilon}}{\dot{\varepsilon_0}}\right)^{\frac{1}{m}}\left(1 - F\frac{\theta_r}{\theta_h}\right)$
Molinari and Ravichandran [68]	$\frac{\delta_r}{\delta_{r0}} = \left\{1 - \left[k_r\left(\frac{T}{T_{r0}}\right)\log\left(\frac{\dot{\varepsilon}_{r0}}{\dot{\varepsilon}}\right)\right]^{p_r}\right\}^{q_r}$ and $\frac{\delta_s}{\delta_{s0}} = \frac{1}{\left\{1-\left[k_r\left(\frac{T}{T_{r0}}\right)\log\left(\frac{\dot{\varepsilon}_{r0}}{\dot{\varepsilon}}\right)\right]^{p_s}\right\}^{q_s}}$
Jonhson and Cook [78]	$\sigma_{eq} = (A + B\varepsilon^n)(1 + C\ln\dot{\varepsilon}^*)(1 - T^{*m})$
Voce and Kocks [98]	$\sigma = \sigma_s + \left[(\sigma_0 - \sigma_s)\exp\left(-\frac{\varepsilon}{\varepsilon_r}\right)\right]$
Lin, Chen and Zhong [101]	$\dot{\varepsilon} = AF(\sigma)\exp\left(-\frac{Q}{RT}\right)$
Khan-Huang-Liang [90]	$\sigma = \left[A + B\left(1 - \frac{\ln(\dot{\varepsilon}^p)}{\ln(D_0^p)}\right)^{n_1}\varepsilon^{n_0}\right](1 - T^{*m})e^{c\ln(\dot{\varepsilon})}$
Khan-Liang-Farrokh [97]	$\sigma = \left[\left(a + \frac{k}{d^{n*}}\right) + B\left(\frac{d}{d_0}\right)^{n_2}\left[\left(1 - \frac{\ln(\dot{\varepsilon}^p)}{\ln(D_0^p)}\right)\left(\frac{T_m}{T}\right)\right]^{n_1}(\varepsilon^p)^{n_0}\right]\left(\frac{T_m - T}{T_m - T_{ref}}\right)^m\left(\frac{\dot{\varepsilon}^p}{\dot{\varepsilon}^{p*}}\right)^C$

6. Dynamic recrystallization (DXR)

A brief explanation of this phenomenon has been presented in section 2.2 and in fact DXR has relevance in the case of work-hardened metals undergoing deformations at temperatures in the range of 40 to 50 percent of melting temperature. It has been shown in the preceding sections that this effect has been ignored in most constitutive equations although in high-strain-rate regimes, particularly in adiabatic strain rate regimes the influence of DXR has Andrade (1994) has shown to be important [103] . Andrade (1994) used the JC model due to its popularity and simplicity. In its original version JC equation considers a gradual thermal softening and cannot accommodate sudden flow stress changes due to DXR. This reduction was achieved by incorporating a reduction function *H(T)* which is based on a unit step function of temperature *u(T)* that takes the zero value when the temperature is below a critical DXR temperature Tc (temperature at which the DXR phenomena or phase transformation occurs) or unity when the temperature is larger than Tc, The reducer function is then:

$$H(T) = \frac{1}{1-(1-\bar{H})u(T)} \tag{139}$$

where $\bar{H}$ is a reducer constant. It is expressed by the ratio of the flow stresses just prior to and after the respectively and gives the fractional change in flow stress at the temperature of the critical phenomenon.

The flow stress of the recrystallized material has to be experimentally obtained to be included into the reducer constant. A plot showing that the sudden drop if flow stress due to DXR can be adequately numerically predicted using this method has been presented in Fig. 27 (a). It represents cold- hardened OFHC copper response as a function of temperature for a given strain-rate. Recrystalliztion occurred at 700 ºC and at a plastic strain of 0.3 (the value of the strain-rate has not been reported). Fig. 27 (b) represents the same experiment bu this time presenting the results as a function of strain and temperature. The remarkable agreement obtained between experiment and numerically obtained results show that the DXR effects can be incorporated with good accuracy in constitutive models.

7. Dynamic strength and fracture

It has been shown above that a large number of constitutive models have been developed to simulate the viscoplastic response of metals subject to very high speed impact and intense loading regimes. Most of them do not accurately describe viscoplastic behaviour for strain rates above 10^4 s^{-1} and so some authors developed equations to extend the range of validity of their models to the very high strain rate regime. In the high strain rate regime, single-parameter internal state variable models based on dislocation density are often used. Composite models using two internal variables [104] have also been developed. As explained above, these models are based on glide kinetics that describes the mechanisms of dislocations overcoming obstacles with the assistance of thermal fluctuations. This is valid for applied stresses below the mechanical threshold, corresponding to strain rates not exceeding 10^5 s^{-1}. Above the mechanical threshold the thermally activated dislocation glide no longer controls viscoplastic flow. The production and continuous glide of mobile dislocations that are subject to damping and relativistic effects will be the dominant mechanism. A few constitutive models were proposed, as reviewed above, for the shock loading regime, [6, 35, 37]. Further discussion of these models is available in the literature [2, 63].

Large plastic deformation, large strain rates and temperature softening are generally well described by most constitutive models but a complete treatment of nonlinear response to dynamic loads will have to consider the accumulation of damage and material failure. Two approaches are possible in order to account for damage. In the coupled approach the material damage affects the stress response. Constitutive models including damage can be formulated based on continuum thermodynamics [105] or micro-mechanics of voided materials [106]. Uncoupled methods assume that the stress and strain fields

will remain unaffected by damage. It is clear that damage will introduce some softening in the material and it will be necessary to take into account this softening to be able to capture strain localisation prior to fracture. However, in impact analysis, high strain rates may lead to adiabatic conditions and temperature softening of the material. It follows that it is possible, at least approximately, to describe strain localisation, for instance in adiabatic shear bands, without using a coupled approach if the constitutive equation takes thermal softening into account [107]. The use of coupled models of viscoplasticity to account for damage softening [108, 109] although they provided the best results when compared with experimental data, were found to provide close results to those obtained from uncoupled models [110]. So uncoupled models are often used [107].

A number of models will be capable of predicting the onset of ductile failure when necking appears in the numerical solution. However, in most cases, some form of element deletion will simulate with more realism material rupture under very high loadings. The modelling of failure is rather complex and few models are of practical use but in general there will be a combination of a description of dynamic strain, damage accumulation and failure. So far, various failure criteria have been explored, such as the maximum strain criterion, rupture strain, equivalent plastic work, damage models and energy density models [111].

Impact loading implies large deformations and large strain rates. Each of these poses different demands on the material models used: large deformations require precise descriptions of the yield locus as plastic flow strongly depends on the effects of anisotropy and work hardening. Barlat's models [112] are an example of a set of widely used models for forming applications, where plastic deformations are often large. However, for impact simulations, the dynamic response combined with failure prediction will have to be present in material models. For low strain rates the isotropic von Mises constitutive model or the Gurson model (which proposes a porosity based model in which the yield function is modified by the presence of voids and also describes failure) are often used [113, 114, 115]. Gurson's model (modified by Tvergaard and Needleman) is based on a micromechanical description of growth and nucleation of voids in a rigid-perfectly plastic material. Gurson's model consists of a yield function dependent on hydrostatic pressure and the effective void volume fraction f:

$$\Phi = \frac{q^2}{\sigma_M^2} + 2q_1 f cosh\left(-\frac{3q_2 p}{2\sigma_M}\right) - 1 - (q_1 f)^2 = 0 \quad (140)$$

where σ_M is the actual flow stress in the material, p is the hydrostatic pressure, q is the equivalent von Mises stress and f is the effective void volume fraction which is defined in a cumulative way. The damage evolution consists of void growth due to volumetric plastic straining and nucleation of voids due to deviatoric plastic straining. Void growth is normally the dominant effect in material deterioration under tensile loading. The Gurson method exhibits several problems: it violates the principle of isochoric plastic flow, shows variable values of the plastic Poisson's ratio and cannot describe failure for mean stresses that are near zero or negative. Modifications to the method solved this limitation but made it more difficult to calibrate. These difficulties are avoided by using phenomenological damage models. Of these the Johnson-Cook (JC) is frequently used by researchers. Borvik [108, 109, 110, 116, 117] used the JC coupled constitutive model of viscoplasticity and ductile damage, implemented in the LS-DYNA FEM code. This model assumes that damage accumulates in the material element during straining and that the material breaks when the damage reaches a critical value. In this approach the two equations are coupled, leading to the following unified model:

$$\sigma_{eq} = (1 - D)(A + Br^n)(1 + C \ln \dot{r}^*)(1 - T^{*m}) \quad (141)$$

where D is the damage variable and $r = (1 - D)p$ is the damage-accumulated plastic strain. The model was complemented with an element deletion algorithm that removes elements in which the damage variable reaches a critical value D_c. This approach is perhaps the most widely found in ballistic penetration, blast loading and other high velocity impact problems.

The concept of the damage variable D derives from Continuum Damage Mechanics (CDM) [21, 118] in which it is defined as

$$D = 1 - \frac{A_{eff}}{A_0} \quad (142)$$

where A_0 is the nominal intersection area (the area of a section of a reference volume element isolated in a damaged solid) and A_{eff} is the effective area of resistance (the nominal area reduced by the presence of microdefects such as cracks and cavities). These three variables are referred to a plane (defined by its normal $\boldsymbol{n}$) and a tensor description is often used. Failure occurs when $D = 1$.

The phenomenological JC model was developed during the 1980s to address impact, ballistic penetration and blast loading problems, and has been extensively used by national and military laboratories or private industry to study large strain, high strain rate problems. Its popularity derives from its simplicity and the availability of constants to be used in the equations for a significant number of engineering materials [113, 114]. Physical models very often require constants that are not available and which require complex experimental apparatus to measure them.

The JC model, often known as a viscoplastic constitutive model [92] was also developed as a ductile fracture model [119] that includes the effects of stress triaxiality, temperature, strain rate and strain path on the failure strain. It is also a cumulative model in which the material will break when damage reaches a critical value. The expression for the JC fracture strain is

$$p_f = (D_1 + D_2 \exp(D_3\sigma^*))(1 + D_4 \ln \dot{p}^*)(1 + D_5 T^*) \tag{143}$$

where D_1 to D_5 are material constants, $\sigma^* = \sigma_m/\sigma_{eq}$ is the stress triaxiality ratio and σ_m is the mean stress. Failure occurs when a damage variable defined as $D = \sum \Delta p/p_f$ reaches unity, where Δp is the increment of effective plastic strain during a load increment. Some drawbacks exist, however: Lesuer (2001) [114] noted that the JC constitutive model was unable to predict the correct variations of flow stress with strain rate. The model predicted for titanium, in compression, a significantly higher ductility than experimentally observed and the numerically obtained tensile failure strain was also significantly higher than the experimentally observed values. For a 6061-T6 alloy significant deviations were noted for the strength increase when the strain rate changes to values above 10^3 s^{-1}, where the experimental values show a pronounced increase (see Fig. 28). These results form two different deformation mechanisms for low and high deformation rates. Different deformation rate equations were developed to represent the two phenomena [115]. Spranghers [117] also reported that generally, the plastic strain is incorrect due to the incorrect hardening parameters obtained from the literature, leading to incorrect modelling of the yielding behaviour. Since the analysis is transient and plastic deformation occurs first, errors are cumulative, resulting in an incorrect amount of plastic deformation.

All this research in constitutive modelling and failure models is often applied to plates as impulsive loading of plated structures (vehicles or facilities) is an actual concern for engineers and a brief note on the subject follows.

A significant research effort on impulsive loading on plates and beams has been reported in recent decades [120, 121] attempting to model the large inelastic responses observed. In the 1990s investigations began to include other effects such as boundary conditions, plate stiffening and loading conditions to predict not only deformation but also tearing [122, 123, 124, 125]

It is important to refer the seminal work of Menkes and Opat [126] on beams subjected to blast loads. It was one of the first studies that considered loading up to rupture or tearing at the support points of the structure. Three different failure modes were identified for beams:

Mode I – Large inelastic deformation;

Mode II – Tearing in the outer fibres at supports;

Mode III – Transverse shear failure at the supports.

These modes of failure have been found to also apply to plates [122, 127] but for the square plates' case it was found that mode II failure occurs first in the centre of the sides and then progresses to the corners with increasing impulse [124, 127]. This finding led to some additions to Mode II failure [125]:

Mode II* – Partial tearing at the boundary

Mode IIa – Complete tearing with increasing mid-point displacement

Mode IIb – Complete tearing with decreasing mid-point displacement

Other subdivisions were identified for localised loading conditions such as those proposed by Nurick and co-workers [123] and these modes of failure can be identified in many published experimental results, e.g. [128]. Failure in plates subjected to blast or impact loading is not limited to Modes II or III ductile fracture because some other forms of tearing (e.g. petalling or dishing) may also occur. Tearing was predicted using the CTOD criterion [129] or considering the equivalent plastic strain times the average stress triaxiality [130, 131]. Based on the critical damage value, calculated distributions and

histories of stress and strain, Lee and Wierzbicki (2005) [130, 131] observed that crack length and final deformed shapes of plates are strongly influenced by the spatial distribution and intensity of impulsive loading.

Many experimental results for stiffened plates have been reported in the last few decades [132, 133, 135, 135]. Some of these researchers did not include strain rate or temperature effects in their numerical models. Instead they used (a) an energy balance equation to assess plate or beam inelastic response and tearing [136], (b) the deflecton theory of von Karman and the von Mises yield criterion [137], or (c) use rigid-plastic methods [111, 127, 132, 133, 138, 139, 140, 141]. These methods were shown to give good agreement when the ratio of initial kinetic energy to elastic strain energy is larger than 10 and the load duration is sufficiently short with respect to the natural period of the structure [142].

Another field of interest for ductile failure models (and also under intense investigation) is plate penetration and plugging in ballistic problems [109, 143]. Most work on terminal ballistics has been based on the Johnson-Cook fracture criterion [110, 143, 144, 145, 146, 147, 148, 149, 150]. Sorensen (2008) [149] used the Johnson-Cook damage-accumulation fracture model in conjunction with a threshold maximum tensile stress criterion and a Weibull statistical distribution for the initial failure strain for a 7039 aluminium alloy target material. This allowed the representation of a non-uniform, stochastic failure of the aluminium plate.

When damage of a material occurs, the stress-strain relationship does not accurately represent its behaviour. The use of a true stress-strain relation during material damage introduces strong mesh dependency in results based on strain localisation such that the energy dissipated decreases as the mesh is refined. A fracture energy approach reduces mesh dependency by creating a stress-displacement response after the damage is initiated. The energy required to open a unit area of crack, G_f, may be defined as

$$G_f = \frac{\sigma_{y0}\bar{u}_f^{pl}}{2} \tag{144}$$

where σ_{y0} is the ultimate stress and $\bar{u}_f^{pl}$ is the equivalent plastic displacement failure. With this approach the softening response after damage initiation will be characterised by a stress-displacement response rather than a stress-strain response. However, in the majority of published work, the use of constitutive

models and fracture strain models has been frequently preferred. Due to its simplicity the Johnson-Cook constitutive model and fracture strain model [80, 119] combined with ductile damage mechanics [105] to include material degradation due to damage into the model is the mostly widely present in the available published work involving impact loads. This constitutive equation can be used uncoupled or coupled with different physical phenomena such as damage, temperature and strain-rate. The full model includes linear thermoelasticity, von Mises yield criteria, an associated flow rule, isotropic strain hardening, strain-rate hardening, softening due to adiabatic heating, softening due to isotropic damage evolution and a fracture criterion. Coupling the model with an element-kill algorithm that removes damaged elements from the mesh when the damage variable reaches a critical value may also be adopted to speed up calculations [110].

Other authors, particularly in investigations concerning blast-loaded plates, followed a different approach to add strain rate effects by adjusting the yield stress σ_y, in the finite element analysis, with a Cowper-Symonds relation [111, 122, 123, 124, 151, 152, 153]:

$$\sigma_y = \sigma_0\left[1 + \dot{\varepsilon}/D^{1/n}\right] \tag{145}$$

where *D* and *n* are material parameters. These methods are either based on von Mises plasticity with isotropic hardening/softening behaviour [138] or on plastic work criteria, as rigid-plastic methods are shown to give design level accurate estimates for the response of structures subjected to blast loads [155]. Another approach using fictitious stiff springs at the plate boundary [155] to simulate the variation of the transverse shear stress along that boundary was used to predict Modes II and III failure. Elastic analysis of blast loaded square plates assuming large deflections has also been addressed [156]. It is evident that the range of approaches used to tackle blast-loaded plates is quite wide.

Rigid-plastic methods can predict the maximum loads which cause failure due to excessive transverse shear forces on the material. These shear forces play an important role in the process of failure but they add complexity to the analysis [124]. It has been reported [122] that boundary conditions may determine the tearing mechanism at the plate boundaries. This was investigated for clamped circular plates [123] and for rectangular plates [157] showing that thinning and rupture are highly dependent on

the boundary fixation conditions. Mode I predictions were in good agreement with experimental results but for other modes of failure, variations were observed.

For engineering purposes more straightforward solutions can be obtained by means of equivalent single-degree-of-freedom (SDOF) systems, also known as spring-mass systems or modal approximations methods [134], but these are outside the scope of this review.

8. Conclusion

A review of constitutive models highlighting their main assumptions and features as been presented, together with a brief summary of available methodologies for the analysis of ductile failure. Application to plates was also highlighted which gave some indication on the constitutive modelling methods that are being preferred for these analysis. Theoretical derivations have been developed but at present numerical modelling is used most of times to predict material response. The empirical models are simpler and do not call for an understanding of the physical foundation of the phenomena being simulated. Regression analysis is used to determine the parameters necessary to run the models. The study of a particular material led many users to introduce modification to improve the correlation between experimental data and numerical results. This had resulted in many variations of the models, in particular of the JC equation, one of the most widely cited and used. Typically regression models tend to be accurate only within the range of the data used to calibrate the model, which limits the generality of such models. Also the coupling effects between the influencing factors that affect flow stress (e.g. temperature, strain and strain-rate) must be considered in future models or refinements of existing ones. Obviously future models may become more difficult to implement and might need much more testing to obtain the required data to run them, and this will challenge researchers as industry will maintain a need for simple and more straightforward techniques to use in engineering work.

Physically-based models take into account the thermal deformation mechanism of the material under deformation. Work hardening due to dislocations and their interactions and dynamic softening resulting from temperature increase will result in opposing effects special in hot deformation processes, which remains a field of intense investigation in pursuit of constitutive equations that can adequately models both effects. The solid physical foundation of these models makes them more suitable for certain loading regimes but many of them include parameters that require specialized laboratory equipment to determine them. Their implementation in hydrocodes is therefore difficult.

The prediction of ductile fracture and the development of criteria to predict the fracture processes associated with large plastic deformation and high strain rates are essential for the analysis of

structures subject to blast load. Macroscopic quantities, such as the strain-energy density, have been proposed but in general it is difficult to base predictions on single parameter models.

Future work will resort more often to technology. For instance shock pressure driven by Laser are being used to study the dynamic yield strength of metals using in-situ X-Ray diffraction [158][159]. This shows that on-going research is increasingly sophisticated and continuously in pursuit of the most accurate knowledge on dynamic viscous-plasticity and strength.

Bibliography

[1] Zukas, J. (2004). *Introduction to Hydrocodes.* Baltimore: Elsevier.

[2] Remington, B., Allen, P., Bringa, E., & Hawreliak, J. (2006). Material dynamics under extreme conditions of pressure and strain rate. *Materials Science and Technology, 4*, pp. 474-488.

[3] Chaboche, J. (2008). A review of some plasticity and viscoplasticity constitutive theories. *International Journal of Plasticity, 24*, pp. 1642-1693.

[4] Lee, B. J., Ahzi, S., & Asaro, R. J. (1995). On the plasticity of low symmetry crystals lacking five independent slip systems. *Mechanics of Materials, 20*, pp. 1-8.

[5] Armstrong, R., & Walley, S. (2008). High strain rate properties of metals and alloys. *Internatiional Materials Review, 53-No-3*, pp. 105-127.

[6] Preston, D., Tonks, D., & Wallace, D. (2003). Model of plastic deformation for extreme loading conditions. *Journal of Applied Physics, 93*, pp. 211-220.

[7] Meyers, M. (1994). *Dynamic behaviour of materials.* John Wiley & Sons.

[8] Read, H., Triplett, J., & Cecil, R. (1970). *Dislocation dynamics and the formulation of constitutive equations for rate-dependent plastic flow in metals.* Defense Atomic Support Agency, 01-70-C-0055.

[9] Klepaczko, J. (1974). *Thermally activated flow and strain rate history effects for some polycrystalline FCC metals.* Providence: Brown University - Divisio of Engineering.

[10] Walley, S., Church, P., Townsley, R., & Field, J. (2000). Validation of a path-depemdent constitutive model for FCC and BCC metals using "symmetric" Taylor impact. *Journal Pfysics IV France, 10*, pp. 69-73.

[11] Gould, P., & Goldthorpe, B. (2000). A path-dependent sonstitutive model for gilding copper. *Journal of Physics IV France, 10*, pp. 39-45.

[12] Meyers, M., Benson, D., Voringer, O., Kad, B., Xue, Q., & Fu, H.-H. (2002). Constitutive description of dynamic deformation: physically-based mechanisms. *Materials Science and Engineering A, 322* , pp. 194-216.

[13] Perzyna, P. (1988). Temperature and rate dependent theory of plasticity of crystalline solids. *Revue de Physique Appliquée, 23*, pp. 445-459.

[14] Nemat-Nasser, S., & Li, Y. (1998b). Flow stress of FCC polycrystals with application to OFHC Cu. *Acta Materiallia, 46*, pp. 565-577.

[15] Murr, L., Meyers, M., Niou, C., Chen, Y., Pappu, S., & Kennedy, C. (1997). Shock-induced deformation twinning in tantalum. *Acta Materialia, 45*, pp. 145-175.

[16] Kocks, U. (2001). Realistic constitutive relations for metal plasticity. *Material Sciences and Engineering A, 317*, pp. 181-187.

[17] Follansbee, P., & Kocks, U. (1988). A constitutive description of the deformation of copper based on the use of the mechanical threshold stress as an internal state variable. *Acta Metall., 36*, pp. 81-93.

[18] Sung, J., Kim, J., & Wagoner, R. (2010). A plastic constitutive equation incorporating strain, strain-rate, and temperature. *International Journal of Plasticity, 26*, pp. 1746-1771.

[19] Voyiadjis, G., & Almasri, A. (2008). A physically based constitutive model for FCC metals with applications to dynamic hardness. *Mechanics of materials, 40*, pp. 549-563.

[20] Panov, V. (2006). *Modelling of behaviour of metals at high strain rates.* Cranfield University.

[21] Lemaitre, J., & Chaboche, J. L. (1990). *Mechanics of Solid Materials.* Cambridge University Press.

[22] Rice, J. (1971). Inelastic constitutive relations for solids: an internal-variable theory and its application ro metal plasticity. *Journal of Mechanics and Physics of Solids, 19*, pp. 433-455.

[23] Gao, C., & Zhang, L. (2012). Constitutive modelling of plasticity of FCC metals under extremely high strain rates. *International Journal of Plasticity, 32-33*, pp. 121-133.

[24] Lin, Y., & Chen, X. (2011). A critical review of experimental results and constitutive descriptions for metals and alloys in hot working. *Materials and design, 32*, pp. 1733-1759.

[25] Gronostajski, Z. (2000). The constitutive equations for FEM analysis. *Journal of Materials Processing Technology, 106*, pp. 40-44.

[26] Etse, G., & Carosio, A. (1999). Constitutive equations and numerical approaches in rate dependent material formulations. *MECOM99.*

[27] Cheng, Y., Zhang, H., Chen, Z., & Xian, K. (2008). Flow stress equationof AZ31 magnesium alloy sheet during warm tensile deformation. *Journal of Processing Technology, 208*, pp. 29-34.

[28] Taylor, G. (1934). The mechanism of plastic deformation of crystals. Part I.-Theoretical. *Proceedings of the Royal Society of London A, 145*, pp. 362-387.

[29] Taylor, G. (1938). Plastic Strain in metals. *Journal of the Institute of Metals , 62*, pp. 308-324.

[30] Bodner, S., & Partom, Y. (1975). Constitutive equations for elastic viscoplastic strain-hardening materials. *Journal of Applied Mechanics*, pp. 385-389.

[31] Liang, R., & Khan, A. (1999). A critical review of experimental results and constitutive models for BCC and FCC metals over a wide range of strain rates and temperatures. *International Journal of Plasticity, 15*, pp. 963-980.

[32] Chen, S., Huang, C., Wang, C., & Duan, Z. (2008). Mechanical properties and constitutive relationships of 30CrMnSiA steel heated at high rate. *Materials Science and Engineering A, 483-484*, pp. 105-108.

[33] Song, S., Duan, Z., & Tan, D. (2001). The application of B-P constitutive equations in finite element analysis of high velocity impact. *International Journal of Solids and Structures, 38*, pp. 5215-5222.

[34] Wilkins, M., & Guinan, M. (1973). Impact of cylinders on a rigid boundary. *Journal of Applied Physics, 44*, pp. 1200-1206.

[35] Steinberg, D., Cochran, S., & Guinan, M. (1980). A constitutive model for metals applicable at highstrain rate. *Journal of Applied Physics, 51*, pp. 1498-1504.

[36] Hoge, K., & Mukherjee, A. (1977). The temperature and strain rate dependence of the flow stress of tantalum. *Journal of Materials Science, 12*, pp. 1888-1672.

[37] Steinberg, D., & Lund, C. (1989). A constitutive model for strain rates from 10-4 to 106 s-1. *Journal of Applied Physics, 65*, pp. 1528-1533.

[38] Zerilli, F., & Armstrong, R. (1987). Dislocation mechanicas based constitutive relations for material dynamics calculations. *Journal of Applied Physics, 61*, pp. 1816-1825.

[39] Zhang, H., Wen, W., Cui, H., & Xu, Y. (2009). A modified Zerilli-Armstrong model for alloy IC10 over a wide range of temperatures and strain rates. *Materials Science and Engineering A, 527*, pp. 328-393.

[40] Samantaray, D., Mandal, S., Borah, U., Bhaduri, A., & Sivaprasad, P. (2009). A thermo-viscoplastic constitutive model to predict elevated-temperature flow behaviour in a titatnium-modified austenitic stainless steel. *Materials Science and Engineering A, 526*, pp. 1-6.

[41] Lee, W., & Liu, C. (2006). The effects of temperature and starin rate on the dynanic flow behaviour of different steels. *Materials Science and Engineering A, 426*, pp. 101-113.

[42] Abed, F., & Voyiadjis, G. (2005). A consistent modified Zerilli-Armstrong flow stress model for BCC and FCC metals for elevated temperatures. *Acta Mechanica, 175*, pp. 1-18.

[43] Meyer, J. H. (2006). *A modified Zerilli-Armstrong constitutive model describing the strength and localizing behaviour of Ti-6Al-4V.* Army Research Laboratory, Aberdeen Proving Ground.

[44] Gao, C., & Zhang, L. (2010). A constitutive model for dynamic plasticity of FCC metals. *Materials Science and Engineering A, 527*, pp. 3138-3143.

[45] Mecking, H., & Kocks, U. (1981). Kinetics of flow and strain-hardening. *Acta Metallurgica, 29*, pp. 1865-1875.

[46] Dorward, R., & Hasse, K. (1995). Strain rate effects on tensile deformation of 2024-0 and 7075-0 aluminum alloy sheet. *Journal of Materials Enginnering and Performance, 4*, pp. 216-220.

[47] Zhao, H., & Gary, G. (1995). The testing and behaviour modelling of sheet metals at strain rates from 10-4 to 104 s-1. *Materials Science and Engineering A, 207*, pp. 46-50.

[48] Banerjee, B. (2007). The mechanical threshold stress model for various tempers of AISI 4340 stell. *International Journal of Solids and Structures, 44*, pp. 834-859.

[49] Nemat-Nasser, S., & Okinaka, T. (1996). A new computational approach to crystal plasticity:FCC single crystal. *Mechanics of Materials, 24*, pp. 43-57.

[50] Nemat-Nasser, S., & Isaacs, J. (1997). Direct measurement of isothermal flow stress of metals at elevated temperatures and high strain rates with application to Ta and Ta-W alloys. *Acta Materialia, 45*, pp. 907-919.

[51] Nemat-Nasser, S., Okinawa, T., & Ni, L. (1998c). A physically-based constitutive model for BCC crystals with application to polycristalline tantalum. *Journal of Mechanics and Physics of Solids, 46*, pp. 1009-1038.

[52] Guo, W., Zhang, X., Su, J., Su, Y., Zeng, Z., & Shao, X. (2011). The characteristics of plastic flow and a physically-based model for 3003 Al-Mn alloy upon a wide range of strain rates and temperatures. *European Journal of Machanics A/Solids, 30*, pp. 54-62.

[53] Nemat-Nasser, S., Ni, L., & Okinawa, T. (1998a). A constitutive model for FCC crystals with application to polycrystalline OFHC copper. *Mechanics of Materials, 30*, pp. 325-341.

[54] Nemat-Nasser, S., Guo, W., & Liu, M. (1999a). Experimentally-based micromechanical modelling of dynamic response of molybdenum. *Scripta Materialia, 40*, pp. 859-872.

[55] Nemat-Nasser, S., Guo, W., & Cheng, J. (1999b). Mechanical properties and deformation mechanisms of a commercially pure titanium. *Acta Materialia, 47*, pp. 3705-3720.

[56] Nemat-Nasser, S., Guo, W., & Kihl, D. (2001). Thermomechanical response of AL-6XN stainless steel over a wide range of strain rates. *Journal of the Mechanics and Physics of Solids, 49*, pp. 1823-1846.

[57] Follansbee, P. (1985). *High strain rate deformation in FCC metals and alloys.* Los Alamos National Laboratory.

[58] Kim, J., & Shin, H. (2009). Comparison of plasticity models for tantalum and a modification of the PTW model for wide ranges of strain, strain rate, and tyemperature. *International Journal of Impact Engineering, 36*, pp. 746-753.

[59] Rusinek, A., & Klepaczko, J. (2001). Shear testing of a sheet steel at wide range of strain rates and a constitutive relation with strain-rates and temperature dependence of the flow stress. *International Journal of Plasticity, 17*, pp. 87-115.

[60] Rusinek, A., & Rodriguez-Martinez, J. (2009). Thermo-viscoplastic constitutive relation for aluminium alloys, modeling of negative strain rate sensitivity and viscous drag effects. *Materials and Design, 30*, pp. 4377-4390.

[61] Rusinek, A., Rodriguez-Martinez, J., & Arias, A. (2010). A thermo-viscoplastic constitutive model for FCC metals with application to OFHC copper. *International Journal of Mechanical Sciences, 52*, pp. 120-135.

[62] Kapoor, R., & Nemat-Nasser, S. (2000). Comparison between high strain-rate and low strain-rate deformation of tantalum. *Metall. Mater. Trans. A, 31*, pp. 815-823.

[63] Rodriguez-Martinez, J., Rusinek, A., & Arias, A. (2011). Thermo-viscoplastic behaviour of 2024-T3 aluminium sheets subjected to low velocity perforation at different tempratures. *Thin-Walled structures, 49*, pp. 819-832.

[64] Austin, R., & McDowell, D. (2011). A dislocation-based constitutive model for viscoplastic deformation of FCC metals at very high strain rates. *International Journal of Plasticity, 27*, pp. 1-24.

[65] Armstrong, R., Arnold, W., & Zerilli, F. (2007). Dislocation mechanics of shock-induced plasticity. *Metallurgical and Materials Transactions A, 38A*, pp. 2605-2610.

[66] Armstrong, R., Arnold, W., & Zerilli, F. (2009). Dislocation mechanics of copper and iron in high rate deformation tests. *Journal of Applied Physics, 105*, pp. 23511-1: 23511-7.

[67] Austin, R., & McDowell, D. (2012). Parametrization of a rate-dependent model of shock-induced plasticity for copper, nickel, and aluminum. *International Journal of Plasticity, 32-33*, pp. 134-154.

[68] Molinari, A., & Ravichandran, G. (2005). Constitutive modeling of high-strain-rate deformation in metals based on the evolution of an effective microstructural length. *Mechanics of Materials, 37*, pp. 737-752.

[69] Clausen, A., Borvik, T., Hopperstad, O., & Benallal, A. (2004). Flow and fracture characteristics of aluminium alloy AA5083-H116 as function of strain rate, temperature and triaxaiality. *Materials Science and Engineering, A364*, pp. 260-272.

[70] Zhang, S., McCormick, P., & Estrin, Y. (2001). The morphology of Portevin-Le Chatelier bands: finite element simulation for Al-Mg-Si. *Acta Materialia, 49*, pp. 1087-1094.

[71] Voyiadjis, G., & Abed, F. (2005). Microstructural based models for BCC and FCC metals with tempearature and strain rate dependency. *Mechanics of materials, 37*, pp. 355-378.

[72] Kocks, U., & Mecking, H. (2003). Physics and ohenomenology of strain hardening: the FCC case, Progress in Material Science. *48*, pp. 171-273.

[73] Holmedal, B. (2007). On the formulation of the mechanical threshold stress model. *Acta Materiallia, 55*, pp. 2739-2746.

[74] Forde, L., Walley, S., Peyton-Jones, M., Proud, W., Cullis, I., & Church, P. (2009). The use of symetric Taylor impact to validadte constitutive models for an FCC metal (copper) and a BCC alloy (RHA steel). In E. Sciences (Ed.), *DYMAT*, (pp. 1245-1250).

[75] Forde, L., Proud, W., & Walley, S. (2009). Symmetrical Taylor Impact studoes on copper. *Proceedings of the Royal Society, 465*, pp. 769-790.

[76] Khan, A., & Huang, S. (1992). Experimental and theoretical study of mechanical behaviour of 1100 aluminum in the strain rate range 10-5 - 104 s-1. *International Journal of Plasticity, 8*, pp. 397-424.

[77] Durrenberger, L., Molibnari, A., & Rusinek, A. (2008). Internal variable modeling of the high strain-rate behavior of metals with applications to multiphase steels. *Materials Science and Engineering A, 478*, pp. 297-304.

[78] Johnson, G., & Cook, W. (1983). A constitutive model and data for metals subjected to large strains, high strain rates and high temperatures. *Proceedings of the Seventh International Symposium on Ballistics, The Hague, 19-21 April 1983, Netherlands*, pp. 541-548.

[79] Borvik, T., Hopperstad, O., Berstad, T., & Langseth, M. (2001a). A computational model of viscoplasticity and ductile damage for impact and penetration. *Eur. J. Mech. A/Solids, 20*, pp. 685-712.

[80] Rule, W., & Jones, S. (1998). A revised form for the Johnson-Cook strength model. *International Journal of Impact Engineering, 21*, pp. 609-624.

[81] Zhang, H., Wen, W., & Cui, H. (2009). Behaviours of IC10 alloy over a wide range of strain rates and temperatures: Experiments and modeling. *Materials Science and Engineering A, 504*, pp. 99-103.

[82] Vural, M., & Cairo, J. (2009). Experimental analysis and constitutive modeling for the newly developed 2139-T8 alloy. *Materials Science and Engineering A, 520*, pp. 56-65.

[83] Lin, Y., Xia, Y., Chen, X., & Chen, M. (2010). Constitutive descriptions for hot compressed 2124-T851 aluminum alloy over a wide range of temperature and strain rate. *Computationla Materials Science, 50*, pp. 227-233.

[84] Lin, Y., Chen, X., & Liu, G. (2010). A modified Johnson-Cook model for tensile behaviors of typical high-strength alloy steel. *Materials Science and Engineering A, 527*, pp. 6980-6986.

[85] Shin, H., & Kim, J. (2010). A phenomenological constitutive equation to describe various flow stress behaviors of materials in wide strain rate and temperature regimes. *Journal of Engineering Materials and Technology, 132(2):021009*.

[86] Wang, Y., Zhou, Y., & Xia, Y. (2004). A constitutive description of tensile behaviour for brass over a wide range of strain rates. *Materials Science and Engineering A, 372*, pp. 186-190.

[87] Hou, Q., & Wang, J. (2010). A modified Johnson-Cook constitutive model for Mg-Gd-Y alloy extended to a wide range of temperatures. *Computational Materials Science, 50*, pp. 147-152.

[88] Lin, Y., & Chen, X. (2010). A combined Johnson-Cook and Zerilli-Armstrong model for hot compressed typical high-strength alloy steel. *Computational Materials Science, 49*, pp. 628-633.

[89] Lin, Y., Li, Q., Xia, Y., & Li, L. (2012). A phenomenological constitutive model for high temperature flow stress precistion of Al-Cu-Mg alloy. *Materials Science and Engineering A, 534*, pp. 654-662.

[90] Khan, A., & Liang, R. (1999). Behaviours of three BCC metal over a wide range of strain rates and temperatures: experiments and modeling. *International Journal of Plasticity, 15*, pp. 1089-1109.

[91] Khan, A., & Liang, R. (2000 a). Behaviours of three BCC metals during non.proportional multi-axial loadings: experiments and modeling. *International Journal of Plasticity, 16*, pp. 1443-1458.

[92] Khan, A., Zhang, H., & Takacs, L. (2000 b). Mechanical response and modeling of fully compacted nanocrystallin iron and copper. *International Journal of Plasticity, 16*, pp. 1459-1476.

[93] Khan, A., Suh, Y., & Kazmi, R. (2004). Quasi-static and dynamic loading responses and constitutive modeling of titanium alloys. *International Journal of Plasticity, 20*, pp. 2233-2248.

[94] Khan, A., Suh, Y., Chen, X., Takacs, L., & Zhang, H. (2006). Nanocrystalline aluminium and iron: Mechanical behaviour at quasi-static and high strain rates, and constitutive modeling. *International Journal of Plasticity, 22*, pp. 195-209.

[95] Khan, A., & Zhang, H. (2000c). Mechanically alloyed nanocrystalline iron and copper mixture: behaviour and constitutive modelung over a wide range of strain rates. *International Journal of Plasticity, 16*, pp. 1477-1492.

[96] Yu, H., Guo, Y., Zhang, K., & Lai, X. (2009). Constitutive model on the description of plastic behaviour of DP600 steel at strain rate from 10-4 to 103 s-1. *Computational Materials Science, 46*, pp. 36-41.

[97] Farrokh, B., & Khan, A. (2009). Grain size, strain rate, and temperature dependence of flow stress in ultra-fine grained and nanocrystalline Cu and Al: Synthesis, experiment, and constitutive modeling. *International Journal of Plasticity, 25*, pp. 715-732.

[98] Voce,E. (1948). The relationship between stress and strain for homogeneous deformation. *Journal of the Institute of Metals, 74*, pp. 537-556.

[99] Kocks, U. (1976). Laws for work-hardening and low temperature creep. *Journal of Engineering Materials and Technology*, pp. 76-85.

[100] Naderi, M., Durrenberger, L., Molinari, A., & Bleck, W. (2008). Constitutive relationships for 22MnB5 boron steel deformed isothermally at ahigh temperatures. *Materials Science and Engineering A, 478*, pp. 130-139.

[101] Lin, Y., Chen, M., & Zhong, J. (2008). Constitutive modeling for elevated temperature flow behaviour of 42CrMo steel. *Computational Materials Science, 42*, pp. 470-477.

[102] Lin, Y., & Liu, G. (2010). A new mathematical model for predicting flow stress of typical high-strength alloy steel at elevated high temperature. *Computational Materials Science, 48*, pp. 54-58.

[103] Andrade U R et al. (1994). Cosntitutive description of work-and shock-hardened copper. *Scripta Metallurgica et Materialia*, 30, pp. 933-938.

[104] Nes, E. (1998). Modelling of work hardening and stress saturation in FCC metals. *Progress in Materials Sciences, 41*, pp. 129-193.

[105] Lemaitre, J. (1992). *A course on damage mechanics.* Springer-Verlag.

[106] Gurson, A. (1977). Continuum theory of ductile rupture by void nucleation and growth: Part 1 - Yield criteria and flow rules for porous ductile media. *Journal of Engineering Materials and Technology*, pp. 1-15.

[107] Borvik, T., Hopperstad, O., & Berstad, T. (2003). On the influence of stress strain triaxiality and strain rate on the behaviour of a structural steel. part II. Numerical study. *European Journal of Mechanics A/Solids, 22*, pp. 15-32.

[108] Borvik, T., Langseth, M., Hopperstad, O., & Malo, K. (1999). Ballistic penetration of steel plates. *International Journal of Impact Engineering, 22*, pp. 855-886.

[109] Borvik, T., Hopperstad, O., Berstad, T., & Langseth, M. (2001). Numerical simulation of plugging failure in ballistic penetration. *International Journal of Solids and Structures, 38*, pp. 6241-6264.

[110] Borvik, T., Hopperstad, O., Berstad, T., & Langseth, M. (2001b). Numerical simulation of plugging failure in ballistic penetration. *International Journal of Solids and Structures, 38*, pp. 6241-6264.

[111] Yuen, S., & Nurick, G. (2005). Experimental and numerical studies on the response of quadrangular stiffened plates. part I: subjected to uniform blast load. *International Journal of Impact Engineering, 31*, pp. 55-83.

[112] Barlat, F., & Lian, J. (1989). Plastic behaviour and stretchability of sheet metals. Part I: A Yield function for orthotropic sheets under plane stress conditions. *UInternational Journal of Plasticity, 5*, pp. 51-66.

[113] Neukamm, F., Feucht, M., & Haufe, A. (2008). Consistent damage modelling in the process chain of forming to crashworthiness simulations. *LS-DYNA Anwenderforum.* Bamberg.

[114] Lesuer, D., Kay, G., & LeBlanc, M. (2001). Modeling large-strain, high rate deformation in metals. *Third Biennal Tri-Laboratory Engineering Conference Modeling and Simulation.* Pleasanton: Lawrence Livermore National Laboratory.

[115] Lesuer, D., Kay, G., & LeBlanc, M. (2001). *Modellng large-strain, high rate deformation in metals.* Lawrence Livermore National Laboratory, UCRL-JC-134118.

[116] Bovirk, T., Hassen, A., Dey, S., Langberg, H., & Langseth, M. (2008). On the ballistic and blastload response of a 20 ft ISO container protected with aluminium panels filled with a local mass - Phase I: Design of protective system. *Engineering Structures, 30*, pp. 1605-1620.

[117] Spranghers, K., Vasilakos, I., Lecompte, D., Sol, H., & Vantomme, J. (2013). Numerical simulation and experimental validation of the dynamic response of aluminum plates under free air explosions. *International Journal of Impact Engineering, 54*, pp. 83-95.

[118] Bonora, N. (1997). A nonlinear CDM model for ductile failure. *Engineering Fracture mechanics, 58*, pp. 11-28.

[119] Johnson, G., & Cook, W. (1985). Fracture characteristics of three metals subjected to various strains, strain rates , temperatures and pressures. *Engineering Fracture mechanics, 21 No. 1*, pp. 31-48.

[120] Nurick, G., & Martin, J. (1989a). Deformation of thin plates subjected to impulsive loading - A review Part I: Theoretical considerations. *International Journal of Impact Engineering, 8*, pp. 159-170.

[121] Nurick, G., & Martin, J. (1989b). Deformation of thin plates subjected to impulsive loading - A review Part II: Experimental studies. *International Journal of Impact Engineering, 8*, pp. 171-186.

[122] Teeling-Smith, R., & Nurick, G. (1991). The deformation and tearing of thin circular plates subjected to impulsive loads. *International Journal of Impact Engineering, 11*, pp. 77-91.

[123] Nurick, G., Gelman, M., & Marshall, N. (1996a). Tearing of blast loaded plates with clamped boundary conditions. *International Journal of Impact Engineering, 18*, pp. 803-827.

[124] Olson, M., Nurick, G., & Fagnan, J. (1993). Deformation and rupture of blast loaded square plates - predictions and experiments. *International Journal of Impact Engineering, 13*, pp. 279-292.

[125] Nurick, G., & Shave, G. (1996b). The deformation and tearing of thin square plates subjected to impulse loads - an experimental study. *Internatiional Journal of Impact Engineering, 18*, pp. 99-116.

[126] Menkes, S., & Opat, H. (1973). Tearing and Shear Failures in Explosively Loaded Clamped Beams. *Exp. Mech., Vol.13*, pp. 480-486.

[127] Nurick, G., Olson, M., Fagnan, J., & Levin, A. (1995). Deformation and tearing of blast-loaded stiffened square plates. *Internatiional Journal of Impact Engineering, 16*, pp. 273-291.

[128] Kazemahvazi, S., Radford, D., Deshpande, V., & Fleck, N. (2007). Dynamic failure of clamped circular plates subjected to an underwater shock. *Journal of Mechanics of materials and Structures, 2*, pp. 2007-2013.

[129] Wierzbicki, T. (1999). Petalling of plates under explosive and impact loading. *International Journal of Impact Engineering, 22*, pp. 935-954.

[130] Lee, Y.-W., & Wierzbicki, T. (2005b). Fracture prediction of thin plates under localized impulsive loading. Part II: discing and petalling. *International Journal of Impact Engineering, 31*, pp. 1277-1308.

[131] Lee, Y.-W., & Wierzbicki, T. (2005a). Fracture prediction of thin plates under localized impulsive loading. Part I: dishing. *International Journal of Impact Engineering, 31*, pp. 1253-1276.

[132] Schubak, R., Olson, M., & Anderson, D. (1993a). Rigid-plastic modelling of blast-loaded stiffened plates - part I: One way stiffened plates. *International Journal of Mechanical Sciences, 35*, pp. 289-306.

[133] Schubak, R., Olson, M., & Anderson, D. (1993b). Rigid-plastic modelling of blast-loaded stiffened plates - part I: Partial end fixity, rate effects and two-way stiffened plates. *International Journal of Mechanical Sciences, 35*, pp. 307-324.

[134] Schleyer, G., Hsu, S., White, M., & Birch, R. (2003). Puilse pressure loading of clamped mild steel plates. *International Journal of Impact Engineering, 28*, pp. 223-247.

[135] Pan, Y., & Louca, L. (1999). Experimental and numerical studies on the response of stiffened plates subjected to gas explosions. *journal of Constructional Steel Research, 52*, pp. 171-193.

[136] Yu, J., & Jones, N. (1989). Numerical simulation of a clamped beam under impact loading. *Computers and Structures, 32*, pp. 281-293.

[137] Koko, T., & Olson, M. (1991). Non-linear analysis of stiffened plates using super elements. *International Journal for Numerical Methods in Engineering, 31*, pp. 319-343.

[138] Balden, V., & Nurick, G. (2005). Numerical simulation of the post-failure motion of steel plates subjected to blast loading. *International Journal of Impact Engineering, 32*, pp. 14-34.

[139] Langdon, G., Yuen, S. K., & Nurick, G. (2005b). Experimental and numerical studies on the response of quadrangular stiffened plates. Part II: localised blast loading. *International Journal of Impact Engineering*, pp. 85-111.

[140] Langdon, G., & Schleyer, G. (2005a). Inelastic deformation and failure of profiled stainless steel blast wall panels. part I: analytical modelling considerations. *International Journal of Impact Engineering, 31*, pp. 371-399.

[141] Langdon, G., & Schleyer, G. (2006). Deformation and failure of profiled stainless steel blast wall panels. part III: finite element simulations and overall summary. *International Journal of Impact Engineering, 32*, pp. 988-1012.

[142] Jones, N., Uran, T., & Tekin, S. (1970). The dynamic plastic behaviour of fully clamped rectangular plates. *International Journal of Solids Structures, 6*, pp. 1499-1512.

[143] Iqbal, M., Khan, S., Ansari, R., & Gupta, N. (2013). Experimental and numerical studies of double-nosed projectile impact on aluminum plates. *International Journal of Impact Engineering, 54*, pp. 232-245.

[144] Abdulhamid, H., Kolopp, A., Bouvet, C., & Rivallant, S. (2013). Experimental and numerical study of AA5086-H111 aluminum plates subjected to impact. *International Journal of Impact Engineering, 51*, pp. 1-12.

[145] Borvik, T., Olovsson, L., Dey, S., & Lanseth, M. (2011). Normal and oblique impact of small arms bullets on AA6082-T4 aluminium protective plates. *International Jounal of Impact Engineering, 38*, pp. 577-589.

[146] Borvik, T., Hopperstad, O. S., & Pederson, K. O. (2010). Quasi-brittle fracture during structural impact of AA7075-T651 aluminium plates. *International Journal of Impact Engineering, 37*, pp. 537-551.

[147] Borvik, T., Forrestal, M., Hopperstad, O., Warren, T., & Langseth, M. (2009). Perforation of AA5083-H116 aluminium plates with conical-nose steel projectiles - calculations. *International Journal of Impact Engineering, 36*, pp. 426-437.

[148] Gupta, N., Iqbal, M., & Sekhon, G. (2006). Experimental and numerical studies on the behavior of thin auminum plates subjected to impact by blunt-and-hemispherical-nosed projectiles. *International Journal of Impact Engineering, 32*, pp. 1921-1944.

[149] Sorensen, B., Kimsey, K., & Love, B. (2008). High-velocity impact of low-density projectiles on structural aluminum armor. *International Journal of Impact Engineering, 35*, pp. 1808-1815.

[150] Borvik, T., Clausen, A., Eriksson, M., Berstad, T., Hopperstad, O., & Langseth, M. (2005). Experimental and numerical study on the perforation of AA6005-T6 panels. *International Journal of Impact Engineering, 32*, pp. 35-64.

[151] Jones, N. (1989). *Structural Impact.* Cambridge University Press.

[152] Ramajeyathilagam, K., Vendhan, C., & Bhujanga Rao, V. (2000). Non-linear transient dynamic response of rectangular plates under shock loading. *International Journal of Impact Engineering, 24*, pp. 999-1015.

[153] Yuan, Y., & Tan, P. (2013). Deformation and failure of rectangular plates subjected to impulsive loadings. *International Journal of Impact Engineering, 59*, pp. 46-59.

[154] Jones, N. (1993). Recent studies on the response of structures subjected to large impact loads. *Ship Structures Symposium '93.* Arlington, Virginia.

[155] Rudrapatna, N., Vaziri, R., & Olson, M. (1999). Deformation and failure of blast-loaded square plates. *International Journal of Imapact Engineering, 22*, pp. 449-467.

[156] Jacinto, A., Ambrosini, R., & Danesi, R. (2001). Experimental and computaional analysis of plates under air blast loading. *International Journal of impact Engineering, 25*, pp. 927-947.

[157] Bonorchis, D., & Nurick, G. (2009). The influence of boundary conditions on the loading of rectangular plates subjected to localised blast loading - Importance in numerical simulations. *International Journal of Impact Engineering, 36*, pp. 40-52.

[158] Wehrenberg, C.,*et all* (2014). Strain anisotropy and shear strength of shock compressed tantalumfrom *in-situ* laue diffraction. Journal of Physics: Conference Series 500.18th APS-SCCM and 24th AIRAPT

[159] Hawreliak, J. *et all* , (2007). In-situ probing of lattice response in shock compressed materials using x-ray diffraction. LLNL, CCRL-PROC-233046

FIGURE CAPTIONS

Fig. 1: Stress-strain curves at different strain rates for material in which work hardening rate is (left) insensitive and (right) sensitive to strain rate (adapted from [7], pp. 367).

Fig. 2: Schematic of a dislocation overcoming barriers with the assistance of a thermal energy (reprinted from [12] Constitutive description of dynamic deformation: physically-based mechanisms. *Materials Science and Engineering A, 322,* Meyers, M., Benson, D., Voringer, O., Kad, B., Xue, Q., & Fu, H.-H., pp. 194-216. Copyright 2002, with permission from Elsevier).

Fig. 3: Schematic illustration of the variation of the strain-hardening rate with $\hat{\boldsymbol{\sigma}}$ as a function of strain rate and temperature. The dashed line shows Voce behaviour (reprinted from [17] A constitutive description of the deformation of copper based on the use of the mechanical threshold stress as an internal state variable. *Acta Metall.*, 36, Follansbee, P., & Kocks, U., pp. 81-93. Copyright 1988, with permission from Elsevier).

Fig. 4: Schematic behaviour of yield stress versus temperature of pure FCC metal (reprinted from [19] A physically based constitutive model for FCC metals with applications to dynamic hardness. *Mechanics of materials*, 40, Voyiadjis, G., & Almasri, A., pp. 549-563. Copyright 2008, with permission from Elsevier).

Fig. 5: Experimental and calculated (fitted) stress-strain curves aluminium at constant strain rates (reprinted from [33] The application of B-P constitutive equations in finite element analysis of high velocity impact. *International Journal of Solids and Structures*, 38, Song, S., Duan, Z., & Tan, D., pp. 5215-5222. Copyright 2001, with permission from Elsevier).

Fig. 6: Comparison of theoretical and experimental values on thermal softening of 30CrMnSiA at a strain rate of 1 s^{-1} (reprinted from [32] Mechanical properties and constitutive relationships of 30CrMnSiA steel heated at high rate. *Materials Science and Engineering A*, 483-484, Chen, S., Huang, C., Wang, C., & Duan, Z., pp. 105-108. Copyright 2008, with permission from Elsevier).

Fig. 7: Experimental (dashed line) and calculated (solid line) shock induced wave profiles showing the motion of aluminium - PMMA interface versus time for various Pressure, Temperature and strain dependencies: (a) pure hydro; (b) constant $\boldsymbol{Y}$ and $\boldsymbol{G}$; (c) adding work hardening; (d) adding the $\boldsymbol{P}$ dependence of $\boldsymbol{Y}$; (f) adding $\boldsymbol{T}$ dependence; (g) adding the Bauschinger model with $\boldsymbol{G_1 = G_0}$; (h) the Bauschinger effect with $\boldsymbol{G_1 = 0.725 G_0}$ (reproduced with permission from [35] Steinberg, D., Cochran, S., & Guinan, M. A constitutive model for metals applicable at highstrain rate. *Journal of Applied Physics, 51*, pp. 1498-1504. Copyright 1980, AIP Publishing LLC).

Fig. 8: Comparison of calculation and experiment for a Ta target shocked to a peak stress of 230 GPa (reproduced with permission from [48] Steinberg, D., & Lund, C. (1989). A constitutive model for strain rates from 10^{-4} to 10^{6} s^{-1}. *Journal of Applied Physics, 65*, pp. 1528-1533. Copyright 1989, AIP Publishing LLC).

Fig. 9: Comparison of model prediction with the experimental data for annealed OFHC copper at different temperatures with the strain rate of 4000 s^{-1} (reprinted from [42] A constitutive model for dynamic plasticity of FCC metals. *Materials Science and Engineering A*, 527, Gao, C., & Zhang, L., pp. 3138-3143. Copyright 2010, with permission from Elsevier).

Fig. 10: Predictions of the model and comparison with experimental results for copper at (a) $\boldsymbol{\dot{\varepsilon} = 0.01}$ s^{-1} and (b) $\boldsymbol{\dot{\varepsilon} = 8500}$ s^{-1}. The calculations for the latter strain rate are for both isothermal ($\boldsymbol{T = 295\ K}$ dashed line) and adiabatic (solid line) (reprinted from [17] A constitutive description of the deformation of copper based on the use of the mechanical threshold stress as an internal state variable. *Acta Metall.*, 36, Follansbee, P., & Kocks, U. pp. 81-93. Copyright 1988, with permission from Elsevier).

Fig. 11: Comparison of model prediction with experimental results for annealed OFHC copper at different strain rates and temperatures using NNL constitutive model (reprinted from [14] Flow stress of FCC polycrystals with application to OFHC Cu. *Acta Materiallia*, 46, Nemat-Nasser, S., & Li, Y. pp. 565-577. Copyright 1998, with permission from Elsevier).

Fig. 12: Comparisons between model and experiment for various strain rates and temperatures: experimental data (dotted), continuum model calculations (dashed) and model calculations using the present constitutive model (solid) (reprinted from [62] A constitutive model for FCC crystals with

application to polycrystalline OFHC copper. *Mechanics of Materials*, 30, Nemat-Nasser, S., Ni, L., & Okinawa, T. pp. 325-341. Copyright 1998, with permission from Elsevier).

Fig. 13: Comparison of model predictions with experimental results at a strain rate of 3500 s^{-1} (reprinted from [66] Thermomechanical response of AL-6XN stainless steel over a wide range of strain rates. *Journal of the Mechanics and Physics of Solids*, 49, Nemat-Nasser, S., Guo, W., & Kihl, D. pp. 1823-1846. Copyright 2001 with permission from Elsevier).

Fig. 14: Description of the flow stress evolution with plastic strain using the MRK model and comparison with experiments at 4000 s^{-1} (a) $\boldsymbol{T_a = 500\ K}$ and (b) $\boldsymbol{T_a = 700\ K}$ (reprinted from [71] A thermo-viscoplastic constitutive model for FCC metals with application to OFHC copper. *International Journal of Mechanical Sciences*, 52, Rusinek, A., Rodriguez-Martinez, J., & Arias, A. pp. 120-135. Copyright 2010, with permission from Elsevier).

Fig. 15: Fixed-point material velocity profiles for 6071-AA computed using steady wave analysis are compared to experimental measurements for shock stress amplitudes of (a) 2.1 GPa; (b) 3.7 GPa; (c) 9.0 GPa; and (d) material velocities profiles plotted on common axes (reprinted from [74] A dislocation-based constitutive model for viscoplastic deformation of FCC metals at very high strain rates. *International Journal of Plasticity*, 27, Austin, R., & McDowell, D. pp. 1-24. Copyright 2011, with permission from Elsevier).

Fig. 16: Localised strain-rate pattern in a tensile round bar specimen for an imposed strain rate of 0.002 s^{-1} (reprinted from [80] The morphology of Portevin-Le Chatelier bands: finite element simulation for Al-Mg-Si. *Acta Materialia*, 49, Zhang, S., McCormick, P., & Estrin, Y. pp. 1087-1094. Copyright 2001, with permission from Elsevier).

Fig. 17: Adiabatic stress-strain curves for OFHC copper, compared with experimental results at 4000 s^{-1} strain rates at different initial temperatures (reprinted from [82] Microstructural based models for BCC and FCC metals with tempearature and strain rate dependency. *Mechanics of materials*, 37, Voyiadjis, G., & Abed, F. pp. 355-378. Copyright 2005, with permission from Elsevier).

Fig. 18: Comparison of VA model for the stress-strain curve at different strain rates with experimental data and the NNL model [14] (reprinted from [19] A physically based constitutive model for FCC metals with applications to dynamic hardness. *Mechanics of materials*, 40, Voyiadjis, G., & Almasri, A. pp. 549-563. Copyright 2008, with permission from Elsevier).

Fig. 19: Comparison of different models' predictions with Clifton's experimental data [17] for the relation of flow stress versus strain in annealed OFHC copper at $\mathbf{6.4 \times 10^5\ s^{-1}}$ and room temperature (reprinted from [23] Constitutive modelling of plasticity of FCC metals under extremely high strain rates. *International Journal of Plasticity*, 32-33, Gao, C., & Zhang, L. pp. 121-133. Copyright 2012, with permission from Elsevier).

Fig. 20: Model prediction for the relations of flow stress versus strain for OHFC copper under very high strain rates at room and elevated temperatures (reprinted from [23] Constitutive modelling of plasticity of FCC metals under extremely high strain rates. *International Journal of Plasticity*, 32-33, Gao, C., & Zhang, L. pp. 121-133. Copyright 2012, with permission from Elsevier).

Fig. 21: Model prediction (solid line) compared with experimental results (circles) for a compression test for annealed copper [17] (reprinted from [78] Constitutive modeling of high-strain-rate deformation in metals based on the evolution of an effective microstructural length. *Mechanics of Materials*, 37, Molinari, A., & Ravichandran, G. pp. 737-752. Copyright 2005, with permission from Elsevier).

Fig. 22: Comparison of experimental stress-strain curves (solid lines) with MJC model predictions: (a) temperature dependence of flow stress at a reference strain rate of 10^{-4} s^{-1}; and (b) effect of strain rate and temperature (reprinted from [95] Experimental analysis and constitutive modeling for the newly developed 2139-T8 alloy. *Materials Science and Engineering A*, 520, Vural, M., & Cairo, J. pp. 56-65. Copyright 2009, with permission from Elsevier).

Fig. 23: Observed and calculated responses for nanocrystalline aluminium at different strain rates by using KHL model for various grain sizes (reprinted from [54] Nanocrystalline aluminium and iron: Mechanical behaviour at quasi-static and high strain rates, and constitutive modeling. *International Journal of Plasticity*, 22, Khan, A., Suh, Y., Chen, X., Takacs, L., & Zhang, H., pp. 195-209. Copyright 2006, with permission from Elsevier).

Fig. 24: The KLF model correlation of the compressive viscoplastic response of 10 h milled (d = 82mm) bulk Al at different temperatures and dynamic strain rates (reprinted from [57] Grain size, strain rate, and temperature dependence of flow stress in ultra-fine grained and nanocrystalline Cu and Al: Synthesis, experiment, and constitutive modeling. *International Journal of Plasticity*, 25, Farrokh, B., & Khan, A. pp. 715-732. Copyright 2009, with permission from Elsevier).

Fig. 25: Stress-Strain correlations between experimental data and constitutive models (a) strain rate 0.1 s^{-1}; (b) strain rate 1 s^{-1} (reprinted from [90] Constitutive relationships for 22MnB5 boron steel deformed isothermally at ahigh temperatures. *Materials Science and Engineering A*, 478, Naderi, M., Durrenberger, L., Molinari, A., & Bleck, W. pp. 130-139. Copyright 2008, with permission from Elsevier).

Fig. 26: Predicted and measured flow stress for 42CrMo steel under different strain rates and different forming temperatures: (a) 850˚C; (b) 950˚C; (c) 1050˚C; and (d) 1150˚C (reprinted from [104] A new mathematical model for predicting flow stress of typical high-strength alloy steel at elevated high temperature. *Computational Materials Science*, 48, Lin, Y., & Liu, G. pp. 54-58. Copyright 2010, with permission from Elsevier).

Fig. 27: (a) Predicted and measured values of flow stress at a plastic strain of 0.3 for cold-worked copper as a function of temperature (b) Predicted and measured stress-strain curves for cold-worked copper as a function of temperature. Scripta Mettalurgica et Materialia, 30, Andrade U R et al.pp. 933-938. Copyright 1994, with permission from Elsevier

Fig. 28: (a) Comparison between the stress-strain rate behaviour predicted by the mechanism-based material model and experimental data for 6061-T6, with regions of the stress-strain rate curve that are dominated by discrete obstacle plasticity and drag controlled plasticity. (b) Similar comparison for Ti-6Al-4V alloy (reproduced from [115] Modeling large-strain, high rate deformation in metals. *Third Biennal Tri-Laboratory Engineering Conference Modeling and Simulation.* Pleasanton: Lawrence Livermore National Laboratory, Lesuer, D., Kay, G., & LeBlanc, M. Copyright 2001; with permission of Lawrence Livermore National Laboratory).

Table 1

Table 1 – Comparison of the major characteristics of physically based constitutive models.

Year	Model	Strain rate	Main features
1975	Bodner and Parton [30]	10^{-3} to 10^{0} s^{-1}	• Based upon separation of the total deformation rate into elastic and plastic components • Incorporates strain hardening effects through a plastic work term • Assumes a dependency on J2 invariant • No temperature effects;
1980	Steinberg and Guinan [35]	10^{5} s^{-1}	• Incorporates temperature effects, • Considers the effect of shock pressure • Based on equivalent plastic strain
1987	Zerilli-Armstrong [38]	$4x10^{3}$ s^{-1}	• Considers temperature effects • Considers grain size. • Based on dislocation mechanics • Considers thermal activation
1988	Mechanical threshold stress [17]	10^{-4} to 10^{4} s^{-1}	• Incorporates temperature effects • Based on thermal activation • Uses the flow stress at 0 K (MTS) • Based on dislocation density as state variable
1989	Steinberg and Lund [48]	10^{-4} to 10^{6} s^{-1}	• Considers thermal activation • Includes the effect of temperature • Extends the Steinberg and Guinan model • Based on equivalent plastic strain • Considers the pressure
1998	Nemat-Nasser and Li [14]	10^{-3} to 10^{4} s^{-1}	• Considers dislocation mechanics • Considers thermal activation • Considers temperature
2001	Nemat-Nasser, Guo and Kihl [66]	10^{-2} to $\approx 10^{4}$ s^{-1}	• Based on dislocation motion mechanics • Includes viscous drag effects on dislocation motion
2003	Preston, Tonks and Wallace [6]	10^{-3} to 10^{9} s^{-1}	• Uses an Arrhenius form for plastic strain rate but with an activation energy • Suitable for explosive loading
2001	Rusinek and Klepaczko [69]	10^{-4} to 10^{3} s^{-1}	• Includes temperature effects • Based on two components of stress: effective and internal • Uses an Arrehnius type eq. for the effective component of stress
2011	Austin and McDowell [74]	10^{4} to 10^{8} s^{-1}	• Based on dislocation densities as state variables • Uses J2 flow theory • First plastic-wave analysis using dislocation mechanics in the weak shock regime
2001	Zhang, McCormick and Estrin [80]	10^{-3}	• Models the Portevin-Le Chatelier effect • Based upon separation of the total deformation rate into elastic and plastic components
1982	Anand [81]	10^{-2}	• Considers temperature • Activation energy • Considers dynamic recovery
2005	Voyadjis and Abed [82]	10^{-3} to 10^{4} s^{-1}	• Modified ZA model • Based on dislocation mechanics • Considers thermal activation
2007	Holmedal [84]	10^{-4} to 10^{9}	• Modification of MTS method
2008	Voyadjis and Almasri [19]	10^{-4} to 10^{4}	• Based on VA model • Based on dislocation density • Considers temperature effects • Considers activation energy
2012	Gao and Zhang [23]	10^{-3} to 10^{4}	• Based on dislocation motion • Considers thermal activation • Considers dislocation drag for high strain rates
2009	Huang et al. [85]	10^{-5} to 10^{6} s^{-1}	• Dislocation mechanics • Thermal activation • Temperature
2000	Gould and Goldthorpe [11]	Not indicated	• Based on Follansbee and Kocks [17] model • Temperature effect • Dislocation motion • Thermal activation

Table 2

Table 2 – Constitutive equations of the indicated models.

Bodner and Partom [30]	$\dot{\varepsilon}_x^p = \frac{2D_0}{\sqrt{3}}\frac{\sigma}{\lvert\sigma\rvert}\exp\left[-\frac{1}{2}\left(\frac{3A^2}{\sigma^2}\right)^n\right]$
Steinberg and Guinan [35]	$Y = Y_0[1+\beta(\varepsilon+\varepsilon_1)]^n\left[1+\left(\frac{Y_p'}{Y_0}\right)\frac{P}{\eta^{\frac{1}{3}}}+\left(\frac{G_T'}{G_0}\right)(T-300)\right]$
Zerilli and Armstrong [36]	$\sigma = \sigma_a + C_2\varepsilon^{\frac{1}{2}}\exp(-C_3T + C_4T\ln\dot{\varepsilon}) + kl^{-\frac{1}{2}}$
MTS [17]	$\sigma = \hat{\sigma}_a + (\hat{\sigma}-\hat{\sigma}_a)\left\{1-\left[\frac{KT\ln\left(\dot{\varepsilon}_0/\dot{\varepsilon}\right)}{g_0\mu b^3}\right]^{\frac{1}{q}}\right\}^{\frac{1}{p}}$
Steinberg and Lund [48]	$\dot{\varepsilon}_p = \frac{1}{C_1}\exp\left[\frac{2U_k}{KT}\left(1-\frac{\sigma_t}{\sigma_p}\right)^2\right]+\frac{C_2}{\sigma_t}$
Nemat-Nasser and Li [14]	$\tau(\dot{\gamma},\gamma,T) = \tau^o\left\{1-\left[-\frac{KT}{G_0}\left(\ln\frac{\dot{\gamma}}{\dot{\gamma}_0}+\ln\left(1+a(T)\gamma^{\frac{1}{2}}\right)\right)\right]^{\frac{1}{2}}\right\}^{\frac{3}{2}}\left[1+a(T)\gamma^{\frac{1}{2}}\right]+\tau_a^o\gamma^{n_1}$
Nemat-Nasser, Guo and Kihil [66]	$\tau^* = \tau^0\left\{1-\left[-\frac{KT}{G_0}\ln\left(\frac{\dot{\gamma}f(\gamma,T)}{\dot{\gamma}}\right)\right]^{\frac{1}{q}}\right\}^{\frac{1}{p}} f(\gamma,T) \quad \text{for } T \le T_c$
Preston-Tonks-Wallace [6]	$\hat{\tau} = \hat{\tau}_s + \frac{1}{p}(s_0-\hat{\tau}_y)\ln\left\{1 - \left[1-\exp\left(-p\frac{\hat{\tau}_s-\hat{\tau}_y}{s_0-\hat{\tau}_y}\right)\right]\exp\left[-p\theta\psi\left[(s_0-\hat{\tau}_y)\left[\exp\left(p\frac{\hat{\tau}_s-\hat{\tau}_y}{s_0-\hat{\tau}_y}\right)-1\right]\right]^{-1}\right]\right\}$
Rusineck-Klepcazko [69]	$\sigma = \frac{E(T)}{E_0}\left[B_0\theta_m^{-\nu}(\varepsilon_0+\varepsilon^p)^{n_0(1-D_2\theta_n)} + \sigma_0^*(1-D_1\theta_m)^m + \sigma_{ns}\right]$
Voyadjis-Abed [82]	$\sigma = B\varepsilon_p^n\left[1-\left(\beta_1T-\beta_2T\ln\dot{\varepsilon}_p\right)^{1/q}\right]^{1/p}+Y_a$
Voyadjid-Almasri [19]	$\sigma = B\varepsilon_p^n\left[1+B_1T\left(\dot{\varepsilon}_p\right)^{1/m}-B_2T\exp\left[A\left(1-\frac{T}{T_t}\right)\right]\right]+Y_a$
Gao-Zhang [23]	$\sigma = \hat{\sigma}_a + \hat{Y}\varepsilon^n\exp\left[C_3T\ln\left(\frac{\dot{\varepsilon}}{\dot{\varepsilon}_{s0}}\right)\right]\left\{1-\left[-C_4T\ln\left(\frac{\dot{\varepsilon}}{\dot{\varepsilon}_0}\right)\right]^{1/q}\right\}^{1/p}$
Huang [85]	$\tau = \alpha\mu b\sqrt{\rho}+\left[B_{wind}^0+\frac{B_{flutter}^0}{1-\left(\frac{\dot{\gamma}}{b\rho_m C_t}\right)^2}\right]\frac{T}{\theta_D}\frac{\dot{\gamma}}{b^2\rho_m}$
Gould and Goldthorpe [11]	$\bar{\sigma} = \sigma_a + \phi\eta\left\{1-\left[\alpha-\theta\frac{\varepsilon}{\eta}+1\right]^{\frac{1}{1-\alpha}}\right\}$

Table 3

Table 3 - Comparison of the major characteristics of some empirical constitutive models.

Year	Model	Strain rate	Main features
2003	Kocks and Mecking [72]	10^{2} to 10^{4} s^{-1}	• Based on dislocation density • Considers thermal activation • Considers flow stress at 0 K
2005	Molinari & Ravichandran [68]	10^{-3} to $8.5x10^{4}$ s^{-1}	• Based on a characteristic length scale of the microstructure • Considers temperature effects • Considers grain size
1983	Johnson and Cook [78]	Up to 10^{4} s^{-1}	• Purely empirical model • Considers the effect of temperature • Considers strain rate effects
1976	Voce and Kocks [98]	10 s^{-1}	• Uses the concept of saturation stress as a function of temperature and strain rate
2008	Lin, Chen and Zhong [101]	$5x10$ s^{-1}	• Defines flow stress in terms of the Zener-Hollomon parameter
1992	Khan and Huang [76]	10^{-5} to 10^{4} s^{-1}	• Does not includes temperature effects • Based upon separation of the total deformation rate into elastic and plastic components • Assumes a dependency on J2 invariant
1992	Khan, Huang and Liang [90]	10^{-6} to 10^{4} s^{-1}	• Adds temperature effects to the KH model
2009	Khan, Liang and Farrokh [97]	10^{-4} to 10^{3} s^{-1}	• Derived from KHL method • Includes temperature effects • Considers grain size
			•
			•

Table 4

Table 4 - Constitutive equations of the indicated phenomenological models.

Kocks and Mecking [72]	$s = \left(\frac{\dot{\varepsilon}}{\dot{\varepsilon_0}}\right)^{1/m} \exp\left(-F\frac{\theta_r}{\theta_h}\right)$ and $s = \left(\frac{\dot{\varepsilon}}{\dot{\varepsilon_0}}\right)^{\frac{1}{m}} \left(1 - F\frac{\theta_r}{\theta_h}\right)$
Molinari and Ravichandran [68]	$\frac{\delta_r}{\delta_{r0}} = \left\{1 - \left[k_r\left(\frac{T}{T_{r0}}\right)\log\left(\frac{\dot{\varepsilon}_{r0}}{\dot{\varepsilon}}\right)\right]^{p_r}\right\}^{q_r}$ and $\frac{\delta_s}{\delta_{s0}} = \frac{1}{\left\{1-\left[k_r\left(\frac{T}{T_{r0}}\right)\log\left(\frac{\dot{\varepsilon}_{r0}}{\dot{\varepsilon}}\right)\right]^{p_s}\right\}^{q_s}}$
Jonhson and Cook [78]	$\sigma_{eq} = (A + B\varepsilon^n)(1 + C\ln\dot{\varepsilon}^*)(1 - T^{*m})$
Voce and Kocks [98]	$\sigma = \sigma_s + \left[(\sigma_0 - \sigma_s)\exp\left(-\frac{\varepsilon}{\varepsilon_r}\right)\right]$
Lin, Chen and Zhong [101]	$\dot{\varepsilon} = AF(\sigma)\exp\left(-\frac{Q}{RT}\right)$
Khan-Huang-Liang [90]	$\sigma = \left[A + B\left(1 - \frac{\ln(\dot{\varepsilon}^p)}{\ln(D_0^p)}\right)^{n_1}\varepsilon^{n_0}\right](1 - T^{*m})e^{C\ln(\dot{\varepsilon})}$
Khan-Liang-Farrokh [97]	$\sigma = \left[\left(a + \frac{k}{d^{n*}}\right) + B\left(\frac{d}{d_0}\right)^{n_2}\left[\left(1 - \frac{\ln(\dot{\varepsilon}^p)}{\ln(D_0^p)}\right)\left(\frac{T_m}{T}\right)\right]^{n_1}(\varepsilon^p)^{n_0}\right]\left(\frac{T_m - T}{T_m - T_{ref}}\right)^m\left(\frac{\dot{\varepsilon}^p}{\dot{\varepsilon}^{p*}}\right)^C$

Figure 1

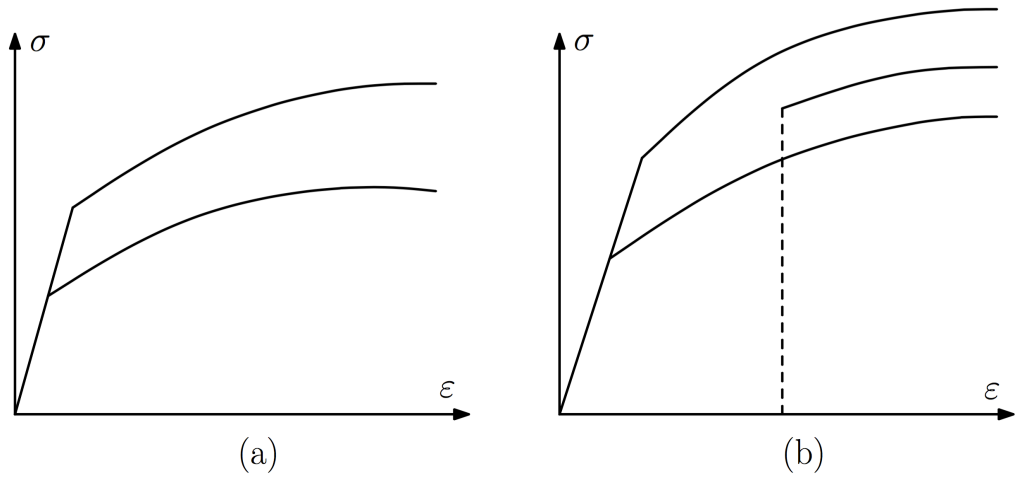

Fig. 1: Stress-strain curves at different strain rates for material in which work hardening rate is (left) insensitive and (right) sensitive to strain rate (adapted from [7], pp. 367).

Figure 2

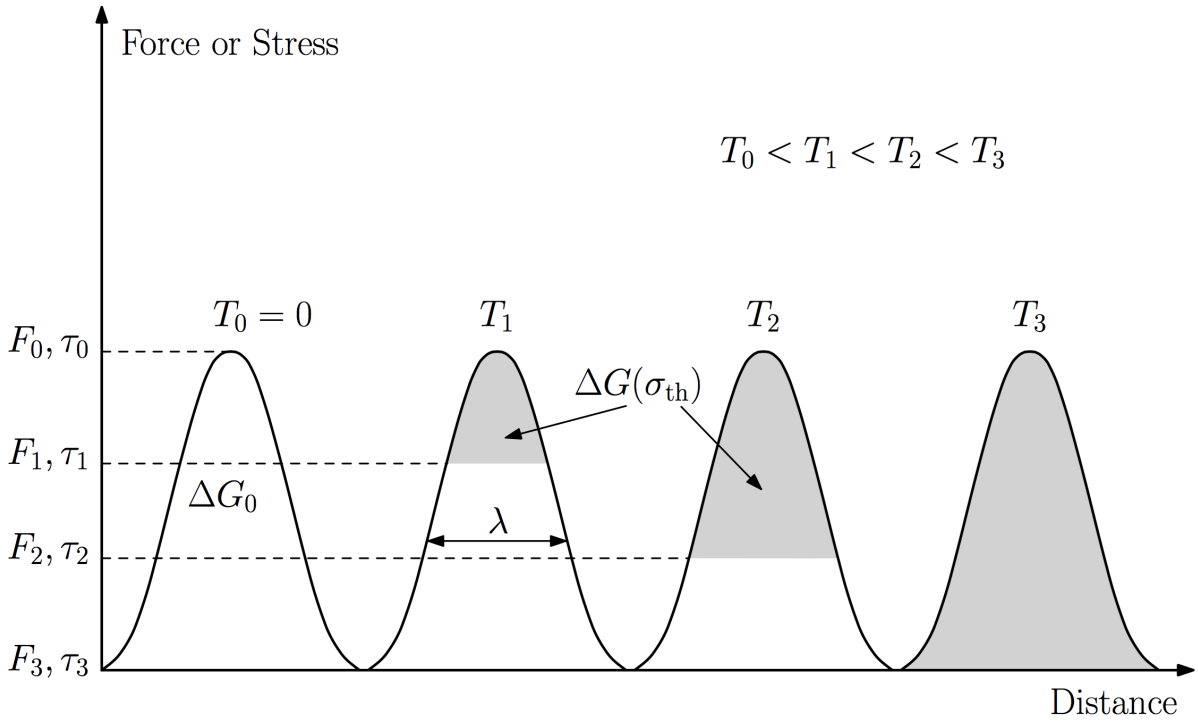

Fig. 2: Schematic of a dislocation overcoming barriers with the assistance of a thermal energy (reprinted from [12] Constitutive description of dynamic deformation: physically-based mechanisms. *Materials Science and Engineering A, 322,* Meyers, M., Benson, D., Voringer, O., Kad, B., Xue, Q., & Fu, H.-H., pp. 194-216. Copyright 2002, with permission from Elsevier).

Figure 3

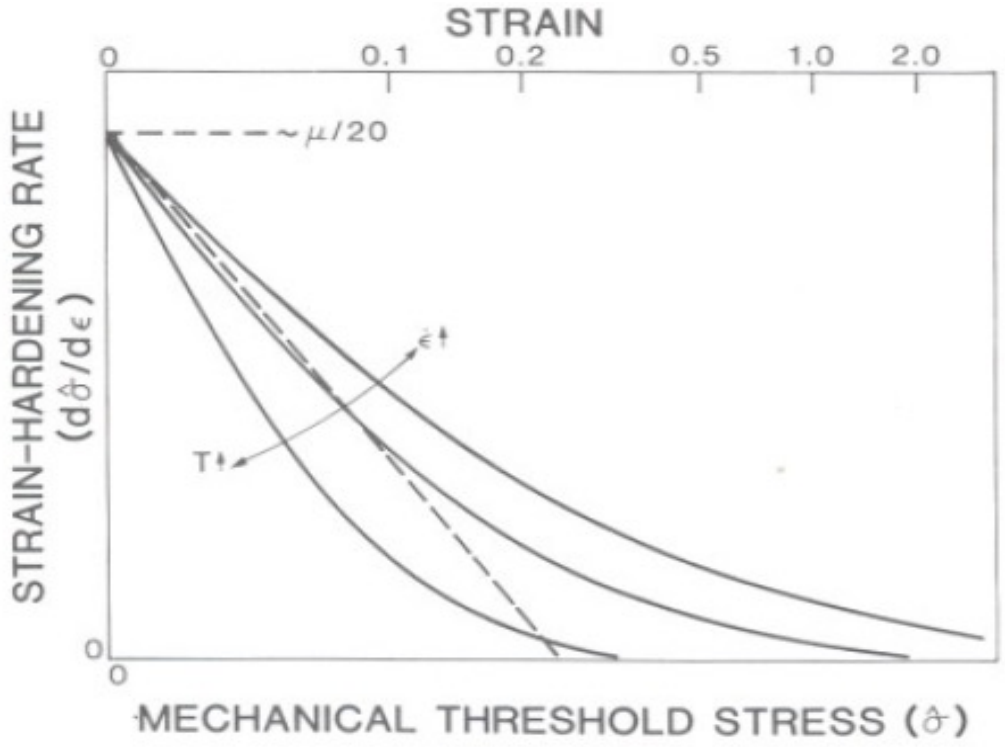

Fig. 3: Schematic illustration of the variation of the strain-hardening rate with $\hat{\boldsymbol{\sigma}}$ as a function of strain rate and temperature. The dashed line shows Voce behaviour (reprinted from [17] A constitutive description of the deformation of copper based on the use of the mechanical threshold stress as an internal state variable. *Acta Metall.*, 36, Follansbee, P., & Kocks, U., pp. 81-93. Copyright 1988, with permission from Elsevier).

Figure 4

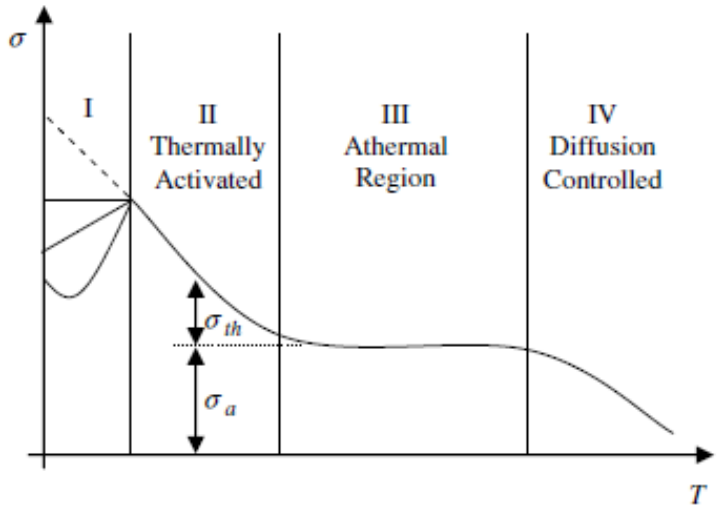

Fig. 4: Schematic behaviour of yield stress versus temperature of pure FCC metal (reprinted from [19] A physically based constitutive model for fcc metals with applications to dynamic hardness. *Mechanics of materials*, 40, Voyiadjis, G., & Almasri, A., pp. 549-563. Copyright 2008, with permission from Elsevier).

Figure 5

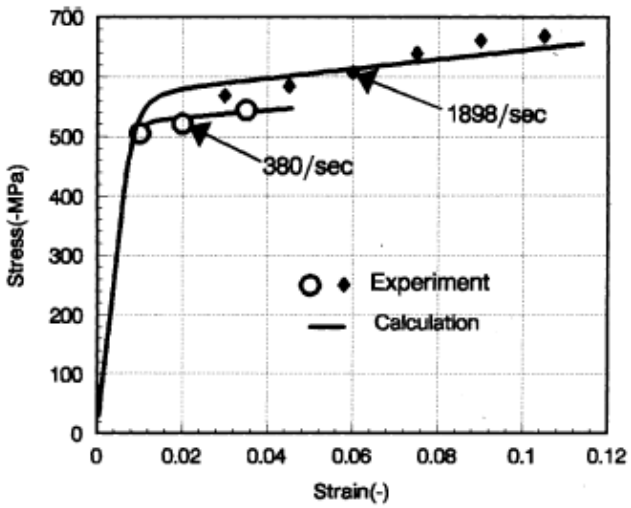

Fig. 5: Experimental and calculated (fitted) stress-strain curves aluminium at constant strain rates (reprinted from [33] The application of B-P constitutive equations in finite element analysis of high velocity impact. *International Journal of Solids and Structures*, 38, Song, S., Duan, Z., & Tan, D., pp. 5215-5222. Copyright 2001, with permission from Elsevier).

Figure 6

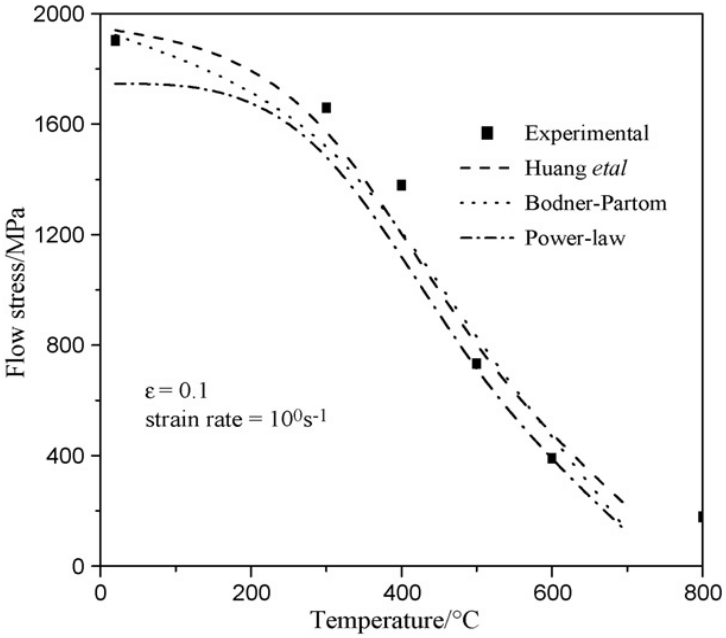

Fig. 6: Comparison of theoretical and experimental values on thermal softening of 30CrMnSiA at a strain rate of 1 s^{-1} (reprinted from [32] Mechanical properties and constitutive relationships of 30CrMnSiA steel heated at high rate. *Materials Science and Engineering A*, 483-484, Chen, S., Huang, C., Wang, C., & Duan, Z., pp. 105-108. Copyright 2008, with permission from Elsevier).

Figure 7

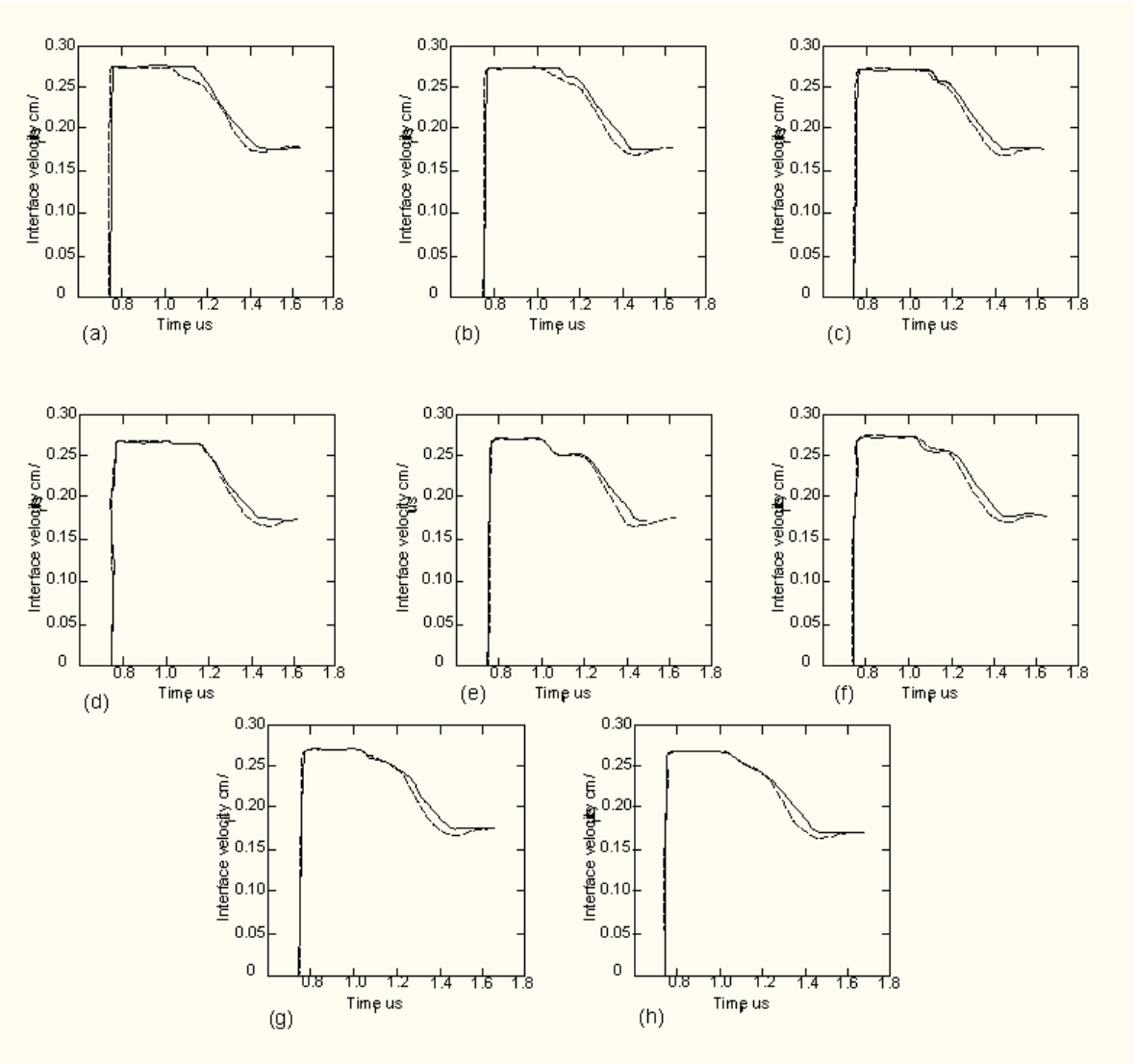

Fig. 7: Experimental (dashed line) and calculated (solid line) shock induced wave profiles showing the motion of aluminium - PMMA interface versus time for various Pressure, Temperature and strain dependencies: (a) pure hydro; (b) constant $\boldsymbol{Y}$ and $\boldsymbol{G}$; (c) adding work hardening; (d) adding the $\boldsymbol{P}$ dependence of $\boldsymbol{Y}$; (f) adding $\boldsymbol{T}$ dependence; (g) adding the Bauschinger model with $\boldsymbol{G_1 = G_0}$; (h) the Bauschinger effect with $\boldsymbol{G_1 = 0.725G_0}$ (reproduced with permission from [35] Steinberg, D., Cochran, S., & Guinan, M. A constitutive model for metals applicable at highstrain rate. *Journal of Applied Physics, 51*, pp. 1498-1504. Copyright 1980, AIP Publishing LLC).

Figure 8

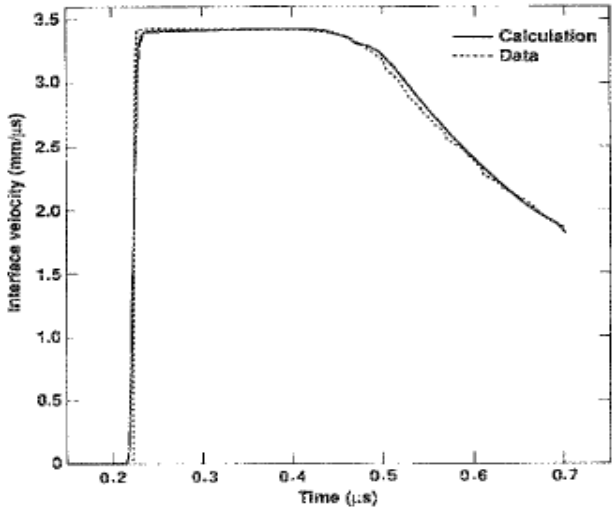

Fig. 8: Comparison of calculation and experiment for a Ta target shocked to a peak stress of 230 GPa (reproduced with permission from [48] Steinberg, D., & Lund, C. (1989). A constitutive model for strain rates from 10-4 to 106 s-1. *Journal of Applied Physics, 65*, pp. 1528-1533. Copyright 1989, AIP Publishing LLC).

Figure 9

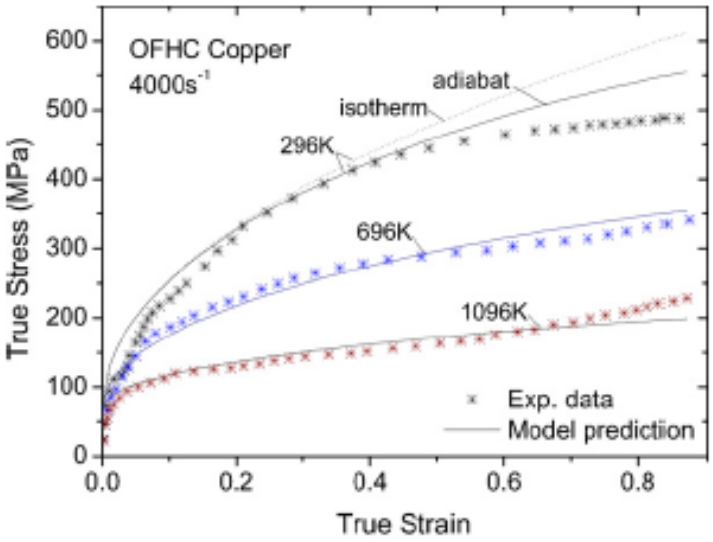

Fig. 9: Comparison of model prediction with the experimental data for annealed OFHC copper at different temperatures with the strain rate of 4000 s^{-1} (reprinted from [42] A constitutive model for dynamic plasticity of FCC metals. *Materials Science and Engineering A*, 527, Gao, C., & Zhang, L., pp. 3138-3143. Copyright 2010, with permission from Elsevier).

Figure 10

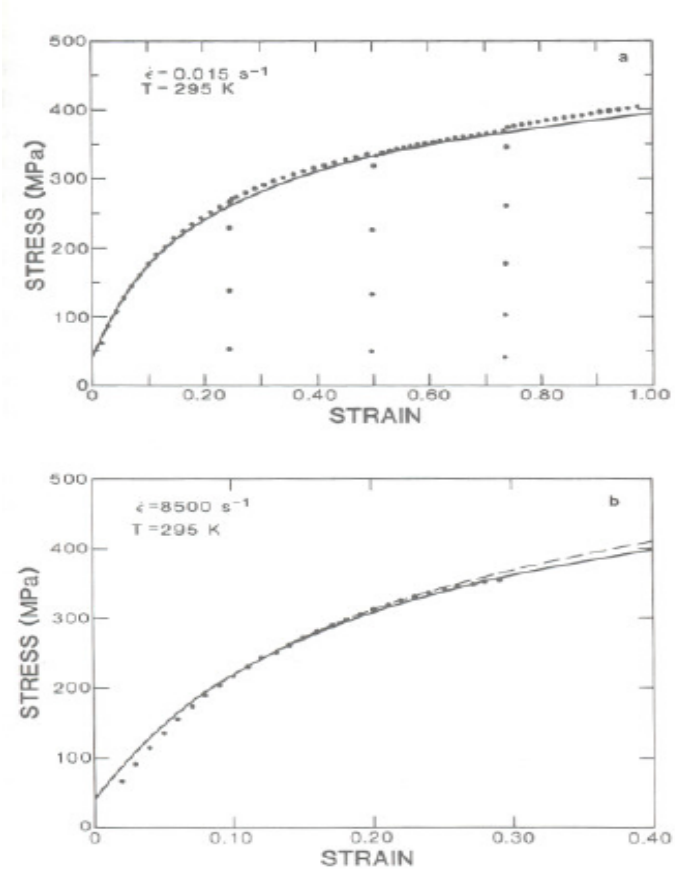

Fig. 10: Predictions of the model and comparison with experimental results for copper at (a) $\dot{\boldsymbol{\varepsilon}} = \mathbf{0.01}$ s^{-1} and (b) $\dot{\boldsymbol{\varepsilon}} = \mathbf{8500}$ s^{-1}. The calculations for the latter strain rate are for both isothermal ($\boldsymbol{T} = \mathbf{295\ K}$ dashed line) and adiabatic (solid line) (reprinted from [17] A constitutive description of the deformation of copper based on the use of the mechanical threshold stress as an internal state variable. *Acta Metall.*, 36, Follansbee, P., & Kocks, U. pp. 81-93. Copyright 1988, with permission from Elsevier).

Figure 11

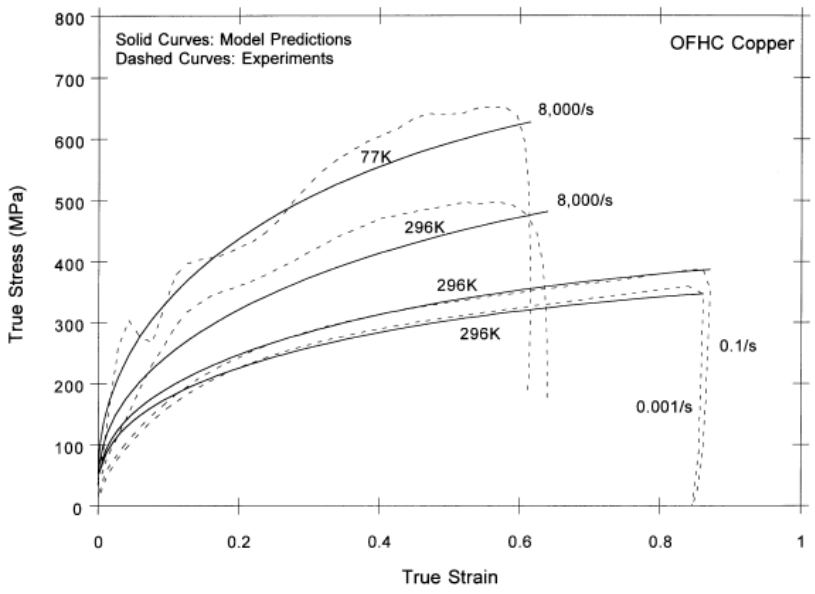

Fig. 11: Comparison of model prediction with experimental results for annealed OFHC copper at different strain rates and temperatures using NNL constitutive model (reprinted from [14] Flow stress of FCC polycrystals with application to OFHC Cu. *Acta Materiallia*, 46, Nemat-Nasser, S., & Li, Y. pp. 565-577. Copyright 1998, with permission from Elsevier).

Figure 12

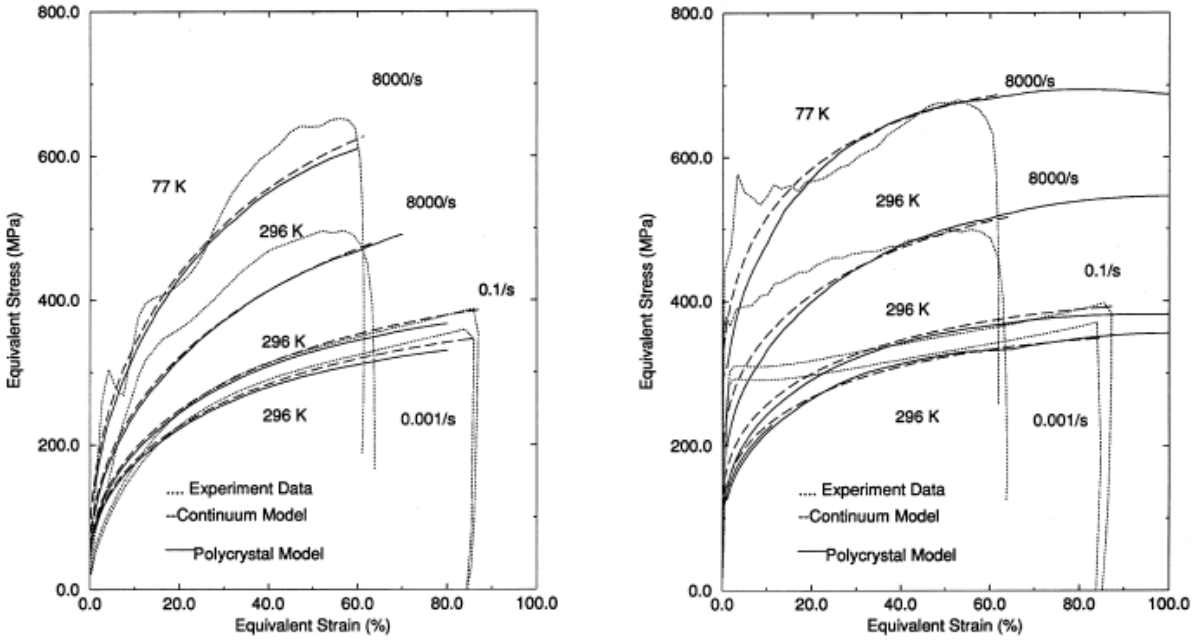

Fig. 12: Comparisons between model and experiment for various strain rates and temperatures: experimental data (dotted), continuum model calculations (dashed) and model calculations using the present constitutive model (solid) (reprinted from [62] A constitutive model for fcc crystals with application to polycrystalline OFHC copper. *Mechanics of Materials*, 30, Nemat-Nasser, S., Ni, L., & Okinawa, T. pp. 325-341. Copyright 1998, with permission from Elsevier).

Figure 13

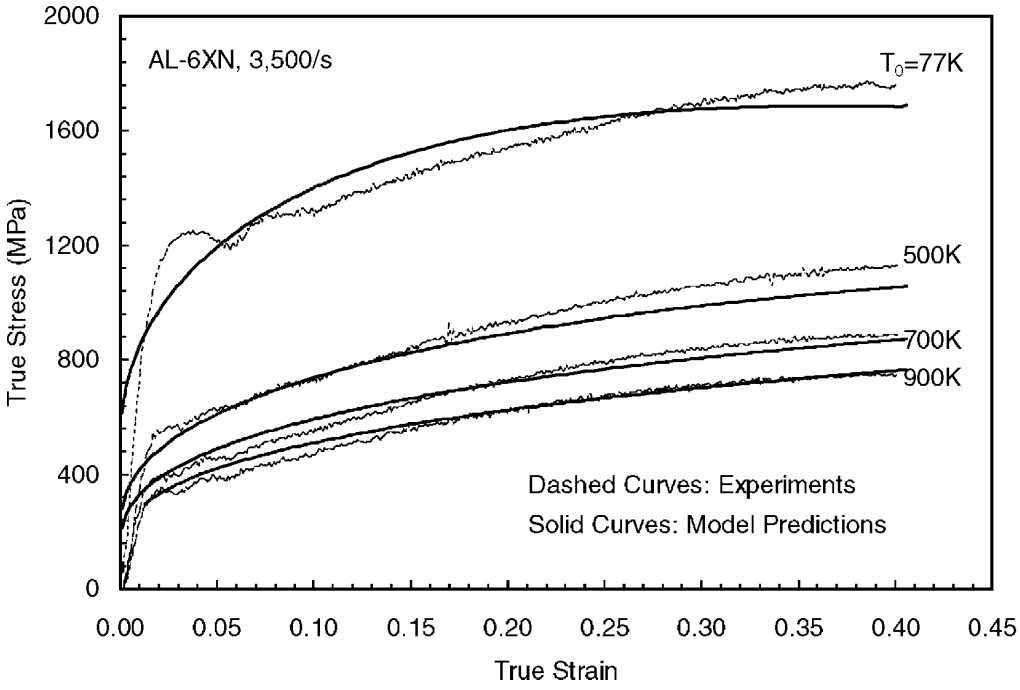

Fig. 13: Comparison of model predictions with experimental results at a strain rate of 3500 s^{-1} (reprinted from [66] Thermomechanical response of AL-6XN stainless steel over a wide range of strain rates. *Journal of the Mechanics and Physics of Solids*, 49, Nemat-Nasser, S., Guo, W., & Kihl, D. pp. 1823-1846. Copyright 2001 with permission from Elsevier).

Figure 14

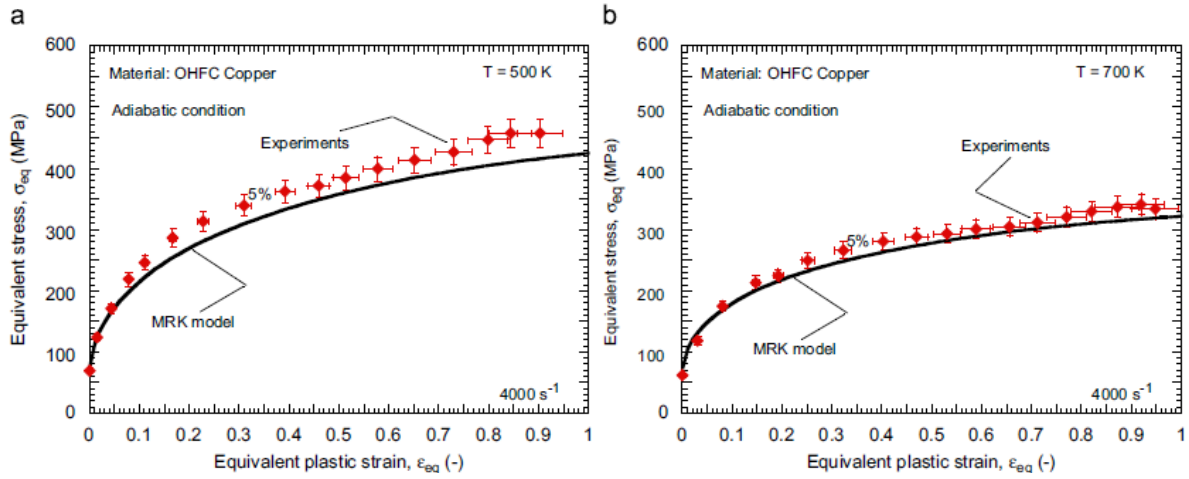

Fig. 14: Description of the flow stress evolution with plastic strain using the MRK model and comparison with experiments at 4000 s^{-1} (a) $\boldsymbol{T_a = 500\ K}$ and (b) $\boldsymbol{T_a = 700\ K}$ (reprinted from [71] A thermo-viscoplastic constitutive model for FCC metals with application to OFHC copper. *International Journal of Mechanical Sciences*, 52, Rusinek, A., Rodriguez-Martinez, J., & Arias, A. pp. 120-135. Copyright 2010, with permission from Elsevier).

Figure 15

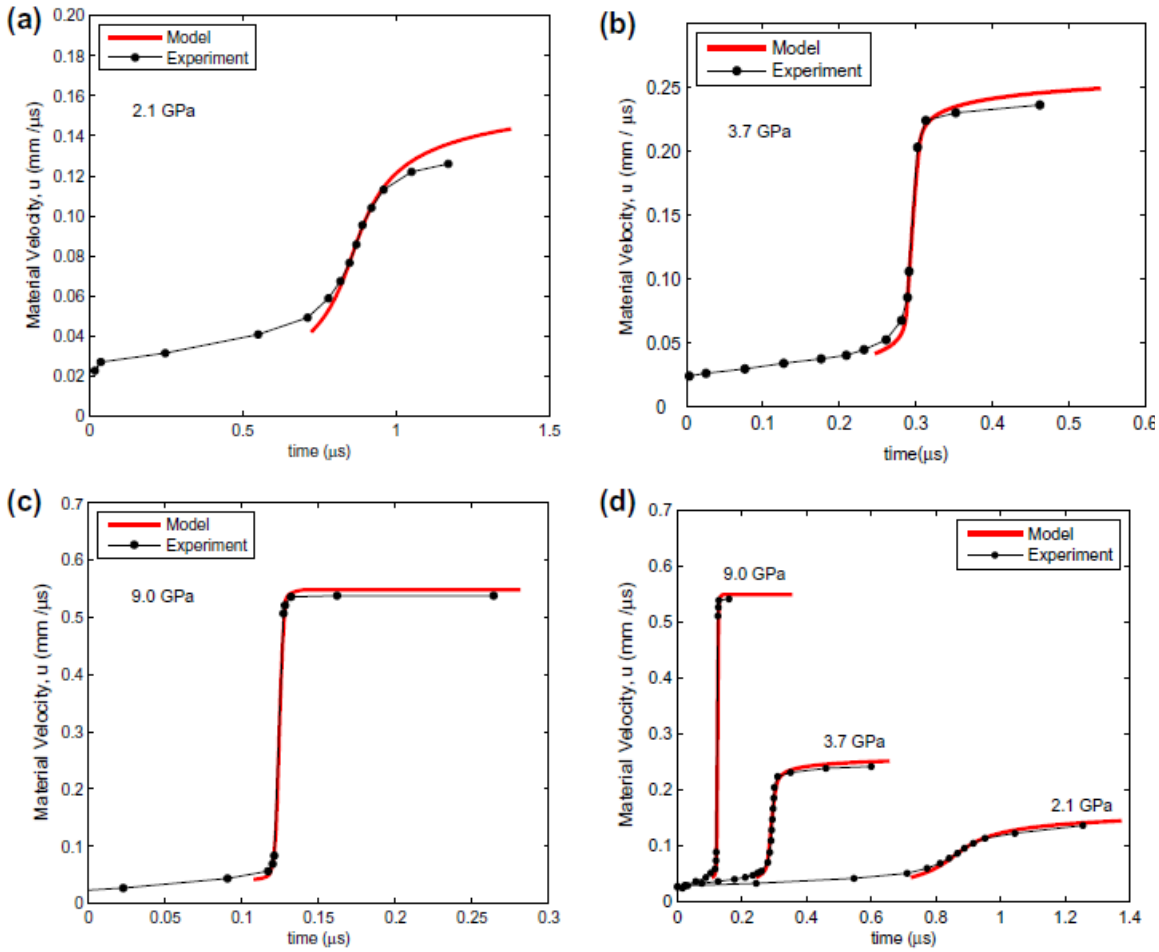

Fig. 15: Fixed-point material velocity profiles for 6071-AA computed using steady wave analysis are compared to experimental measurements for shock stress amplitudes of (a) 2.1 GPa; (b) 3.7 GPa; (c) 9.0 GPa; and (d) material velocities profiles plotted on common axes (reprinted from [74] A dislocation-based constitutive model for viscoplastic deformation of fcc metals at very high strain rates. *International Journal of Plasticity*, 27, Austin, R., & McDowell, D. pp. 1-24. Copyright 2011, with permission from Elsevier).

Figure 16

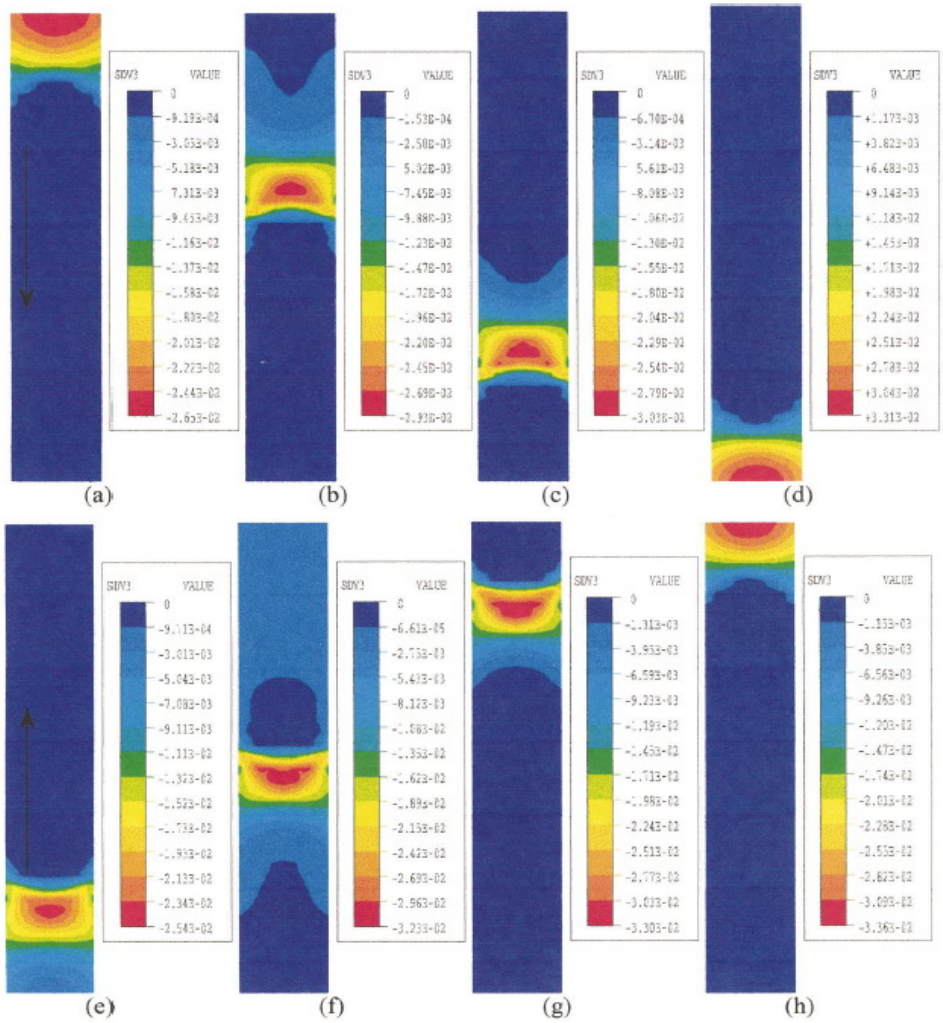

Fig. 16: Localised strain-rate pattern in a tensile round bar specimen for an imposed strain rate of 0.002 s^{-1} (reprinted from [80] The morphology of Portevin-Le Chatelier bands: finite element simulation for Al-Mg-Si. *Acta Materialia*, 49, Zhang, S., McCormick, P., & Estrin, Y. pp. 1087-1094. Copyright 2001, with permission from Elsevier).

Figure 17

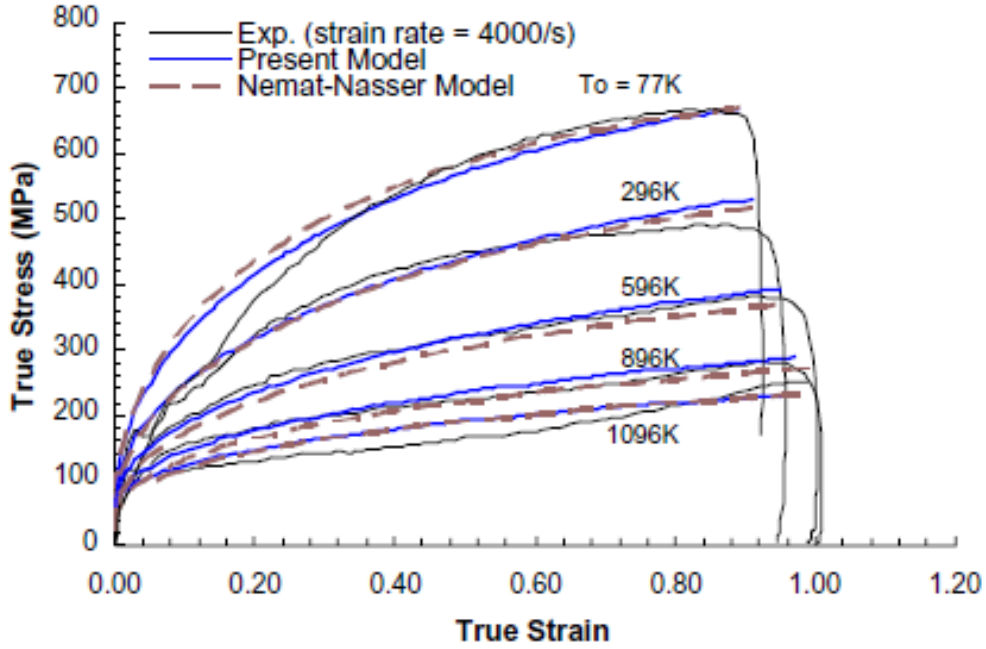

Fig. 17: Adiabatic stress-strain curves for OFHC copper, compared with experimental results at 4000 s^{-1} strain rates at different initial temperatures (reprinted from [82] Microstructural based models for BCC and FCC metals with tempearature and strain rate dependency. *Mechanics of materials*, 37, Voyiadjis, G., & Abed, F. pp. 355-378. Copyright 2005, with permission from Elsevier).

Figure 18

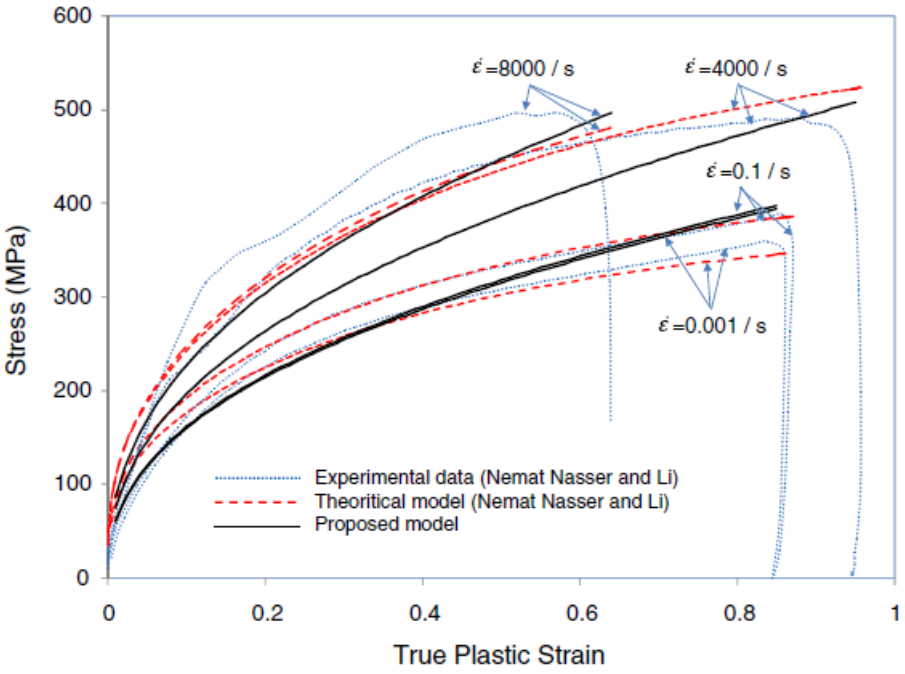

Fig. 18: Comparison of VA model for the stress-strain curve at different strain rates with experimental data and the NNL model [14] (reprinted from [19] A physically based constitutive model for fcc metals with applications to dynamic hardness. *Mechanics of materials*, 40, Voyiadjis, G., & Almasri, A. pp. 549-563. Copyright 2008, with permission from Elsevier).

Figure 19

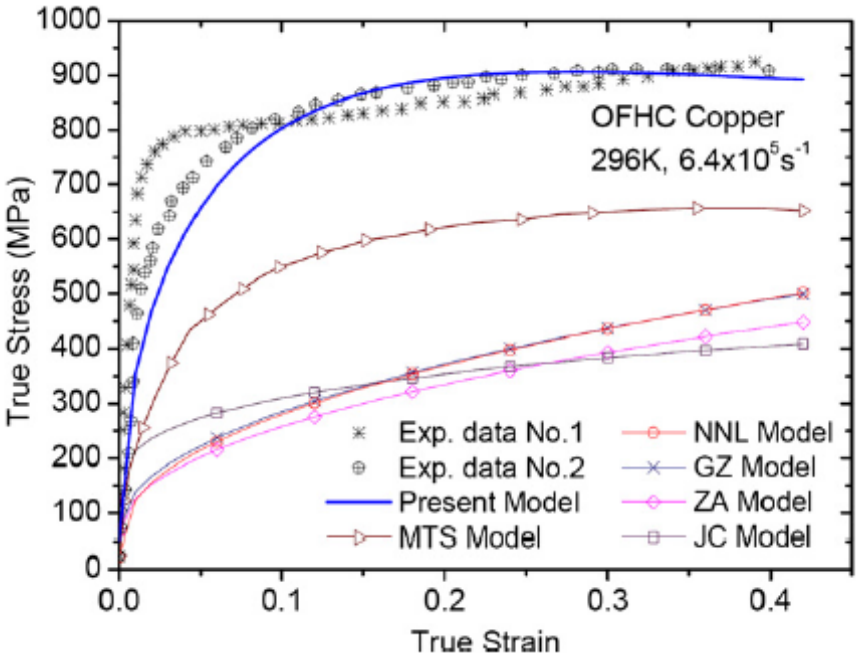

Fig. 19: Comparison of different models' predictions with Clifton's experimental data [17] for the relation of flow stress versus strain in annealed OFHC copper at $\mathbf{6.4\times10^5\ s^{-1}}$ and room temperature (reprinted from [23] Constitutive modelling of plasticity of fcc metals under extremely high strain rates. *International Journal of Plasticity*, 32-33, Gao, C., & Zhang, L. pp. 121-133. Copyright 2012, with permission from Elsevier).

Figure 20

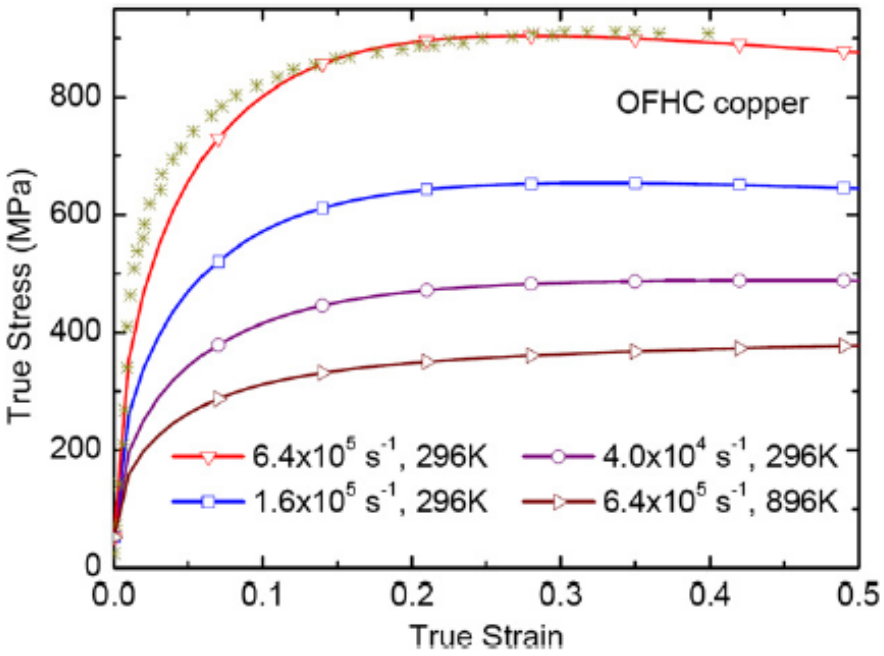

Fig. 20: Model prediction for the relations of flow stress versus strain for OHFC copper under very high strain rates at room and elevated temperatures (reprinted from [23] Constitutive modelling of plasticity of fcc metals under extremely high strain rates. *International Journal of Plasticity*, 32-33, Gao, C., & Zhang, L. pp. 121-133. Copyright 2012, with permission from Elsevier).

Figure 21

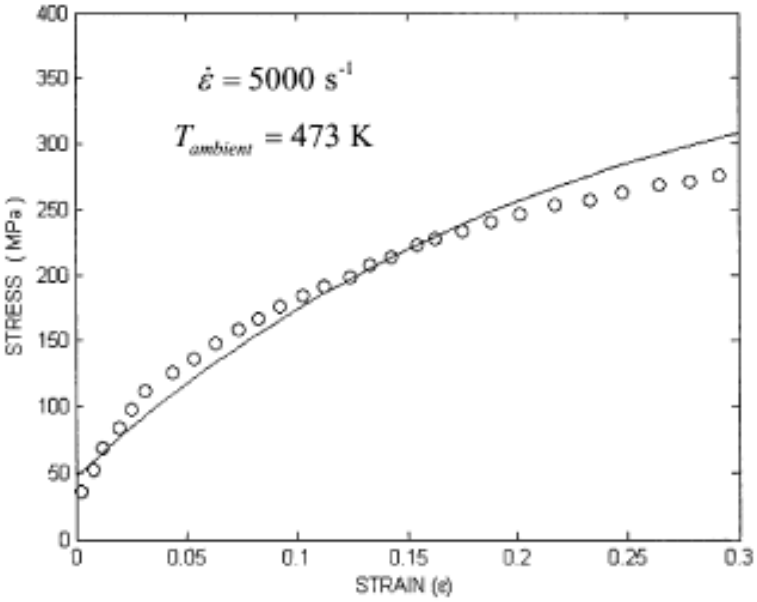

Fig. 21: Model prediction (solid line) compared with experimental results (circles) for a compression test for annealed copper [17] (reprinted from [78] Constitutive modeling of high-strain-rate deformation in metals based on the evolution of an effective microstructural length. *Mechanics of Materials*, 37, Molinari, A., & Ravichandran, G. pp. 737-752. Copyright 2005, with permission from Elsevier).

Figure 22

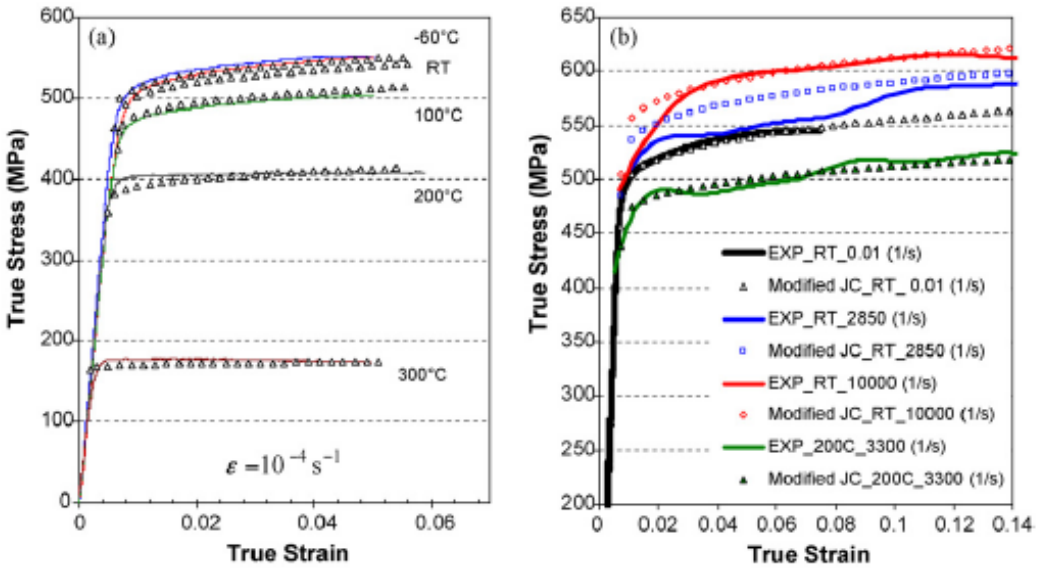

Fig. 22: Comparison of experimental stress-strain curves (solid lines) with MJC model predictions: (a) temperature dependence of flow stress at a reference strain rate of 10^{-4} s^{-1}; and (b) effect of strain rate and temperature (reprinted from [95] Experimental analysis and constitutive modeling for the newly developed 2139-T8 alloy. *Materials Science and Engineering A*, 520, Vural, M., & Cairo, J. pp. 56-65. Copyright 2009, with permission from Elsevier).

Figure 23

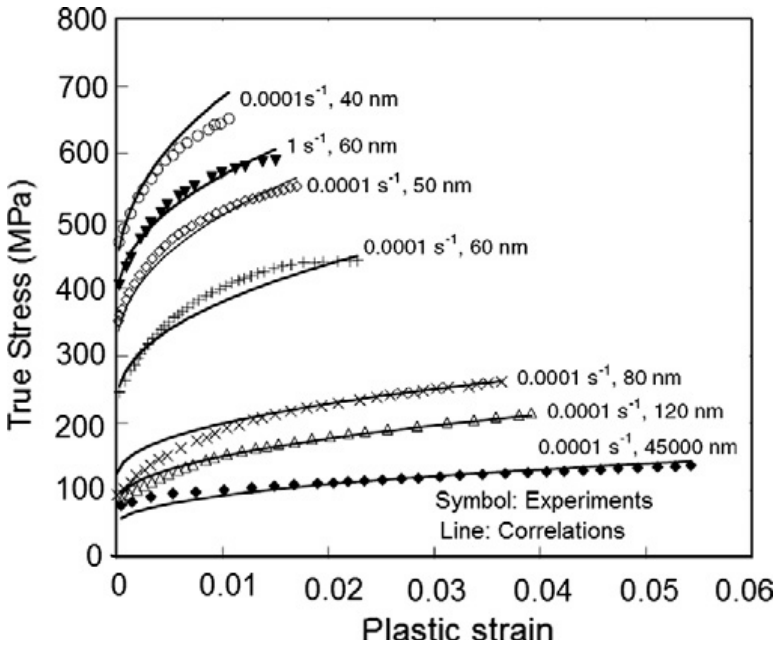

Fig. 23: Observed and calculated responses for nanocrystalline aluminium at different strain rates by using KHL model for various grain sizes (reprinted from [54] Nanocrystalline aluminium and iron: Mechanical behaviour at quasi-static and high strain rates, and constitutive modeling. *International Journal of Plasticity*, 22, Khan, A., Suh, Y., Chen, X., Takacs, L., & Zhang, H., pp. 195-209. Copyright 2006, with permission from Elsevier).

Figure 24

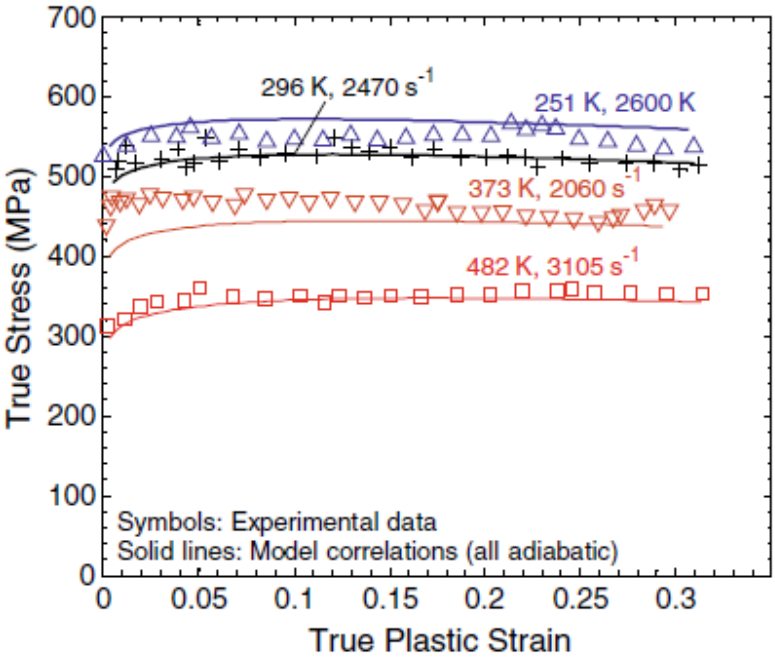

Fig. 24: The KLF model correlation of the compressive viscoplastic response of 10 h milled (d = 82mm) bulk Al at different temperatures and dynamic strain rates (reprinted from [57] Grain size, strain rate, and temperature dependence of flow stress in ultra-fine grained and nanocrystalline Cu and Al: Synthesis, experiment, and constitutive modeling. *International Journal of Plasticity*, 25, Farrokh, B., & Khan, A. pp. 715-732. Copyright 2009, with permission from Elsevier).

Figure 25

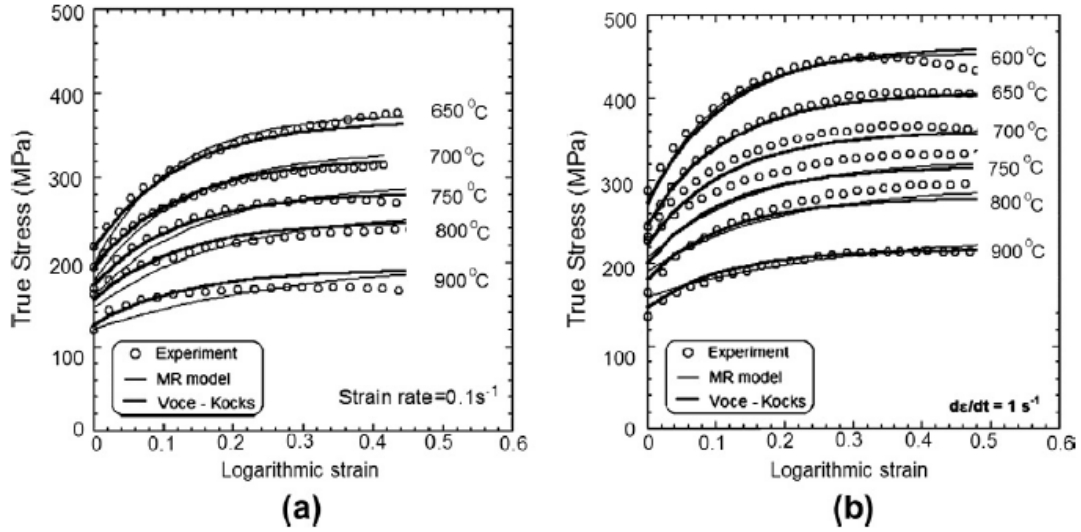

Fig. 25: Stress-Strain correlations between experimental data and constitutive models (a) strain rate 0.1 s^{-1}; (b) strain rate 1 s^{-1} (reprinted from [90] Constitutive relationships for 22MnB5 boron steel deformed isothermally at ahigh temperatures. *Materials Science and Engineering A*, 478, Naderi, M., Durrenberger, L., Molinari, A., & Bleck, W. pp. 130-139. Copyright 2008, with permission from Elsevier).

Figure 26

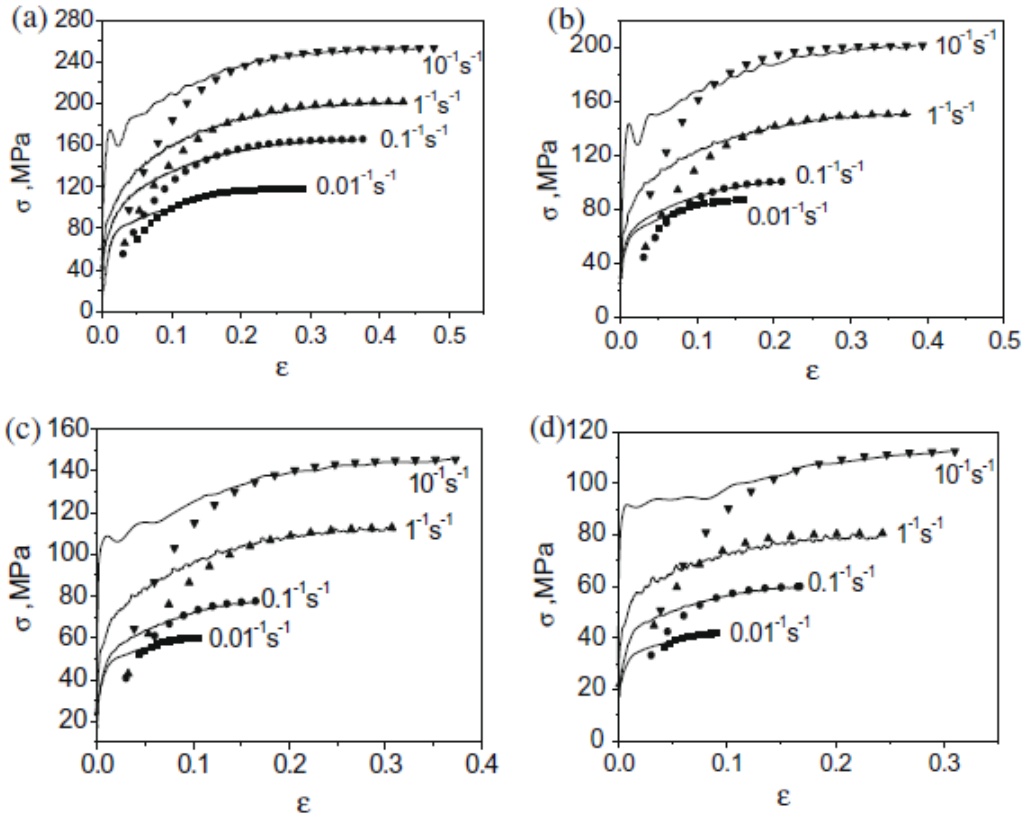

Fig. 26: Predicted and measured flow stress for 42CrMo steel under different strain rates and different forming temperatures: (a) 850˚C; (b) 950˚C; (c) 1050˚C; and (d) 1150˚C (reprinted from [104] A new mathematical model for predicting flow stress of typical high-strength alloy steel at elevated high temperature. *Computational Materials Science*, 48, Lin, Y., & Liu, G. pp. 54-58. Copyright 2010, with permission from Elsevier).

Figure 27

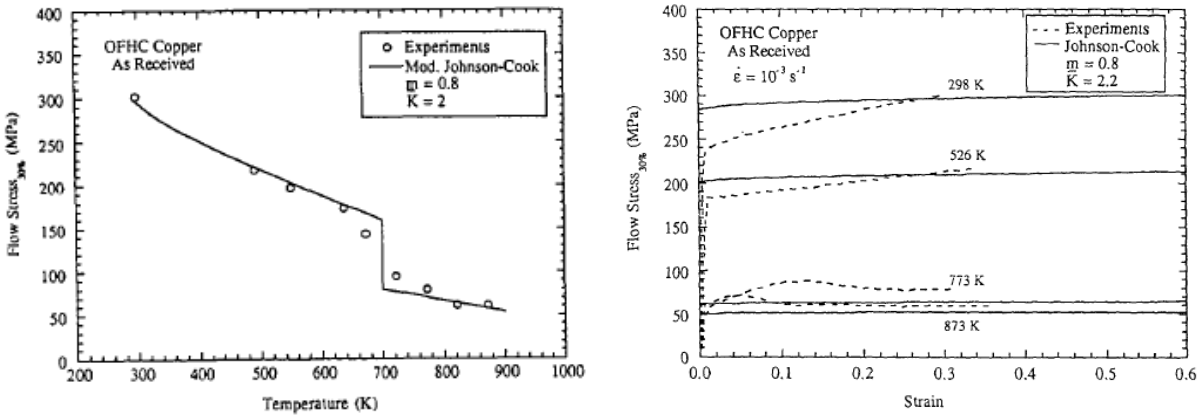

Fig. 27: (a) Predicted and measured values of flow stress at a plastic strain of 0.3 for cold-worked copper as a function of temperature (b) Predicted and measured stress-strain curves for cold-worked copper as a function of temperature. Scripta Mettalurgica et Materialia, 30, Andrade U R et al.pp. 933-938. Copyright 1994, with permission from Elsevier

Figure 28

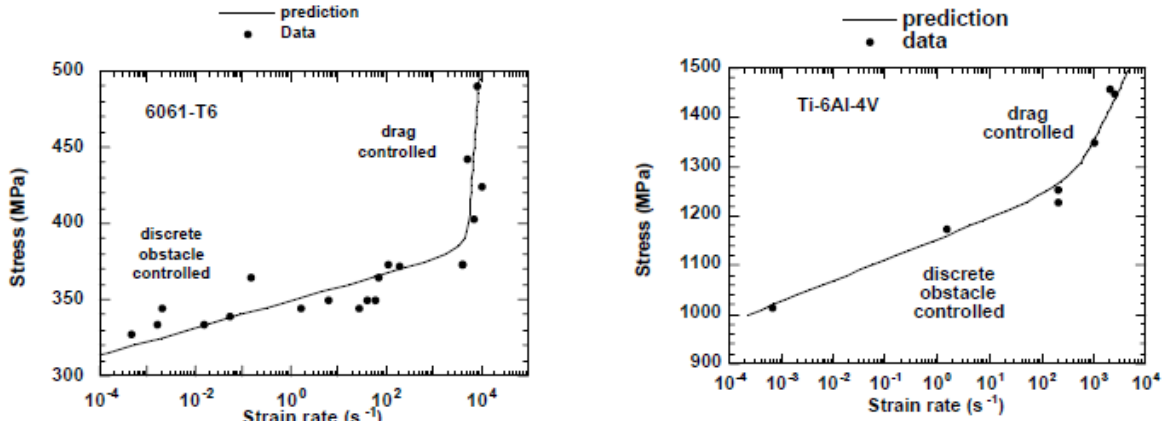

Fig. 28: (a) Comparison between the stress-strain rate behaviour predicted by the mechanism-based material model and experimental data for 6061-T6, with regions of the stress-strain rate curve that are dominated by discrete obstacle plasticity and drag controlled plasticity. (b) Similar comparison for Ti-6Al-4V alloy (reproduced from [115] Modeling large-strain, high rate deformation in metals. *Third Biennal Tri-Laboratory Engineering Conference Modeling and Simulation.* Pleasanton: Lawrence Livermore National Laboratory, Lesuer, D., Kay, G., & LeBlanc, M. Copyright 2001; with permission of Lawrence Livermore National Laboratory).